DEVELOPMENT OF TEXTILE SENSORS TO MEASURE ANTHROPOMETRIC AND PRESSURE INFORMATION OF CHILDREN'S FEET

Sarah Mamaril De Guzman

Primary Supervisor: Associate Professor Andrew Lowe

Secondary Supervisor: Dr. Cylie Williams

A thesis submitted to Auckland University of Technology in fulfilment of the requirements for the degree of Masters of Engineering

2018

School of Engineering, Computer and Mathematical Sciences

Faculty of Design and Creative Technologies

Abstract

Bobux is a manufacturer of children's shoes and approached Auckland University of Technology (AUT) to help solve the pain points that their customers and clinicians have through implement new technology within their products. The aim of this research is to embed knitted smart textile sensors in their children's shoes to sense the growth and development of a child's feet – specifically foot length and weight distribution. The eventual product is envisaged as an Internet of Things (IoT) device connected to a mobile phone application receiving data meaningful to the parent, clinician, and designers.

In this research, a knitted textile sensor system to measure foot length based on capacitive sensing was developed. Two prototype configurations were evaluated on 14 children, who each inserted their feet for ten seconds inside the instrumented shoes. Capacitance readings were related to the proximity of their toes to the sensor and validated against foot length and shoe size. A linear regression model was developed on capacitance readings and foot length. This regression model was found to be statistically significant (p-value = 0.01, Standard error = 0.08). Results of this study indicated that knitted textile sensors can be implemented inside shoes to measure foot length.

Furthermore, this research developed a low cost, built-in shoe plantar pressure measurement system. This is useful for podiatrists and designers, as they are interested how pressure distribution changes from infants to toddlers. The capacitive sensors were laminated using copper tape sheet on plastic backing with adhesive, elastomer layers, and combination of conductive and non-conductive fabrics. Constructed sensors were characterised using compression tests with repeated loads. Results showed that the sensors exhibited rate-independent hysteresis in estimation of pressure, for which a

calibration model was developed. The system can mimic, at lower fidelity, more expensive plantar pressure measurement systems.

This research found that it is feasible to produce low-cost shoe-embedded capacitive sensors that can provide information about the development of children's feet.

Table of Contents

List of Figures

xii

List of Tables

Attestation of Authorship

I hereby declare that this submission is my own work and that, to the best of my knowledge, it contains no previous material previously published or written by another person (except where explicitly defined in the acknowledgements), nor material which to a substantial extent has been submitted for the award of any other degree or diploma of a university or other institution of higher learning

Sarah De Guzman

Acknowledgements

I wish to thank Dr. Andrew Lowe for his patience, support, advice and guidance throughout this research. I would also like to thank, Sam Burton, Andrew Sharp and Bobux staff for supporting this research, this work would not exist without you.

I would like to express my gratitude to the following:

- Dr. Andrew Lowe for his patience, support, advice and guidance throughout this research.

- Sam Burton, Andrew Sharp and Bobux staff for supporting this research and letting me break numerous shoes for this research

- Dr. Cylie Williams from Monash University for imparting knowledge and all the wonders of paediatric podiatry.

- Textile and Design Lab especially Gordon Fraser and Peter Heslop for providing their knowledge around textiles and CNC knitting machine skills.

- To wider AUT Community, thank you for your support and offering a welcoming approach.

Sincere thank you to helpful friends especially to Andries Meintjes for creating a data collection app and mentoring me in embedded programming, participants in my research, and School of Engineering staff for their encouragement and support during this Master's Degree in Auckland University of Technology.

I would like to thank all my Mum, Dad, 4 siblings, and friends for constant support and for lending a helping hand when needed.

Ethics Approval

Phase 1, as detailed in chapter 3 of this thesis needed to be tested on children between ages 11 to 36 months old. Full ethics approval for this was approved on 1st December 2017, AUTEC Reference Number 17/381.

Ethics Approval document is included in Appendix 3.

Chapter 1 Introduction

1.1 Background of Study

Bobux is a New Zealand children's shoe company that started creating soft sole shoes for infants in 1991. This started as the former owners Chris and Colleen Bennett wanted soft soled shoes for their 9 month old daughter to let her foot grow naturally (Harris, 2015). At present, the shoes Bobux designs ranges from infants, toddlers and pre-school aged children. Their motivations and design mantra are to create stylish functional shoes that help with children's foot development. In addition to that, Bobux have been actively seeking podiatrists' advice in making their shoes. Their input is valuable because it helps the design team in creating shoes that are good for children.

Children's feet are relatively flatter and have less structure due to the bones not being fully calcified. For this reason, barefoot activity is important for children as it functions as touch sense organ, that is, children should be able to feel the changing terrain while playing or running (Baadh, 2014). Children's feet during the walker stage (between 9 – 14 months) only have cartilage and padding tissues. These will develop to bones, ligaments and tendons over time through play, use and different environmental exposure (Sessoms, 2017). Bobux' shoes are designed based on the barefoot model, to help develop feet in a more natural way while protecting from environmental dangers such as shards of glass, grass prickles and hot concrete. Additionally, Bobux shoe lasts[1] are shaped in a unique way compared to normal lasts, as they are more flat footed compared to normal lasts.

---

[1] Last is a mechanical form that has a shape similar to human foot. This is used by shoe makers to manufacture and repair shoes.

Foot Morphology literature indicates that in the first 3 years of life, the foot length grows approximately 2 mm per month. It also recommends that children aged 2 to 6 years old need to change shoes every 2 months (Wenger, 1983). Later, more detailed studies indicate different foot growth rates for children ages one to five years old.

- Children under 15 months of age required to change half size footwear in less than two months
- From 15 months to 2 years of age, half size foot wear increase occurred every two to three months
- From 2 to 3 years of age, half size footwear increase happened every three to four months
- From 3 to 5 years of age, half size foot wear increase occurred every 4 months.

Both genders grow at similar rates, however, boys' feet are likely to grow one size longer and one size wider (Gould et al., 1990). It is also indicated that the development of the child's foot is strongly influenced at the point at which the child starts to stand and start walking. During infancy there is no need for a shoe as they will not be walking. From the phase when they start to walk, from ages 1 – 2 years, the sole purpose of the shoe is protection from weather and environment. Therefore, at this age, shoes must be very soft and flexible to allow for freedom to move like it is barefooted. Thick soles would impinge foot development as it adds strain on the foot and ankle joints. (Maier, 1999)

From ages 2 – 4 years old is when children start to become active. This is also the time when short bones in their feet start to harden or ossify. The loads induced on the bones play a significant role in development of bones. It is necessary for children to be able to feel the changes in terrain for more natural bone development. (Walther, Herold, Sinderhauf, & Morrison, 2008)

Although the references stated in the previous paragraphs are nearly 20-30 years old, information about foot growth is still lacking. Foot growth information can provide information such as – child growth spurt occurrence and time indication when to buy new shoes (Busscher et al., 2011). Additionally, podiatrists still do not have enough evidence as to whether footwear influences structural development of the feet and associated locomotor behaviours (Morrison, Price, McClymont, & Nester, 2018). Existing views on children's footwear have left unchallenged with outdated literature (Staheli, 1991) thus, remaining an area where more research attention is necessary. Parents are willing to buy an inexpensive brand because children's shoes are deemed expendable due to their rapid foot growth. Consumers are not fully aware of footwear literacy, hence views of consumers on children's shoes are left unchallenged.

Parents usually buy shoes that are bigger so that they do not need to keep buying shoes. Similarly, parents would then let their child grow into these shoes, not knowing that they should have changed shoes a long time ago. Children, especially the ones who have just started walking, 10 – 14 months old, are incapable of specifically telling their parents how their shoes fit. Currently, parents are required to guess which size to choose when buying their child's footwear. This is a pain point from the parent's point of view, and if this is solved, this would empower parents in helping choose the correct shoes for this child. Usually, parents are biased in what the child wants just because the child likes to wear their favourite shoes even though the shoes may not be a good fit for them. During the buying stages, a child may choose shoes that are attractive to their eye, but again, this may not necessarily fit them.

According to Bobux internal customer research, parents, particularly first-time parents, deal with a lot of uncertainty and issues such as:

1. What is the optimal age to put children into walking shoes?
2. Is their child walking properly?
3. How long should parents keep their children in a pair before upgrading to a bigger size?

In addition to solving parents' issues, Bobux is also interested in deciphering podiatrists' issues around children's foot development. In this thesis, new techniques of shoe manufacturing and new materials will be explored to help solve issues mentioned and to contribute to the lack of research in paediatric podiatry while creating an awareness to foot health while the child is young.

Bobux advocates for children's foot health and for empowering parents upon deciding whether what is best for their child, but also collate this information into a large dataset which can be used in clinical research.

Although foot growth research is known to be one of the best indicators in growth spurt and possibly various diseases, information regarding when the parents bought new shoes and also how their feet grow inside these shoes is lacking. (Busscher et al., 2011) Unknown foot and other physiological problems are put inside the basket term of 'idiopathic' as clinicians do not really know how the problem came about.

1.2   Research Aims

The aim of this research is to study the technical feasibility of textile sensors in measuring foot anthropometrics, specifically foot length and plantar pressure. This is divided in two phases:

1.   Creation and validation of in shoe foot length measurement system.
2.   Creation and validation of built-in shoe plantar pressure measurement

The motivations behind the creation of these two aims are to alleviate pain points of both parents and podiatrists as described in Section 1.1.

1.3   Research Methods

This research was based on relevant theory and supported by experimental work to concluding the feasibility of the overall research project. The literature review covers the theory, motivations and the underlying technologies used in creating prototypes for the two topics. The two main topics covered are – use of textile sensors to measure anthropometric foot parameters and viability of built in insole plantar pressure measurement system. These topics are described in their own separate chapters. Each topic includes its respective introduction, methodology, results and discussion. The introduction lightly describes the objectives of the topic. The methodology describes the processes used in creating a way to answer the topic. The results section shows the results acquired from the several testing procedures done in that topic. The discussion ties in all the investigation done with the literature review to provide conclusions. A conclusion chapter compares the two topics together by creating enough input for the motivations from the introduction.

Research analysis methods such as mixed methods paradigm (qualitative and quantitative methods) and inductive research analysis are used in Chapter 4, due to insufficient amount

of research in this area. Research about the underlying theories are accessible, but applications to such specific topics are not available. In Chapter 5, mixed methods paradigm and deductive research analysis was applied due to more breadth of research done in this area.

1.4 Thesis Structure

Chapter 1 introduces the research questions and the context of topics covered in this thesis.

Chapter 2 covers the literature review on the topics around paediatric podiatry, children's foot development in physiological aspects and how footwear plays a role between these two. This chapter also discusses the emergence of smart materials and how this can be used for unknowns that both footwear industry and clinicians may have.

Chapter 3 covers the literature review of the enabling technology, capacitive sensing. This chapter discusses basic configuration of sensors and how this can be implemented on footwear.

Chapter 4 tackles the design and development process of creating a knitted shoe sensor that can measure anthropometric foot parameters of children from the walker age (11 months old to 36 months old). Chapter 5 examines the feasibility of creating a built-in shoe plantar pressure measurement of children of the same age range as the former.

Chapter 6 concludes this thesis, answering the research questions and aims introduced in Chapter 1.

Chapter 2 Literature Review

This chapter contains topics of children's foot growth and development, issues around paediatric podiatry and how footwear can play a role in children's foot development. Emergence of smart materials and enabling technologies are also discussed in this chapter.

2.1 Infant to Toddler Foot Growth and Development

The phases of infant growth and development from rolling over, sitting, crawling then to walking are important milestones for the child and exciting for the parent, as these represent development of motor control and coordination. The first 12 months is a crucial stage of development as the anatomy, neuromuscular and sensory systems undergo rapid changes (Price, Morrison, Hashmi, Phethean, & Nester, 2018). This is the stage where, the body weight increases to more than 50% from birth and lengths of lower limbs to approximately 50%, linearly from birth up until the age of 18 months (Wells, Hyler-Both, Danley, & Wallace, 2002).

Alongside these changes, the shape structure and function of the foot continues to change and grow as the child starts to explore and interact with physical and social environments. The foot is primarily used for reaching and grasping before it develops as a weight bearing structure (Galloway & Thelen, 2007). There is rapid foot growth from learning to stand upright and beginning to walk. It is known that half of the final foot length will be reached at an average age of 12-18 months (Anderson, Blais, & Green, 1956). The foot growth velocity decreases rapidly until the age of 5 years. Between 5 and 12 years of age, the feet of girls grow on average by 0.9 cm per year. For boys, the growth period lasts until the age of 14 years (Niethard, 1997). However, these studies are dated and cannot claim to

be conclusive as the impact of physical and social environments on growth and health continue to change.

Infants are heavier on their 12th month than they were at birth. This impacts their ability to stand and walk. Therefore, their bones need to develop, so they can support their increased weight, during initial stages of walking. As children's mass change, their bone structures also change. The typical range where a child starts to cruise and independently walk is between 10 and 20 months with an average time of about 12 months. At birth, some bones are present but there is a rapid ossification in the first 12 months to 6 years. During this time, the foot is supported by partially ossified centres (Hallemans et al., 2006). A large fat pad is present underneath the foot up to the age of six. It is thought to distribute plantar pressure to protect delicate soft cartilage and tissues and help increase the surface contact with the ground during learning complex walking and running skills (Gould, Moreland, Alvarez, Trevino, & Fenwick, 1989).
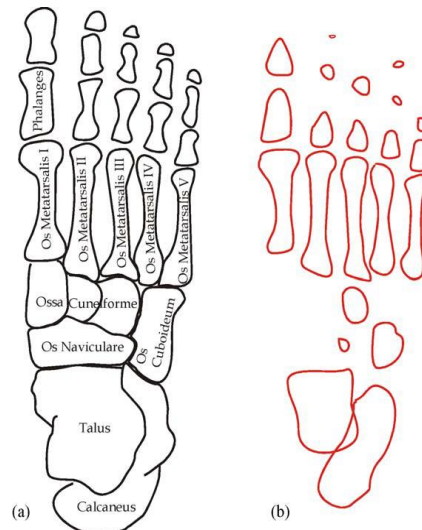
Figure 2.1 left) Bony skeleton of adult; right) Skeleton of toddler foot. Soft cartilage surrounding the ossification centres.(Hallemans, Clercq, Dongen, & Aerts, 2006)

The foot is covered with skin, which is a sensory organ containing receptors that help relay information to the brain. It contributes to the control of the posture and movement (Inglis, Kennedy, Wells, & Chua, 2002). When the child starts to walk, he/she learns through movement to engage with their environment. Locomotion also aids children's mental development, and it is through walking, that they can start to distinguish which surfaces are safe to walk on and, how to adjust their body posture so that they do not fall over.

As children start to walk independently, the fat pads remain on the plantar surface to protect the under developed soft bones. As the complex bony structures develop, the fat pad recedes and the longitudinal arch starts to develop around five years of age (Gould et al., 1989). The longitudinal arch functions as space for soft tissues with elastic properties. These soft tissues acts as springs and shock absorbers, which spread ground contact forces over time during weight bearing physical activities (Kirby, 2017). Over time, the child's body learns how to support these weights more sophisticatedly during the development of the longitudinal arch. This holds passive and active components – passive components which automatically increase stiffness of the longitudinal arch; active components which allow the central nervous system to modify its stiffness and redirect ground reaction forces along the plantar surface for more effective load distribution on weight bearing activities, on certain terrains (Kirby, 2017).

There is a wide inter-individual variety of foot shape and gait during infancy and childhood. Therefore, a differentiation between physiological and pathological features can be extremely difficult. Children's feet can be assessed in clinical environments by facilitating a thorough knowledge of dynamic plantar pressure patterns (Simon, Quesada, Pisciotta, & Leurgans, 1994). For plantar pressure assessment to be indicated, a child

would have to pose serious feet problems that are causing immobility. Normal developing children are not necessarily checked by a podiatrist or researcher very often, hence the lack of normative information.

This thesis describes the development and validation of in-shoe monitoring tools to observe two aspects of children's foot growth and development– foot shape and structure (i.e. anthropometric parameters) specifically foot length and plantar pressure. Foot length is chosen because it is one of the indicators of foot growth, however, as indicated by research on foot length of normal developing children was conducted by Wenger (1983). This thesis will help create technologies that can be implemented inside shoes to detect foot length. Similarly, plantar pressure rapidly increases during the infant to toddler stage as their weight increases rapidly. More information on plantar pressure can help clinicians identify early stage foot related diseases that could occur later when children grow up to be adults. This information also helps designers create better shoes.

2.2 Podiatry Research in Children Footwear and Foot Development and use of Research in Co-Design

There is a vast amount of research available on how adults' feet react and respond while these are inside shoes. A simple Google Scholar search of keywords "adult feet inside shoes" yields 133,000 search results (excluding patents) and "toddler feet inside shoes" yields 25,800 search results (excluding patents). This may be due to the adult population percentage worldwide outnumbering children population (25.44% on age bracket 0-14 years) (Indexmundi), although, this can also be influenced by other factors. One of the biggest factors is that, adults are more capable of verbally communicating how something feels like, whereas complex communication and quantitative measures are used in children especially infants and toddlers as they are incapable of giving constructive verbal communication like adults. Another aspect could also be that not much interest is taken in this field of research due to the difficulties of dealing with children in a controlled environment.

Clinicians, podiatrists and other researchers face distinct challenges, one of which is making sense of emerging problems in the paediatric foot and lower limb research area. Many areas of health care and medicine are turning towards evidence-based practice. Therefore more information is needed to shape the clinician's understanding around paediatric foot and lower limb issues (Evans, Morrison, & Williams, 2015). With a plethora of information and if interpreted correctly, clinicians can make faster diagnoses and create preventive measures.

To create more information for clinicians, there needs to be an accessible database containing useful data. An example of this could be a database for normative values of plantar pressure measurements in children. This is an accepted measure in clinical assessment for foot function. Bosch et al. (2007) started to curate normative values for

plantar pressure data for 100 healthy German children over four years, as there was no information that existed to determine the normality of an individual pressure pattern. This research team noticed there was a gap in longitudinal studies observing paediatric foot developments. This knowledge provided information about normal growth related changes of foot shape and foot loading parameters (pertaining to plantar pressure) This information is relatively hard to extract within a non-longitudinal study, as this infancy to toddler stage is the times of fastest foot growth (Bosch et al., 2007).

Information curated in such research can help clinicians make diagnoses but also can be used to improve the design of children's shoes. Most manufacturers create shoes that are a miniature of an adult shoe. However, children and specifically toddlers do not have the same foot anatomy and characteristics as adult feet (Morrison et al., 2018).

Though normative studies like Bosch et al. (2007) exist, Morrison et al. (2018) draws upon how there needs to be more research on children's footwear science and advanced understanding of interaction between the foot and the shoe. Evidence-based practice may apply to children's feet, however this is still an issue in designing children's footwear (Morrison et al., 2018). Often, shoe designers and manufacturers ask children how they feel when wearing newly designed shoes but end up observing how the shoes are used. Children lack the ability to distinguish tactile input changes and cannot exactly describe how the shoes make their feet feel (Herbaut et al., 2017). This is an issue that shoe designers and manufacturers face when trying to understand what really is a good shoe fit for young children.

Footwear literacy and education is needed to manage foot and any lower limb complaints of pain from children. However, this remains a challenge for both clinicians and parents

(Penkala, 2012). There is little literature regarding footwear purchasing habits. Therefore, attitudes and behaviours of parents buying shoes aren't clearly understood.

There are existing studies that discuss how shoes affect gait. A study done by Buckland, Slevin, Hafer, Choate, and Kraszewski (2014) on children learning how to walk in 5 months or less evaluated barefoot and 3 shoes of varying torsional flexibilities. It was found that children were able to perform a wider step when wearing a very flexible shoe, compared to medium and low flexibility shoe (Buckland et al., 2014). Another study from a different research team looked at how the shoe flexibility contribute to plantar pressure loading of children learning to walk. Similar shoes were used, and it was found that a very flexible shoe showed the same plantar pressure as a barefoot pressure reading, whereas the medium to low flexibility shoes gave lower plantar peak pressures (Hillstrom et al., 2013). Even though the changes of shoe flexibility are documented, it does not indicate as to whether this is a good shoe for the child or not. This could also depend on what the child needs. If the child needs more support and they have a growing pain, a less flexible shoe may be preferable.

Furthermore, little is understood about the foot inside the shoe (Barisch-Fritz, Schmeltzpfenning, Plank, & Grau, 2016). This is highlighted by the gap in amount of existing research and current practices on issues like musculoskeletal symptoms of childhood obesity. If little is understood in normative foot development, it is hard to pinpoint other problems in an abnormal foot development. This information can also impact shoe designers and manufacturers. If little information is understood about foot growth, there is also an information gap in shoe design. It is hard to quantify how good is the fit of the shoe.

2.3 Footwear

Footwear is classified as an article of outer clothing for the feet. Footwear may include but is not limited to, sandals, shoes and boots. Historically, shoes were created to protect feet from the harsh environment. The earliest known shoe dates approximately between 7000 – 8000 BC and were found near central Oregon in North Western America's vast desert. The population traveling across these places needed some protection from the heat of the sand and surface terrain (Connolly, 2012). It is also thought that shoes were used long before this article of footwear was dated. However, due to highly consumable materials and extensive wear, it is difficult to find evidence of the earliest footwear.

Footwear still has an unknown impact on the foot anatomy of children. Parents, clinicians, and shoe manufacturers presume that children's shoes do not hinder normal locomotion and foot function. It has long been thought of that ill fitted and designed shoes contribute to paediatric foot and toe deformity, although, experimental results on the tests are not recorded deeming the research ambiguous (Wegener, Hunt, Vanwanseele, Burns, & Smith, 2011).

Existing literature is available on biomechanical effects of shoes on gait patterns of children. These are described using various biomechanical variables like kinetics, kinematics, spatio-temporal, plantar pressure and muscle function (Wegener et al., 2011). Information about children's foot shape inside shoes is not as available compared to adults.

For a child to start wearing a shoe, he/she must be at a certain age where they need to start wearing it. Young infants aged 11months to 24 months old are still learning how to walk and therefore the main purpose of the shoe is for protection. Children's feet do not need to be boxed inside a shoe where it does not allow free movement. This can add strain on

the foot and the ankle joint which could lead to improper foot growth (Walther et al., 2008).

Footwear may be categorised as athletic and non-athletic footwear. The former tends to have more functional purposes such as more protection from the environment, increased friction from the ground, increased foot stability and variable shock absorption from weight bearing activities. Many athletic shoes are designed to prevent injuries. Non-athletic footwear, such as dress shoes, working shoes or high heeled shoes, may not necessarily provide all the same functional purposes as athletic footwear. While many will still provide some shock absorption or protection from the elements or ground surface, these footwear types cater more for fashion and aesthetic aspects (McPoil, 1988). Athletic shoes are becoming more popular as everyday wear due to being more comfortable to wear than non-athletic shoes. Also, as other cultural aspects like fashion evolving throughout the decades, it is becoming more acceptable to wear athletic shoes every day (Williams, 2014).

Athletic shoes and non-athletic shoes have distinct types of shoe features and construction. Both shoes would always have the following parts shown in Figure 2.2: an upper, lining/sock liner and an outsole.

Figure 2.2: Parts of the shoe (Ethical Elephant, 2017)

- Upper – Refers to the parts of the shoe that covers the back of the heel, toes, top and sides of the foot. This is attached to the outer sole of the shoe. Depending on the style, the materials it is made of can include leather, natural fabrics to synthetic leathers and fabrics. Additionally, depending on the style of the shoe, the upper can be cut as a single piece, or it can be made of many different pieces sewn together (Stimpert, 2018b). The part of the upper that covers the sides and the back of the heel is called a quarter. A Heel counter is a component that can be added to the quarter which stiffens the back of the heel for a better support. The vamp covers the front and top of the foot. The vamp can be a single material or made of several parts including the toe cap and toe puff. Some shoe manufacturers choose to extend the vamp all the way over the toes, whereas others choose to integrate a toe cap for decorative purposes or for extra protection if sturdier materials are in place (i.e. scuff protection). Some manufacturers may include a toe puff in their shoes to reinforce and hold the shoe shape in the toe box area (Stimpert, 2018b)

- Lining and Sock - The lining is the material inside the shoe that touches the entire foot. Its main purpose is to cover the sewn on seams of the upper and the sole. The lining is made of comfortable materials that cushion the foot and/or draw out moisture. Like the upper, the lining can be made of various materials. Leather is one of the most favoured linings as it conforms to the foot shape over time, is durable, allows airflow, and lets moisture evaporate (Stimpert, 2018a). However, leather is expensive and heavy. Shoe manufacturers opt for polyester and acrylic materials due to being inexpensive and light, but they do not absorb moisture like leather. The sock or sock liner can also be called the insole. This is usually the

layer of foam which the sole of the foot rests on inside the shoes (Asics, 2017) and can be attached to the lining. Manufacturers opt to make the insole removable as it is easier to install inside the shoes. A common material of an insole is Ethylene Vinyl Acetate (EVA) Foam, which is a shock absorbent material (Whelan, 1994). Consumers may choose to buy other types of insoles made of other materials to make the shoes more comfortable.

- Outer Sole – The outer sole is the bottom most part of the shoes that directly contacts the ground. Outer soles can be made from various materials such as natural and synthetic rubber, PVC and Polyurethane compounds (Stimpert, 2017). Like the lining and upper, the materials used are dependent on the purpose of the shoe. Its main purpose is to protect the feet from the environment and the changing terrain.

Newer manufacturing techniques such as knitting have emerged in shoe manufacturing, also referred to as 4D knitting. This combines the full upper and the lining of the shoe. A one-piece design is created by a CNC knitting machine. The machine can be programmed to use a variety of threads, which can also vary the amount of stretch and structure of each knitted upper (Motawi, 2017). Shoe manufacturers choose to have knitted uppers due to it being more sustainable as less materials are needed to achieve the same purpose as a normal shoe would have.

2.3.1 Footwear Selection Technologies and Foot Problem Diagnostics

Apart from all the processes of shoe making, there is also a psychological aspect to parents' culture of buying shoes. Parents decide based on what they think is correct. Children do not have cognitive abilities to understand what good fitting shoes are. At shoe retailers, a common device to help parents decide on their child's shoe size is the Brannock device (Figure 2.3). Shoe manufacturers like Clarks and Bobux have simpler versions of this (Figure 2.4 and Figure 2.5. These devices work by having the child put the heel at the back of the device while standing, and a slider that moves up and down is adjusted, measuring the child's foot length. Simply enough, foot length can also be measured using ruler and/or tape measure.
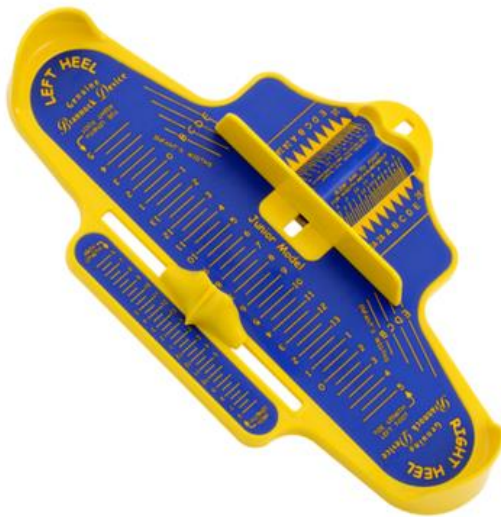
Figure 2.3: Ultra Fit Brannock Foot Measuring Device (Brannock USA)
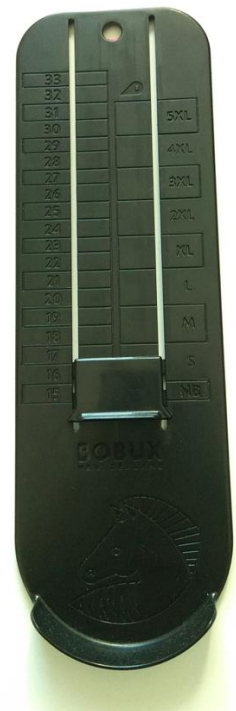
Figure 2.4: Bobux Shoe Ruler

Figure 2.5: Clarks Measure at home Children's Foot Gauge (Clarks)

Pedobarography

Pedobarography is the study of pressure acting between the plantar surface of the foot and supporting surface during static and dynamic loading (Skopljak, Muftic, Sukalo, Masic, & Zunic, 2014). This is mainly used by clinicians to make diagnosis for people with pains in the lower limbs. Pedobarography is also important in gait and posture research for further diagnosing lower limb issues, sports biomechanics, injury prevention and footwear design (Razak, 2012).

There are two categories for these foot pressure measurement devices: a) in-shoe based system and b) platform-based system.

In-shoe based pressure mapping system gives flexibility of movement to the researchers and user because it can be placed inside the shoe. The researcher would not have to worry whether the person stepped on the correct area of the sensor. In-shoe based system like Pedar (Figure 2.8), F-Scan (Figure 2.7) and Orpyx (Figure 2.6) are portable, allowing for variety of studies and biomechanical characteristics to be observed such as, different gait modes in different terrains (Razak, 2012). Pressure measurements acquired in an in-shoe system reflects the characteristic of the foot and the shoe.
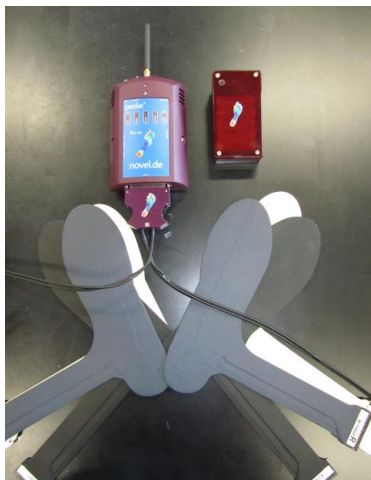
Figure 2.8: Pedar in-shoe foot pressure measurement device (Pedar)

Figure 2.7: F-Scan TekScan (TekScan)

Figure 2.6: SurroSense Rx (Orpyx, 2018)

19

Platform based pressure mapping systems are required to be fixed in one place, hence this is not as portable as the in-shoe based systems. Platform based system like e-med (Figure 2.9), assess the barefoot pressure data, and cannot measure pressure data between a terrain or a shoe. Other platform systems include pressure mapping walkways and mats.

Figure 2.9: emed Pedobarography Platform (Novel)

Pressure measurement devices are expensive. A used Pedar system is priced at USD 27000 (Biomch-L, 2016). Not all clinicians and research institutes can afford to have foot pressure measurement systems in place. These devices are important in helping clinicians diagnose and create preventive treatments for people with lower limb diseases. Hence lower cost versions of these systems are needed.

2.4   Smart textiles role in sensing and challenges

2.4.1   Smart textiles and sensing

Smart textiles are defined as:

> textiles and fabric materials that can sense stimuli from the environment, to react to
> them and adapt to them by integration of functionality in the textile structure. The
> stimulus and response can be electrical, thermal, chemical, magnetic or other origin
> (Van Langenhove & Hertleer, 2004).

Smart textiles can be divided into three groups (Zhang & Tao, 2001a, 2001b, 2001c);

a) Passive smart textiles – these act as sensors and can only sense the environment

b) Active smart textiles – these acts as sensors by sensing the environment. These
   also act as actuators as they can react to the stimuli from the environment.

c) Ultra-smart textiles – act as both sensors and actuators and able to adapt their
   behaviour to certain situations.

Textiles can be defined as any material made of intertwining fibres (also known as yarns
or thread). Yarns are produced by spinning organic fibres – such as cotton, hemp, flax,
pineapple, wool; and/or synthetic fibres such as nylon, polyester, rayon, and lycra.
Textiles and fabrics are formed by knitting, weaving, felting, crocheting these yarns
together (Textile School, 2018) .

Manufacturing of smart textiles does not deviate much from classic fabric production
techniques. The addition of other materials and processes associated with it makes it
smart. An example of smart textile is an electrically conductive yarn comprising of metal
fibres. These are used for variety of apparel and flooring applications such as creation of
carpets that dissipate static electricity in factories (Kessler & Fisher, 1997), technical

clothing made for flammable environments, and anti-microbial clothing used for hospitals and clean rooms (Uddin, 2010).

Sensors are materials or devices which detect or measure a change in a physical property (Oxford Dictionary, 2018). Passive smart textiles can be used as sensors as they can sense changes in the environment. An example of this is the use of textile electrodes for Electrocardiography (ECG). Ankhili, Tao, Cochrane, Coulon, and Koncar (2018), implemented washable and reliable textile electrodes in a sports bra to monitor ECG around the heart area. The textile electrodes were connected to an electronic system to enable reading of the person's ECG. Passive smart textiles do not have any computing power, hence the need for an external electronics unit (Chandra Das & Chowdhury, 2014).

Textile sensors can change traditional clothing into a more functional and performance enhancing garment. There are fabrics which help regulate body temperature, which are useful to people who need more flexibility in colder regions reducing the amount of bulky clothing. Some fabrics can also reduce wind resistance and control muscle vibration, which are useful for improving athletic performance (Gaddis, 2014). In the medical field, textile electrodes are gaining popularity as an alternative to gel electrodes. They can establish a good contact with skin, whereas the gel itself can cause skin irritation and discomfort to the patient. Gel electrodes are only one time use and needs to be replaced from time to time. If this is replaced by textile electrodes, patient monitoring can be done for longer term (Van Langenhove & Hertleer, 2004).

In this thesis, different conductive threads are explored to implement proximity sensing to measure the foot length of children over time. These conductive threads are used as the sensor and these are connected to an electronics unit, to measure the distance of the foot

to the sensor. The same electronics unit is used to measure foot pressure of children. The materials explored for foot pressure measurement are a variety of conductive fabrics and threads. Different manufacturing techniques are also explored to implement the technology.

2.4.2 Smart Textiles and Challenges

Though smart textiles have various potential applications, there are also various challenges. Many smart textile technologies are proven in laboratory studies, but there are still uncertainties in mass production. Initial investigation by Harms, Amft, and Troster (2012) showed positive trends on simulations of predicting behaviour of loose and partially fitting loose garments. Ankhili et al. (2018) also showed promising trends on the washability factors of ECG textile electrodes on sports bras. However, more robust simulations and modelling is needed so that reliable results can be obtained. (Schneegass & Amft, 2017)

Smart textiles technology is relatively new, and so there is an insufficient amount of technical regulation around it. Mass produced textile technology need to comply with user requirements and technical regulations from electronics and textile fields. Certain regulations in the electronics field may not be the same as for the textile industry. This can result to the textile industry needing to change their requirements to meet the same criteria in the electronics field. An example of this is the mechanical handling of textiles and electronics. Some electronic components are designed to bend with a limited bending radius, however, textiles can be bent with smaller bending radius and can be exposed to much larger forces and strains (Cherenack & van Pieterson, 2012)

Chapter 3

Chapter 3 Capacitive Sensors

Capacitive sensors or capacitors operate based on changes in electrical capacitance of a material. The basic structure of this is any two conductive materials separated by any insulator.

Capacitance is a measure of the ability of a capacitor to store energy or electric charge.(Young & Freedman, 2008)
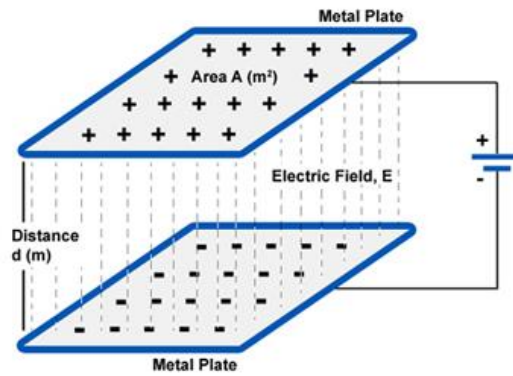
Figure 3.1: Simple Parallel Plate Capacitor

Consider one of the simplest forms of a capacitor, called the parallel plate capacitor. Two plates parallel to each other contain a certain amount of charge per unit potential difference. The standard equation for a parallel plate capacitance is given by the following equation.

$$C = \epsilon_0 \epsilon_r \frac{A}{x_1}$$

Equation 3-1

where ϵ_0 is the permittivity of free space, ϵ_r is the relative permittivity or dielectric constant of the material between two plates, A is the surface area of the conductive plate and x_1 is the distance between the plates or the thickness of the insulating material at any given time.

Referring to Figure 3.1and Equation 3-1, the change in capacitance depends on changing the area, the dielectric constant and the spacing between the two plates.

In addition to the parameters mentioned in Equation 3-1, other capacitor design guidelines need to be followed such as;

1. Appropriate design of capacitor plates to measure desired variables.

2. Maximizing capacitance over a large area of closely spaced plates

3. Appropriate shielding and/or grounding pattern to minimise stray capacitance

4. Selection of excitation frequency (operating frequency) which is high enough to filter out low frequency noise.

5. Design of an appropriate circuit to meet accuracy requirements and to deliver protection from the environment.

(Baxter, 2000)

Knowing that capacitance can change due to influence of varying, surface area, distance between two plates and dielectric constant, there needs to be a circuit to enable measurement of these changes. Simply enough, capacitive sensors can be such areas on the Printed Circuit Boards (PCB) that have been filled with conductive traces like copper and connected a microprocessor (μP) using a conductive trace. The μP measures the sensor in a way that allows detection of minimal changes in capacitance. The capacitance is continuously recorded using a software and when there is change, the system will read and recognise this change on that sensor. (Davidson, 2011)

There are two common ways that a circuit can measure capacitance, some common integrated circuits (ICs) are;

- Charge Time Measurement Unit – A constant current source is set in the µP, this charges the electrode at a constant time. This leaves two variables that can change, capacitance and voltage, if there is increase in voltage, there would a decrease in capacitance (Bilal, 2017)

$$i = C\frac{dV}{dt}$$

$$i = C\frac{V}{t}$$

where $i = current$, $C = capacitance$, $t = time$ and $V = voltage$

- Capacitive Voltage Divider – A voltage divider circuit with two known capacitors are setup in series. The applied equation to measure voltage is;

$$V = \frac{Q}{C}$$

where $V = voltage$, $Q = charge$ and $C = capacitance$

The equation 3-4 shows that, voltage is inversely proportional to capacitance. Using the equation above, if the voltages are known capacitance can be calculated.
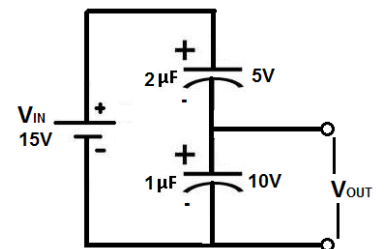
Figure 3.2: Capacitive Voltage Divider DC Circuit (Electronics)

For this thesis, the selected capacitance measurement IC is MPR121 (NXP Semiconductors) uses the Charge Time Measurement Unit (CTMU). (Davidson, 2011) This involves the measurement of voltage, as the system assigns a known current on the

sensor. The circuit then examines for a shift in the amount of voltage while constant current is being applied. The operation and software algorithm of MPR121 is discussed in Section 4.1.3.4.

Capacitive sensors are analogue devices and so any noise can affect the accuracy of the measurement. There are many sources as to where this noise can come from,

1) Noise can come from between the sensing device pin to the electrode itself

2) Neighbouring sensor electrodes being too close to each other

3) Environmental interference such as other humans surrounding the sensor, touch, water, radiated electromagnetic signals, and noise from other electronic devices.

Noise and interference can be minimised by placing appropriate ground patterns and/or by applying active shielding. By placing appropriate ground patterns, the nearby ground traces can block the unnecessary electric field lines (noise). A good ground pattern for preventing noise is a mesh pattern (Renesas, 2017) as this physically filters out the unwanted electric field lines. Electromagnetic field lines have certain frequencies and so the spacing between the mesh needs to be small enough so that it doesn't let unwanted frequencies pass through (Ohmura, Ogino, & Okano, 2014).

Capacitive sensors can detect many physical parameters such as – proximity, position, force, humidity, fluid level and acceleration. (Du, 2015) As materials used to create the sensor can almost be made of anything conductive, and these are readily available everywhere.

3.1.1 Proximity Sensing

Capacitive sensors can be used for proximity sensing. The advantage of this is that it can sense both conductive and non-conductive targets. This sensing technique is also non-contact, has minimal moving parts and can be environmentally sealed.

A simple capacitive sensor configuration can be formed by creating an isolated sensor plate out of a conductive patch on a circuit board and applying charge to it. When an object or a finger approaches the sensor plate, the dielectric constant changes due to it being different from air therefore changing the capacitance. (Digi-Key North American Editor, 2016) The finger influences the change in capacitance due to it displacing the air between the finger and sensor. The human finger is mostly made of water; therefore, it has a higher dielectric constant ($\epsilon_r = 80$) than air ($\epsilon_r = 1$). The interaction of the finger with the electrode's electric field represents an increase in the dielectric constant resulting in capacitance increase (Keim, 2016).
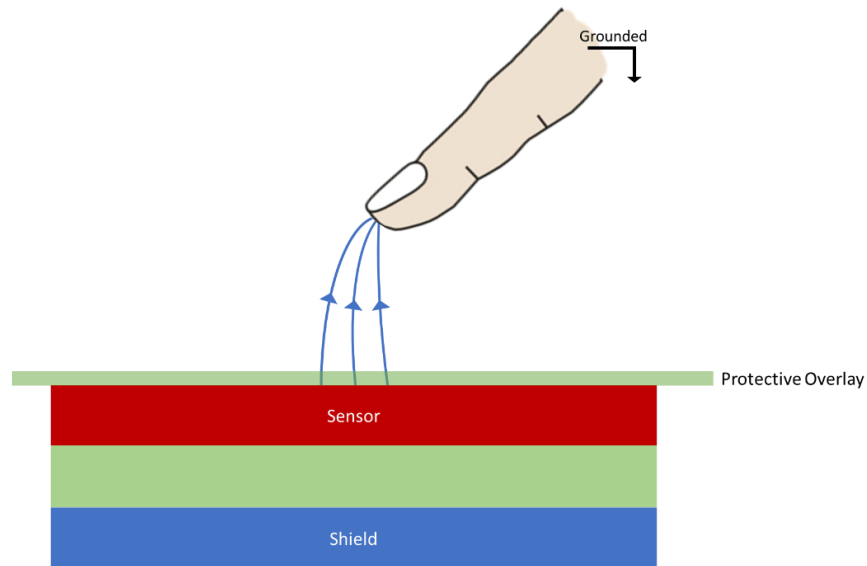
Figure 3.3: Interaction of human body (finger) with a capacitive plate/capacitive touch sensor

Apart from the finger acting as a dielectric, it will also act as a conductor. The human body contains about 75% water containing ions, which is one of the reasons that the human body is conductive. This extends to the skin. However, skin is not fully conductive like metals, as it contains some components which inhibit the flow of electricity through the body (Gusev, Demin, Galina, & Mikhal'chenko, 2009). Although skin is conductive, direct conduction does not occur. This means that the finger does not discharge the electrode, due to the protective overlay shown in Figure 3.4. The skin contributes to the capacitance, as this becomes the second conductive plate of an additional capacitor (Keim, 2016). Hence a new capacitor is created by the finger. This is in parallel with the existing sensor electrode. Despite, the person not being electrically connected to the PCB Ground, the human body has large enough capacity to absorb an electric charge, and thus behaves as a virtual ground as shown in Figure 3.4
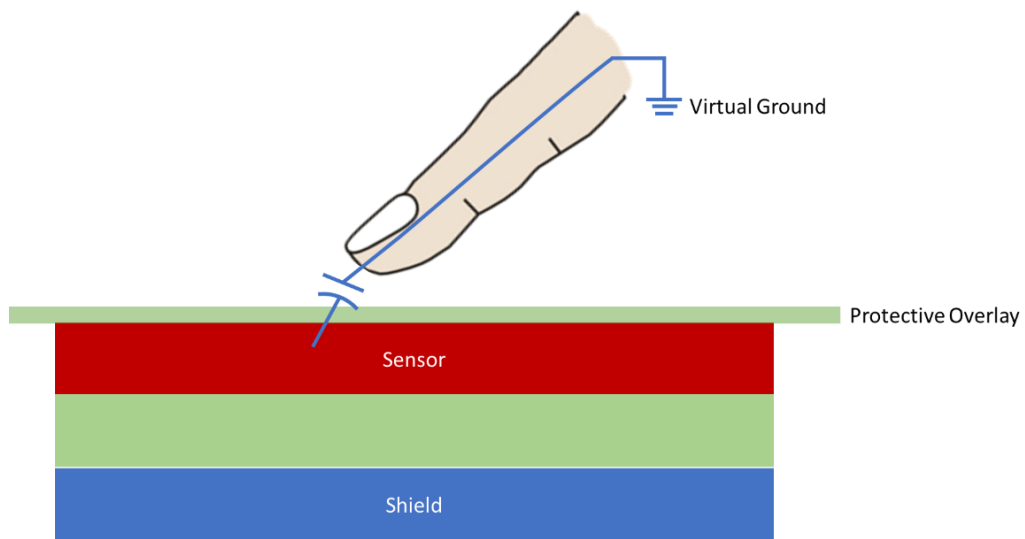
Figure 3.4: Skin on the finger becomes 2nd conductive plate with air and protective overlay as the dielectric

As the finger moves closer to the sensor electrode, the distance between the two conductive plates (finger and sensor electrode) decreases. Hence capacitance increases, which indicates the proximity of the finger to the sensor.

In Chapter 4, proximity sensing is implemented. The sensor design contains one electrode and no dielectric media. It relies on the target's dielectric material (Figure 3.5 and Figure 3.6). The closer the foot gets to the electrode, the capacitance increases (Du, 2015), indicating the foot length inside the shoe.
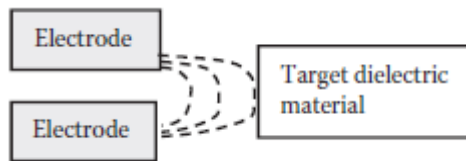
Figure 3.6:Taeget dielectric material approaching sensor electrodes
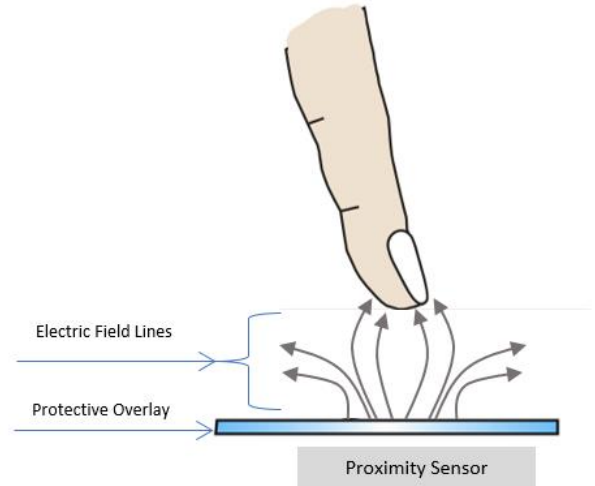
Figure 3.5: Finger changes the electric field lines when it closer to the proximity sensor

An appropriate design of a capacitor electrode chosen is a non-planar electrode plate. This is due to the foot's non-planar shape. The sensors need to conform to the shape of the shoe.

Shielding (or placing of ground planes) of the sensors is considered during the design of the capacitive sensors.

3.1.2 Parallel Plate Configuration for Force Sensors

There are many ways that a capacitive sensor can be configured. In Chapter 5 the parallel plate capacitance design is configured, where a force sensor can be constructed by separating the two conductive plates with an insulating material that acts like dielectric and spring. As force is applied on the metal plate, the insulating material is deformed therefore changing the capacitance.
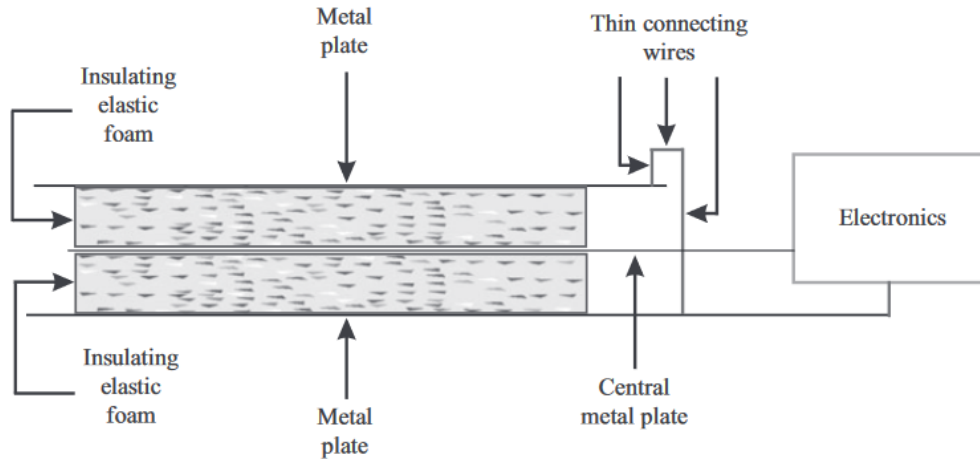
Figure 3.7: Schematic Diagram of a capacitive force sensor (Chappell, 2016) p.203

The capacitive sensor in Figure 3.7 has three conductive plates as opposed to the one in Figure 3.1 which only has two. The extra conductive plate at the top and bottom are electrically connected, which minimises the effects of interference signals (Chappell, 2016)

If an elastic insulating material with no hysteresis is sandwiched between the two metal plates, the applied force and distance between these two can be related by Hooke's Law,

$$F = k \ (d - x_1)$$ *Equation 3-5*

where F is the force applied, k is spring constant, d is the distance between the plates when no force is applied, and x_1 is the distance between the two plates when certain force is applied.

Manipulating Equation 3-1 and Equation 3-5, capacitance can be characterised by force which gives the following equation

$$C = \frac{\epsilon_0 \, \epsilon_r \, A \, k}{k \, x_1 - F}$$

where ϵ_0 is the permittivity of free space, ϵ_r is the relative permittivity or dielectric constant, A is the surface area of the conductive plate, x_1 is the distance between the plates of the thickness of the insulating material at any given time.

From the equation above, capacitance is an inverse function of force applied. Therefore, if variables like A, k, d, ϵ_0 and ϵ_r are known and are set as constants, C and F can then be analysed.

The materials used to construct the force sensor in parallel plate configuration is discussed in Chapter 5.

3.1.3 Understanding the Ground Planes

In Chapter 4.2, two prototypes were created with slight differences. Both prototypes follow the capacitive proximity sensing principle and have the same sensor pattern in the toe cap area. The two prototypes are distinguished as Grounded Heel (GH) and Non-Grounded Heel (NGH). GH shoe sensor prototype (Figure 3.9) has an extra conductive pad on the heel of the knitted sensor and is connected to the ground pin of the electronics circuit. NGH shoe sensor prototype (Figure 3.8), only contains the conductive knitted sensor on the toe area.
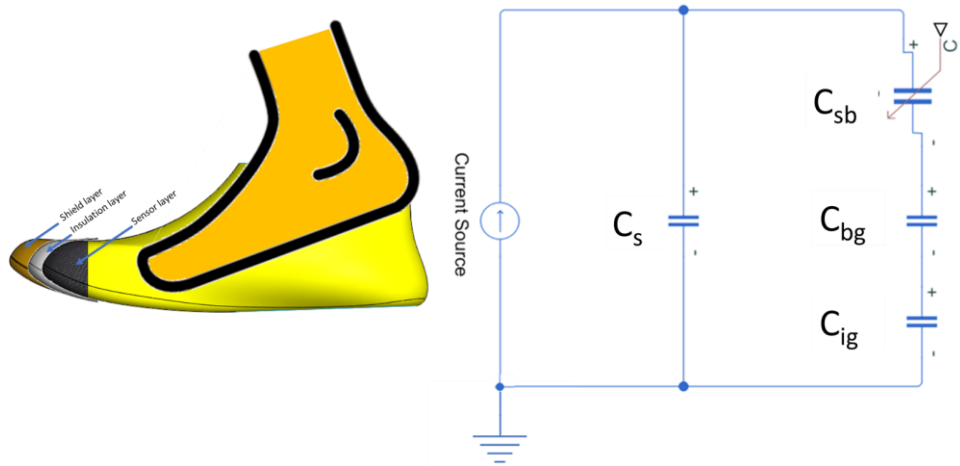
Figure 3.8: (Left) NGH Shoe Prototype layer layout, (Right) Circuit Layout of Sensor Prototype 1
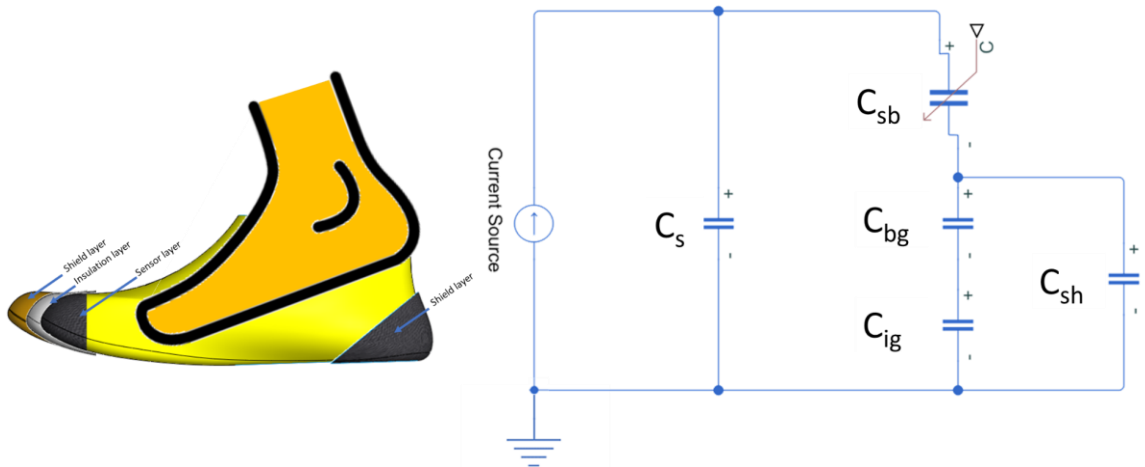
Figure 3.9: (Left) GH Shoe Prototype layer layout (Right) Circuit Layout of Sensor Prototype 2

The capacitive sensing system MPR121 operates by CTMU, whereby voltage changes when there is a change in properties of the electrode. GH and NGH prototypes are use the MPR121 which is driven by a constant current source and has a floating ground as it is not connected to the mains (battery powered). Whenever there is a floating ground, a parasitic capacitance component is present between the system ground and any conductive object from the environment. Parasitic capacitance is denoted as C_{ig} and C_{bg} in Figure 3.8 and Figure 3.9, other parameters and their definitions in both figures are as follows:

- C_{ig} – parasitic capacitance between local instrument ground and earth ground
- C_{bg} – parasitic capacitance component from the human body to the earth ground.
- C_s – capacitance between the sensor plates and instrument ground
- C_{sb} – capacitance between the human body and the sensor
- C_{sh} – capacitance of the extra conductive pad to the earth ground.

Since C_{bg} and C_{ig} are both factors of parasitic capacitance relative to earth ground this can be lumped together as C_t, where;

$$C_t = \frac{C_{ig}C_{bg}}{C_{ig} + C_{bg}}$$

Equation 3-7

The circuit configuration in Figure 3.8 can be simplified as,
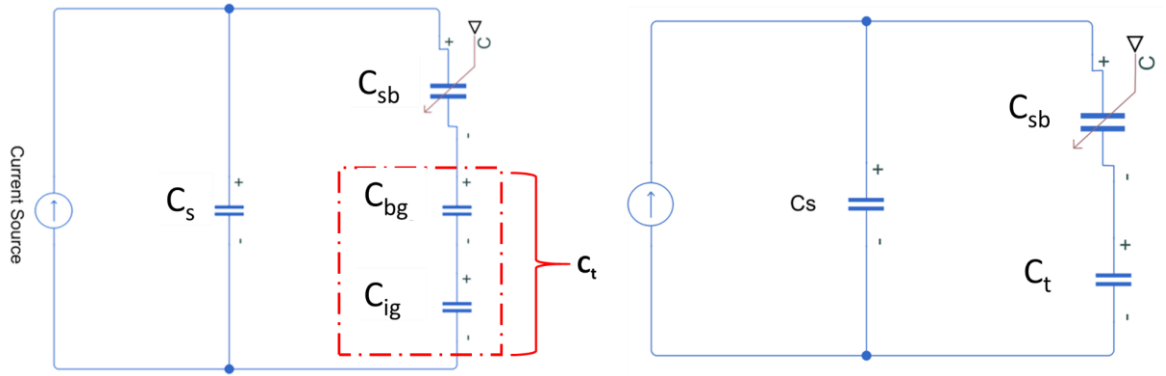
Figure 3.10: (Left) old NGH Configuration (Right) New NGH Configuration

Similarly, circuit configuration in Figure 3.9 can be simplified as;
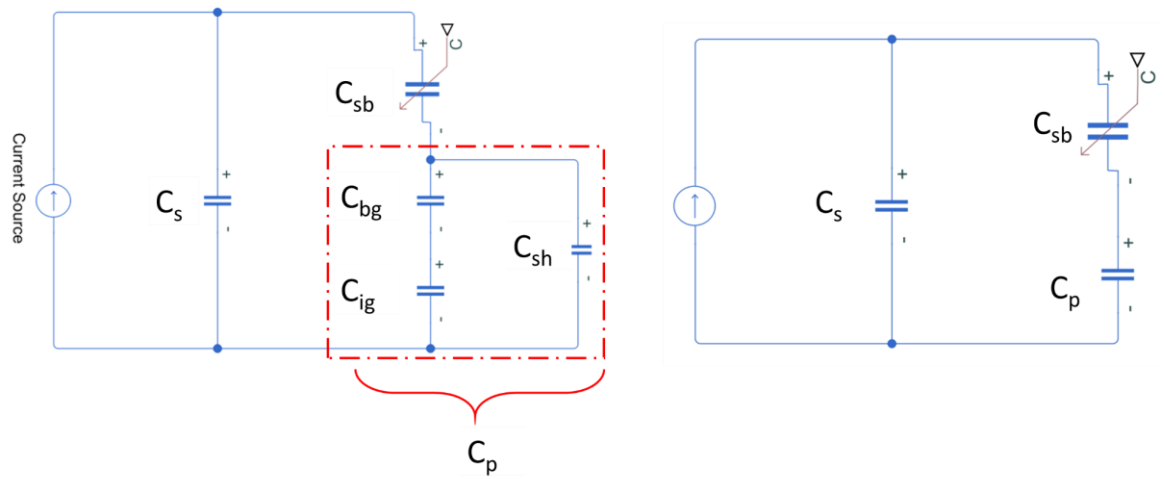
Figure 3.11: (Left) Old GH Circuit Configuration (Right) New GH Circuit Configuration

In Figure 3.11 the parasitic ground and the extra added conductive pad is compounded together as C_p and it is a function of C_t and C_{sh}, where;

$$C_p = C_t + C_{sh}$$

$$C_p = \frac{C_{ig}C_{bg}}{C_{ig} + C_{bg}} + C_{sh}$$

The capacitance equations of GH and NGH shoe sensor prototypes are modelled by the following equations:

$$C_{ngh} = C_s + \frac{C_t C_{sb}}{C_t + C_{sb}}$$

$$C_{gh} = C_s + \frac{C_p C_{sb}}{C_p + C_{sb}}$$

where C_{ngh} is the capacitance of the NGH shoe sensor prototype and C_{gh} is the capacitance of GH show sensor prototype.

In Equation 3-10 and Equation 3-11 we're interested in how the capacitance of the GH and NGH shoe sensor prototypes change relative to human body capacitance C_{sb}, when there is an added influence to the ground referred to as C_p and C_t.

To predict relevant changes to C_{ngh} and C_{gh}, the GH and NGH shoe is physically measured using Agilent E4980A LCR Meter. A scenario is simulated by having a large conductive sheet, which act as the connection of a person to the earth ground. No actual foot is inside the shoe. Capacitance values are measured using an Agilent E4980A LCR Meter using the settings in Table 1.

Table 1: Settings used to measure capacitance in components

Function Settings	Cp-Rp
Frequency	1 kHz
Voltage Level	3.3 V

The meter mode is set at Cp-Rp as we are replicating the configuration in Figure 3.10 and Figure 3.11. Voltage Level is at 3.3 V because that is the capacitive sensing unit operating voltage. From Equation 3-10 and Equation 3-11 there are 2 variables that need to be measured.

- Ct is a mixture of parasitic capacitances between the Earth Ground, instrument and the body. The LCR Meter measured capacitance between the large piece of Copper Taffeta and GND Wire of the electronics unit (Figure 3.12).
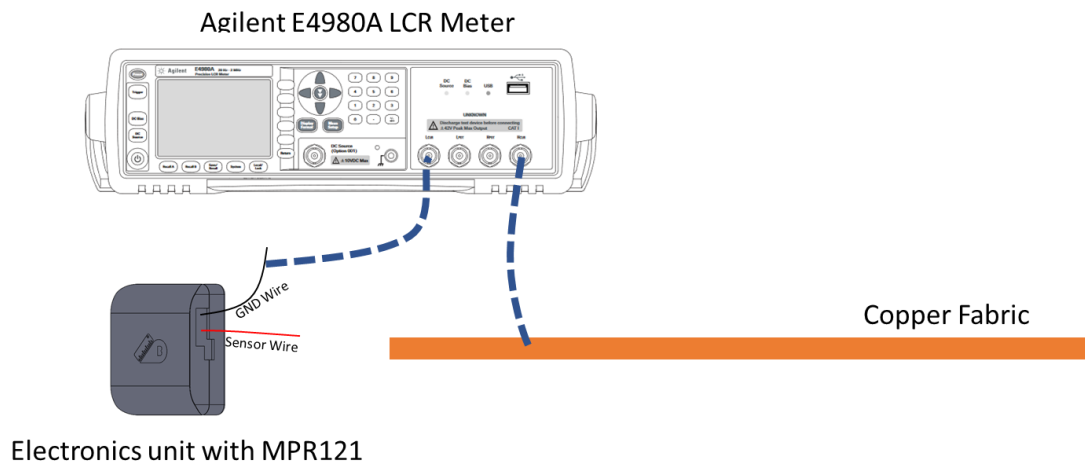
Figure 3.12: Measurement Configuration of C_t

- Csh is the capacitance of the added conductive pad relative to the Earth Ground.
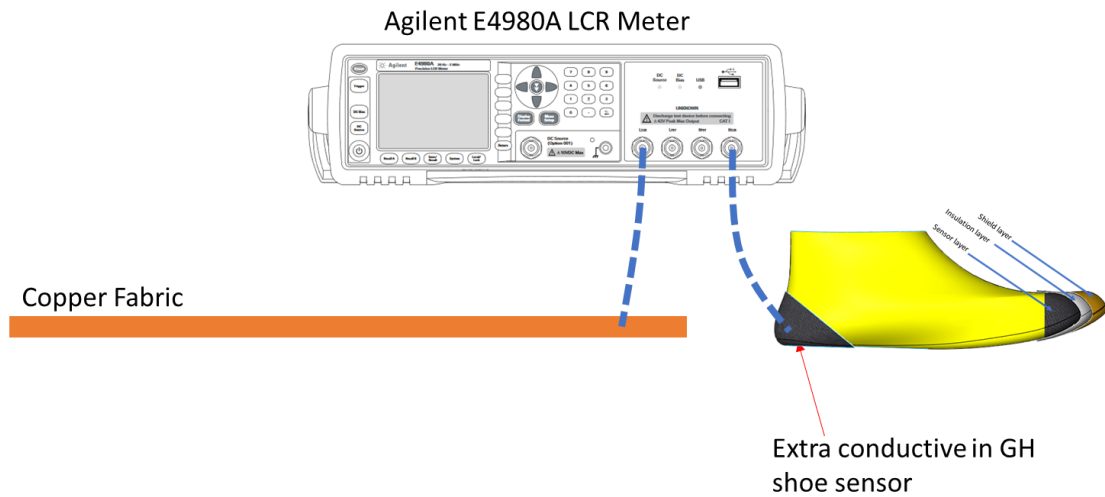
Figure 3.13: Measurement Configuration of C_{sh}

In this simulation, the LCR Meter leads were not directly connected to the Earth Ground on the wall socket. However, this is imitated by using a larger piece of conductive fabric, which serves as both the pseudo body and the Earth Ground as seen in Figure 3.12 and Figure 3.13.

C_{sb} is the human body capacitance, typical human body capacitance varies between 111 pF to 3.90 nF (R.E. Serrano, 2003). The literature provides a broad range due to different people having different charges. Human body capacitance is also affected by the footwear worn, thus creating a large range of capacitance. It can also be affected by the orientation of the human body, a person lying down on a bed with a metal frame is different from a person standing up on the same metal frame bed (Aliau-Bonet & Pallas-Areny, 2013). Even if it is affected by orientation and many other factors, the human body model defined by industrial standards for capacitance is 100 pF capacitor in series with a 1.5 kΩ resistor.(ESD, 2010)

Cs is the capacitance of the sensor, it is calculated using the parallel plate concept in Equation 3-1. The relevant variable that can be measured in this equation is the area (A). To determine A of overlapping plates, the template used to create GH and NGH shoe sensor layer is drawn in Rhino, giving a value of 2259.51 mm^2 (Figure 3.14).

Area of toe cap sensor = 2259.51 mm^2
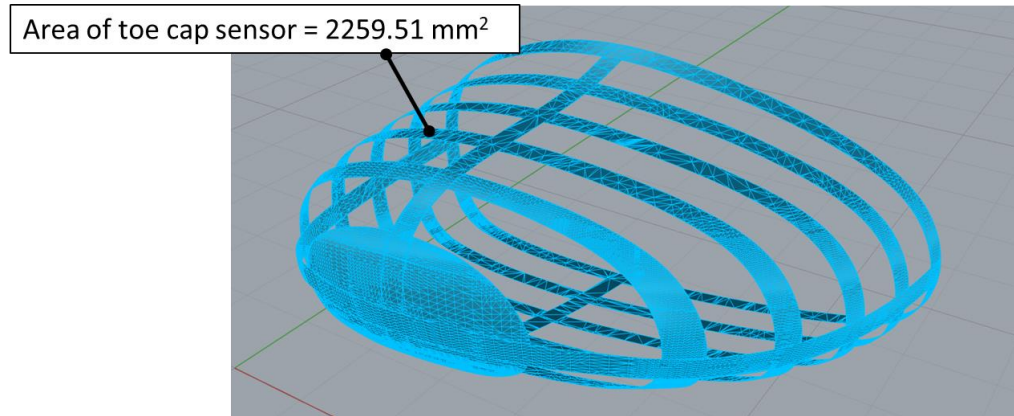
Figure 3.14: Template of Toe cap area of GH and NGH shoe sensor

The shield layer is drawn in Solidworks, this is represented by the toe cap template and has an area of 3868.99 mm^2 (Figure 3.15)

| Area: | 3868.99mm^2 |
| Perimeter: | 274.34mm |
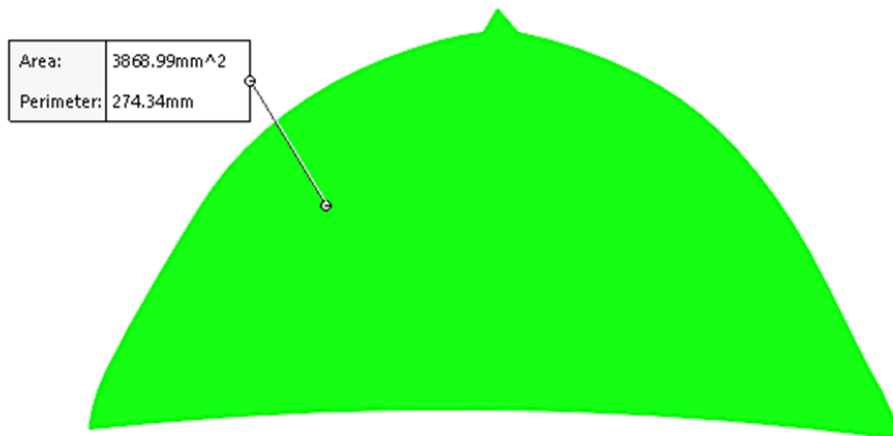
Figure 3.15: Shield layer Area

This areas in Figure 3.14 and Figure 3.15 are close approximations of the plates as this is the base template for the shield layer and the sensor layer, as shown in Figure 3.16.
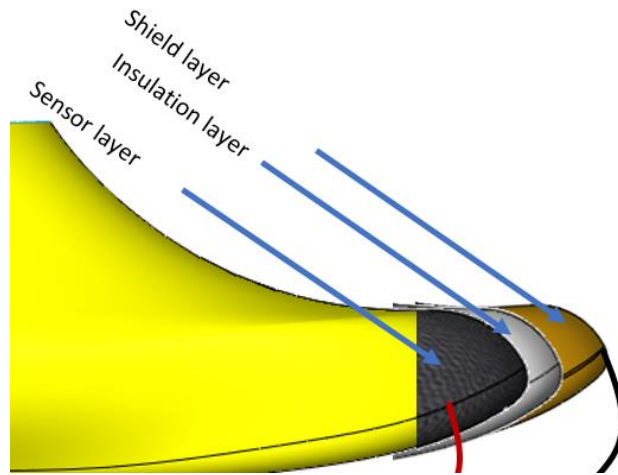
Figure 3.16: Layer layout of the toe are of GH and NGH sensors

Since the areas of the sensor and the shield layer are different, the larger area is taken for the approximate calculation of C_s.

The insulation layer itself is made up of various materials. This insulation layer is mainly the shoe upper, which contains polyurethane, canvas and leather. Dielectric constants, ϵ_r, (relative permittivity) are derived from Material and Processes Database, CES Edupack (Granta Design, 2018). More detailed information can be found in Appendix 1. Most of the insulation material is made of leather for which, its dielectric constant ranges from 2 – 10, an average value is taken as 4.

The spacing (d) between the two plates is determined by measuring the cross section of the shoe upper on the toe cap area. This measured at 4 mm. Table 2 below shows the values used to calculate theoretical C_s value.

Table 2: Values used for C_s calculation

ϵ_0	$8.854 \times 10^{-12} \frac{F}{m}$
ϵ_r	4
A	$3869.99 \; mm^2 \, or \; 3.87 \times 10^{-3} \; m^2$
x_1	$4 \; mm \; or \; 4 \times 10^{-3} m$

Calculating C$_s$ using the variables from Table 2 and substituting them in Equation 3-1;

$$C_s = 8.854 \times 10^{-12} \frac{F}{m} . 4 . \frac{3.87 \times 10^{-3} \; m^2}{4 \times 10^{-3} \; m} = 3.43 \times 10^{-11} \; F$$

Equation 3-12

$$C_s = 34.3 \; pF$$

3.1.3.1 Simulation of Extra Ground Layer.

The values in Table 3 are used to simulate the outputs of the sensor over a range of reported values of human body capacitance values using Equation 3-10 and Equation 3-11.

Capacitance values for C_{sh} and C_t are presented as range as the recorded values using the LCR Meter were fluctuating.

Table 3: Values used for simulating C_{gh}

C_s	$34.3 \times 10^{-12}\ F$
C_{sh}	$1.9 - 2.6 \times 10^{-12} F$
C_{sb}	$100 \times 10^{-12} - 3.9 \times 10^{-9} F$
C_t	$17 - 29.9 \times 10^{-12}\ F$
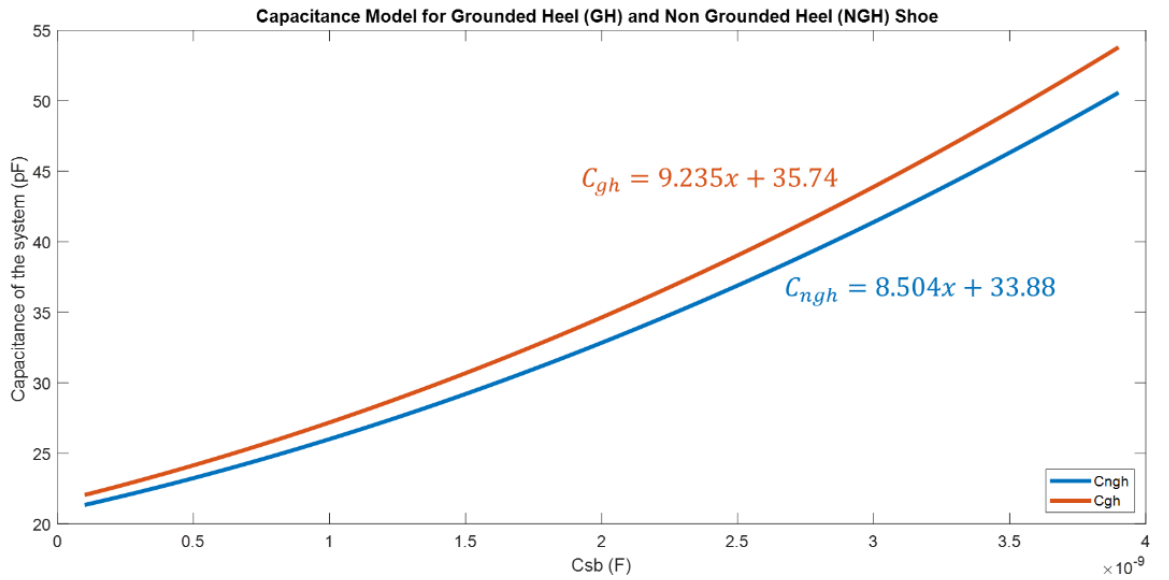
Figure 3.17: Capacitance model of GH and NGH Shoe Sensors

Equation 3-10 and Equation 3-11 are graphed in Figure 3.17, with C_{gh} and C_{ngh} on the y axis and C_{sb} on the x axis. As an approximation, a linear curve is fitted to the data, with

r^2 values of both curves around 0.98 (Cgh = 0.9885; Cngh = 0.9875). Figure 3.17 indicates that GH and NGH capacitance model have differences as these two capacitance models have different slopes as the line for C_{gh} is above C_{ngh}, indicating that the extra conductive pad in the heel affected the capacitance of the system.

Though it is apparent that there are slope changes between the GH and NGH shoe sensors, we are more interested in seeing how much of a difference the extra conductive pad on the heel contributes to sensor sensitivity. This can be observed by taking the partial derivatives of both GH and NGH systems.

$$C_{ngh} = C_s + \frac{C_t C_{sb}}{C_t + C_{sb}}$$

Equation 3-13

$$\frac{dC_{ngh}}{dC_{sb}} = \frac{C_t^2}{(C_t + C_{sb})^2}$$

Equation 3-14

$$C_{gh} = C_s + \frac{C_p C_{sb}}{C_p + C_{sb}}; where \; C_p = C_t + C_{sh}$$

Equation 3-15

$$\frac{dC_{gh}}{dC_{sb}} = \frac{C_p^2}{\left(C_p + C_{sb}\right)^2} = \frac{(C_t + C_{sh})^2}{(C_t + C_{sh} + C_{sb})^2}$$

Equation 3-16

The same capacitance values as in Table 3 are substituted in Equation 3-14 and Equation 3-16 and graphed in Figure 3.19, where the derivative values of GH and NGH are plotted on the y axis, and C_{sb} is are plotted on the x axis. The percentage difference of the derivative between the two derivative values is calculated using Equation 3-17 and plotted in Figure 3.18.

$$Sensitivity \; difference = \frac{dC_{gh} - dC_{ngh}}{dC_{ngh}}$$

Equation 3-17

43
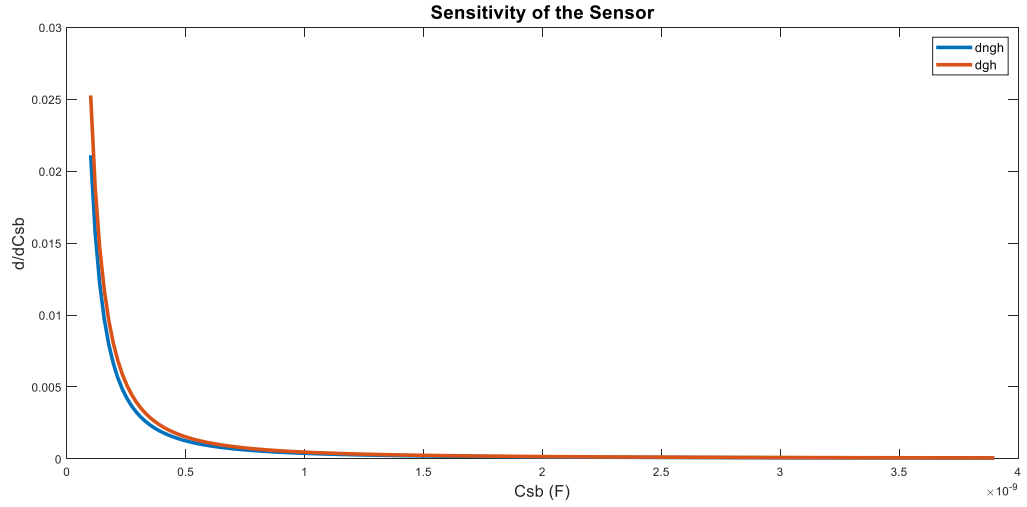
Figure 3.19 Sensitivity of GH and NGH sensor
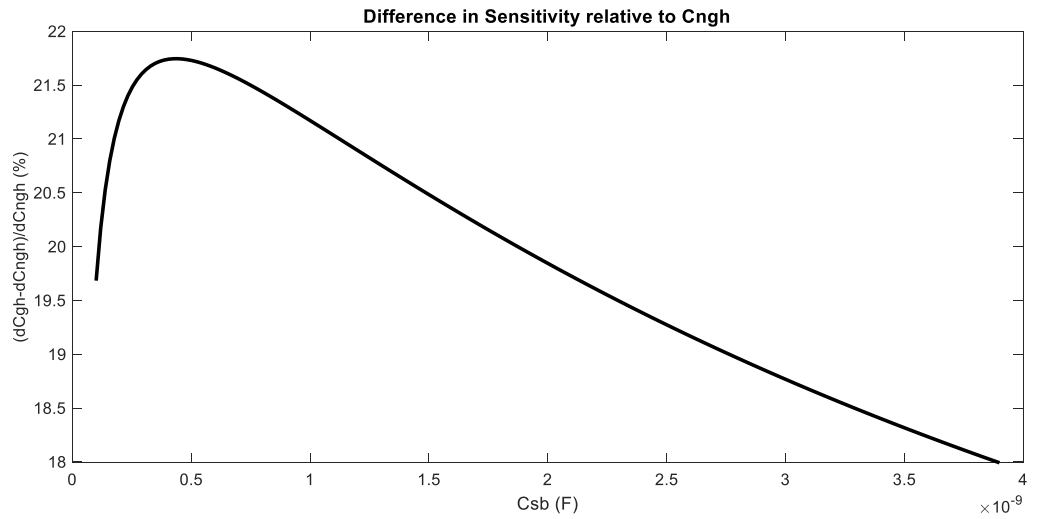
Figure 3.18: Difference in sensitivity relative to C_{ngh}

Figure 3.19 indicates that the larger the body capacitance, the less sensitive the sensor is regardless whether it is the GH or the NGH shoe sensor. This is evident as the graph starts to plateau at 0.5 nF.

Figure 3.18, shows that there is a 19.55% increase in sensitivity by adding the extra conductive pad on the heel, this is indicated by the starting point of the graph when C_{sb} is at 100 pF. The difference in sensitivity changes throughout the given C_{sb} range, where the slope is positive at $C_{sb} < 0.2$ nF, between 0.2 nF $< C_{sb} < 0.61$ nF the gradient is always

changing as it is curved, peaking at $C_{sb} = 0.5$ nF at 21.55%. The slope at $C_{sb} > 0.61$ nF shows a somewhat linear decrease until $C_{sb} = 3.9$ nF.

The differences in the shape of the gradient in Figure 3.18 show a graph of sensitivity range given a human body capacitance. This can be used as a part of an algorithm to better predict a child foot length, given a known body capacitance reading.

Chapter 4 Foot Length Measurement

In this chapter, the development and feasibility of textile sensors to better indicate the foot length of a child while it is still inside the shoe is discussed. There are two prototypes developed to test out its feasibility – Sensor Prototype 1 and Sensor Prototype 2.

Sensor Prototype 1 explains the process of selecting suitable sensing materials, sensing configuration and electrical components. The materials and sensing configuration are evaluated quantitatively and qualitatively.

Sensor Prototype 2 is a design iteration of the previous prototype. It uses the selected materials from Sensor Prototype 1 and refined design configuration. The effectiveness, reliability and feasibility of this prototype is tested and evaluated with children using a wireless electronics module.

Both prototypes follow the proximity capacitive sensing principle. The desired sensing electrodes are made of conductive textiles located at the toe cap of the shoe. These are connected by coaxial cables to the Arduino 101 and MPR121 Capacitive sensing chip. These two make up the embedded electronics unit to enable reading the fabric sensor's output. The output is then passed on to a data logger for further analysis and evaluation. In sensor prototype 1, Arduino 101 is connected to a PC to enable data logging. In sensor prototype 2, Arduino 101 is replaced by a smaller electronics unit Pycom to enable wireless communication from the electronics unit to an Android Mobile phone. A wireless communication is implemented as it created a safer testing environment during evaluation of the prototype with children.

4.1   Sensor Prototype 1

Sensor Prototype 1 explores the selection of materials that can be used for proximity sensing and verification of the selected capacitive sensing chip, MPR121 fore reading the textile sensors.

The proposed concept is to equip the toe cap with conductive textiles to sense elongation of a child's foot over time. It senses elongation using proximity sensing. The capacitance readings from the proximity sensing will be read by a capacitive chip (MPR 121) connected to both knitted conductive textiles and a microprocessor, Arduino 101. The system components are as follows:

Hardware

- Knitted conductive thread at the toe cap as proximity sensor
- Sensor to the electronics using coaxial cables to prevent outside noise from interfering with the sensor signal.

Embedded Electronics

- Electronic components are connected to the knitted conductive threads at the toe cap to acquire capacitance readings
- Off the shelf circuitry

Software

- The embedded electronics is programmed in the Arduino IDE to follow the manufacturer's specification, to enable correct reading of capacitance. The capacitance readings from Arduino 101 and MPR121 are verified by comparing results to a Keysight E4980A LCR Meter.

4.1.1 Objectives

The objectives used to complete Sensor Prototype 1 included qualitative and quantitative analysis. These design requirements are put together so that suitable materials layer layout and electronics can be chosen before creating the next version (Sensor Prototype 2)

The Sensor Prototype 1 design requirements are broken up into two categories: Mechanical Aspects and Electrical/Electronic Components and Software.

Mechanical Aspects include:

- Sensor placement, size and layer layout

- Materials and knitting techniques used for prototypes

Electrical/Electronic Components and Software

- Physical Connections from the knitted conductive textiles sensors and other E-textile Components

- Interfacing of MPR121 (Capacitive Sensing Chip) to Arduino

4.1.2 Methodology

To create sensor prototype 1, available conductive textile materials from AUT Textile and Design Lab were obtained and samples were knitted by the knitting technician at a specific size of the toe cap. The toe cap dimensions were obtained from Bobux design database. Two different fabric sensors were acquired, and these were installed inside two different shoes of the same size. The fabric sensors are connected with a coaxial cable to reduce outside interference/noise in the readings. The sensors were read initially by the Agilent E4980A LCR Meter and again by the Arduino 101 with MPR121 Capacitive sensing chip. Two tests were carried out,

1. Evaluation of conductive textiles to select suitable sensor materials.

   The evaluation was carried out by inserting different sized phantom foot, as this represents different sized foot. The readings were obtained using the LCR Meter and these results were compared and graphed. The criteria for choosing a suitable sensor material is the linearity of the sensor results.

2. Validation of Arduino Code for reading the corresponding capacitance.

   The same test was carried out in Test 1, however, an added step of using the Arduino and MPR121 setup is connected to the sensor prototypes. The criteria for ensuring that Arduino is reading correctly is that the graphed results exhibit the same behaviour as the LCR Meter Results.

4.1.3 Design Layout (Hardware and Software)

Sensor Prototype 1 is described in 3 aspects:

Sensors – This includes the overall materials and connections used to create the textile sensors.

Electronics Unit and Software – This includes how Arduino 101 and MPR121 are used and coded to create a standalone capacitive sensing system.

Data Acquisition and Visualisation – Arduino 101 is connected to a PC and data is logged through Arduino's built in Serial Monitor.
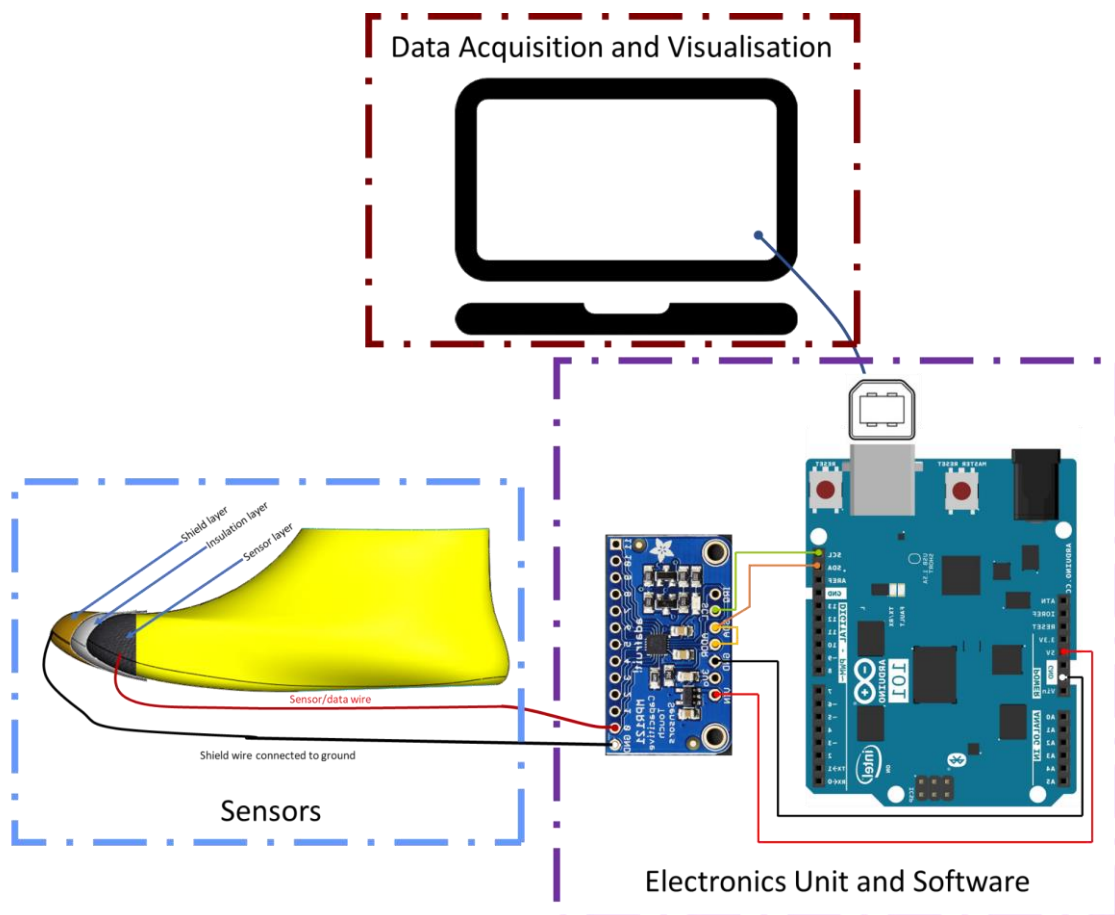
Figure 4.1: System Layout

4.1.3.1 Sensor placement, size and layer layout

Normally, foot length is measured outside the shoes. The proper use of the typical foot measuring devices stated in Section 2.3 is that the heel of the child needs to coincide with the curved part of the device, a horizontal bar is moved until it touches the longest part of the toe. The number that this bar stops at indicates the size of the child's foot.

Ideally, the heel sits at the heel counter. This is designed so that it can hold the heel in position giving more stability during variable movements, together with the whole shoe upper, which firmly holds the foot inside the shoe (Asics, 2017).

This creates the basis of where to place the sensors. The heel is not going to experience much change because the heel would always stay in the heel counter. Therefore, the toe area is an ideal place to put the sensors, as this would see the most change in length. This area is also ideal as layers can be easily fitted and concealed. In shoe manufacturing, a polyester material is sandwiched between the inner layer of the shoe and the protective outer layer of the shoe Figure 4.2. This polyester material (called a toe puff) hardens the toe area which keeps the shoe in shape and adds more protection from scuffing during child's play.
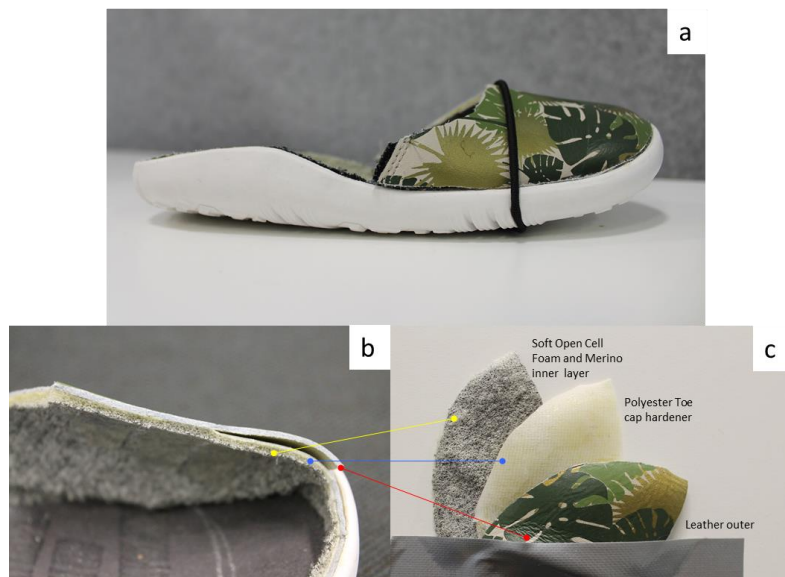
Figure 4.2: a) Example of Bobux Shoe with midsole removed, b and c) Upper of the toe area showing the cross section and layers of the shoe

51

As the sensing technology is based on proximity sensing, there needs to be a conductive area that would serve as the electrode/sensing area. This is achieved by using knitted conductive threads placed in the toe cap area of an existing Bobux shoe.

The sensor shape is based on the toe cap template provided by Bobux shown in Figure 4.3. The print area indicates the sizing limit of the sensor shape.
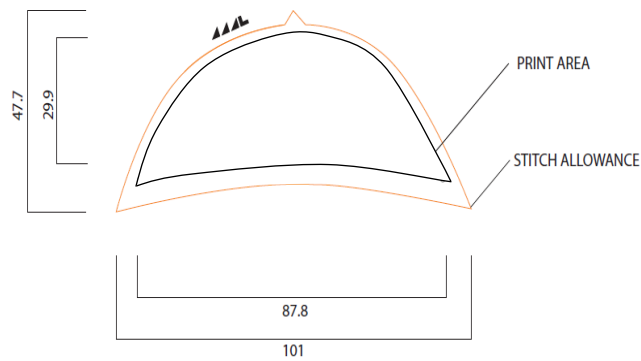
Figure 4.3: Toe Cap Template of a Bobux Shoe

Apart from the sensor, there must also be an insulation layer, to support the sensor in place and a shield layer to protect the sensor from false touches that can happen outside the shoe. This is an unwanted signal that comes from an external influence, not the shoe wearer. Detection of the foot should only happen from the inside of the foot. The shield layer is another conductive fabric which helps decrease the interference from the outside of the shoe. The sensor, insulation and the shield make up the 3 layers of the toe cap area of the shoe.

The textile sensor transmits data to the electronics unit using the black and red wires shown in Figure 4.4. The black wire is connected between the shield and the Ground (GND) Pin of the electronics unit, the red wire is connected between the sensor and the signal pin of the electronics unit.
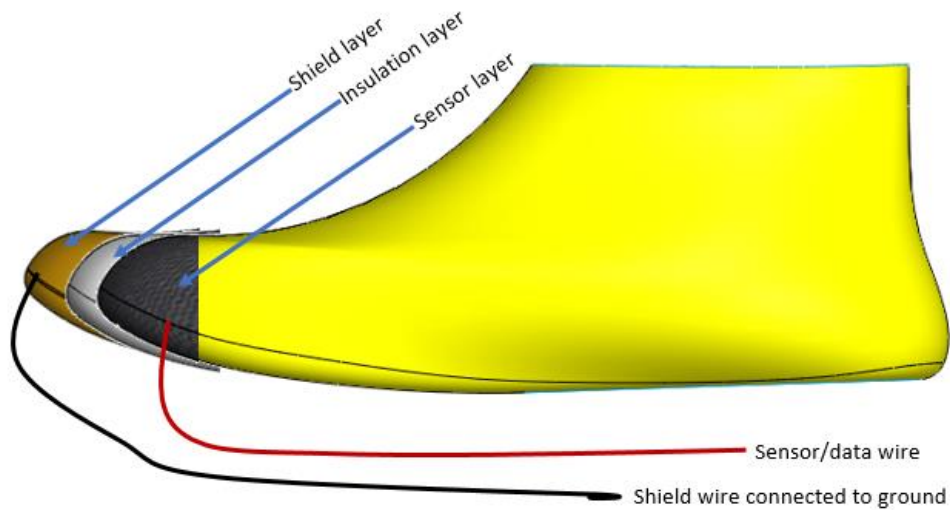
Figure 4.4: Sensor Layer and Wire Layout

Additionally, the red wire (sensor/data wire) needs to also be shielded so as not to transmit false touches. This is achieved by using coaxial cable, where the very inside wire of the coaxial cable is connected to the sensor layer, and the very outside loose braided copper wires are connected to the shield layer. This is discussed more in a later section of this chapter.

Sensor Materials

There were two conductive threads available in AUT Textile and Design Lab with different conductivities, as shown in Figure 4.5:

a) Silver Thread - 2/117 dtex 99% Silver Plated Nylon

   Linear Resistance – 3 kΩ/m (Statex Productions & Vertriebs GMBH, 2010)

b) Stainless Steel Thread – 2/50 Nm, 80% Polyester and 20% Stainless Steel

   Linear Resistance – 530 kΩ/m (Ehrmann, Heimlich, Brucken, Weber, & Haug, 2014)
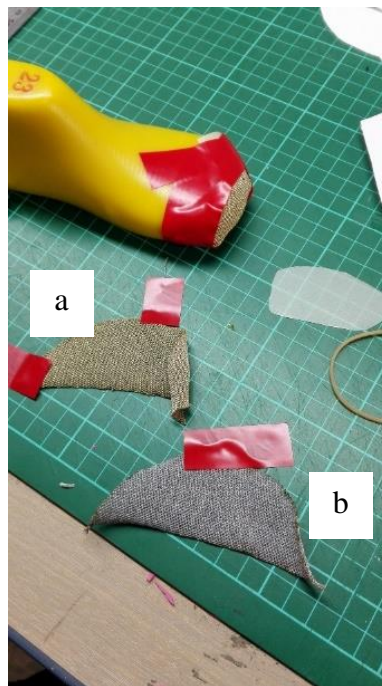
Figure 4.5: Samples cut to shape using toe cap template with a) 99% Silver Thread Sample, b) 80/20% Polyester/Stainless Steel Sample

Both threads were plain knitted as a sheet with ribbed edges using a SIG 123 SV 14 Gauge Knitting machine. The sheets were laser cut with the toe cap template. This is to prevent fraying around the sensor edges. The laser cut sensors were shaped around the toe cap

area of the shoe last using a masking tape. This is done so that the knit would create a solid shape making it easy to attach inside the shoe (Figure 4.6).
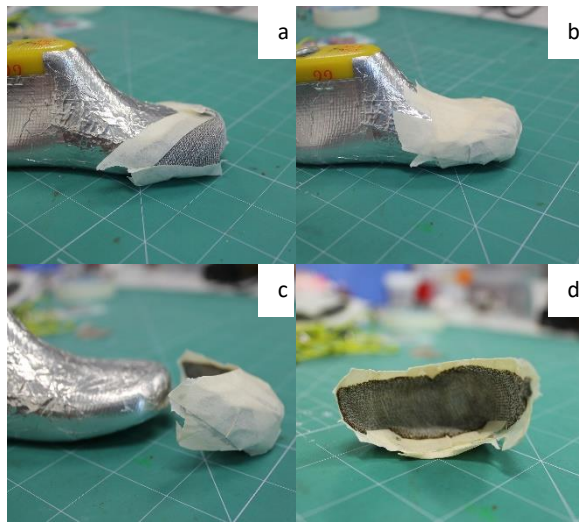
Figure 4.6: Example of the Fabric Sensors are installed using 80/20 PES/SS Sample. a, b, c) Low Tack Masking Tape is used to shape the Fabric Sensor insulating the other layer. d)Completed Sensor to go inside the Toe area of the shoe.

Shielding Material

The material chosen as a shield layer is copper taffeta. This is chosen due to its consistent shielding properties over a large range of frequency (60 – 70 dB between 10-3000 MHz). Additionally, this can be easily adhered to another material with the use of conventional tape adhesives. This can also be laminated with another material which makes it suitable to be layered with other materials.

Figure 4.7: Copper Taffeta (LessEMF)

Copper Taffeta is a desirable material as it does not show a stretch characteristic, present in other conductive fabrics. If the shielding material is flexible and stretchy, there is a high chance that electromechanical properties of the copper taffeta itself could change, which would make it difficult to observe changes to the sensor.

Final Material Layers used for Material Evaluation

Figure 4.8 shows the different layers of sensor, insulation and shielding components of sensor prototype 1. Sensor components shown include stainless steel and silver knitted sensors. These two materials were evaluated for their effectiveness and results presented later in this chapter. Insulation components are the layers of the shoe which includes (top to bottom) sock liner, toe hardener/toe puff and synthetic leather. The shielding component shown is the copper taffeta. The sensor and shielding components are separated by the insulation components.
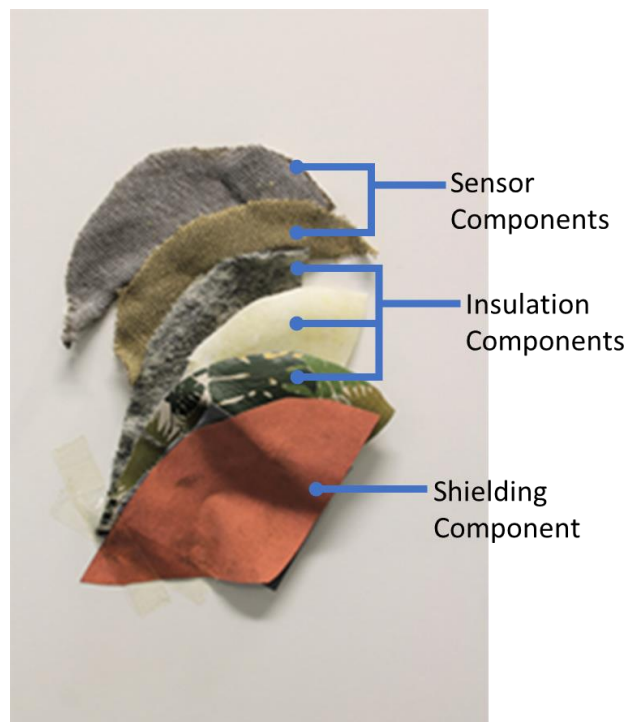
Figure 4.8: Different Layers of sensor prototype 1, showing sensor, insulation and shielding components

4.1.3.3   Connections from the Knitted Conductive Textile Sensors

The aim for this project was to implement an all textile design for the shoe sensors and board connections. E-textile connectors remain an open research field due to diverse application where each solution is unique and needs customization. (Goncalves, da Silva, Gomes, & Simoes, 2018) These connections allow the components to be electromechanically connected. E-textile components need special types of textile threads to ensure robust textile to board connections. The connections also needed to separate the main sense wire to the ground wire. This ensures that no short circuit is going to happen and gets rid of false touch readings

Sensor prototype 1 uses a conventional braided shielded copper wires. This type of wire contains a conductive innermost core, usually copper insulated with PVC. This is surrounded by another set of copper wires braided around it, used for shielding (Figure 3.9). The innermost wire is shielded so that less software filtering is required to isolate the data needing to be read. This gets rid of the interference that can occur when installed inside the shoes. This interference can occur when skin from other parts of the foot touches the wire such as when child inserts their foot inside the shoe. This sliding motion along the wire can cause unwanted readings.

Figure 4.9: Shielded Cable with outside layer stripped (RS Electronics)
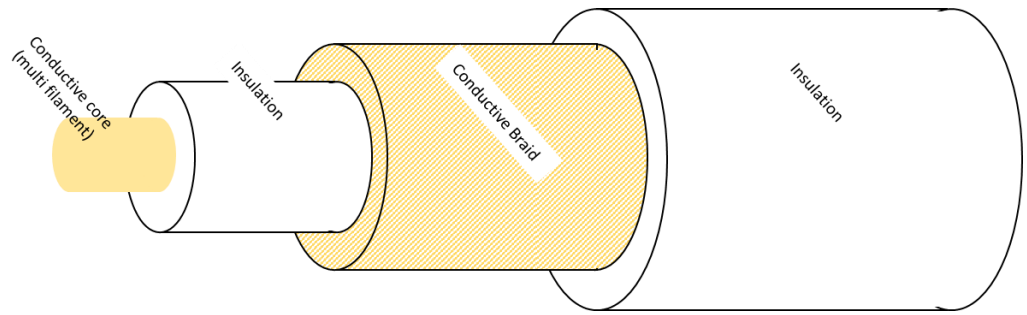
Figure 4.10: Layer Layout of the Shielded Cable

When this wire is installed, both insulations (inner and outer) are stripped, exposing the copper so that it can create contact with the other conductive parts of the sensor.

Pure stainless steel conductive thread is used to connect the inner most wire of the cable to the knitted sensor. Similarly, stainless steel conductive wire is also used and sewn on to connect the outermost part of the cable (conductive braid) to the copper taffeta (Figure 3.12). Pure stainless steel conductive thread is used as it provided a stronger mechanical strength during sewing compared to silver thread with nylon core.
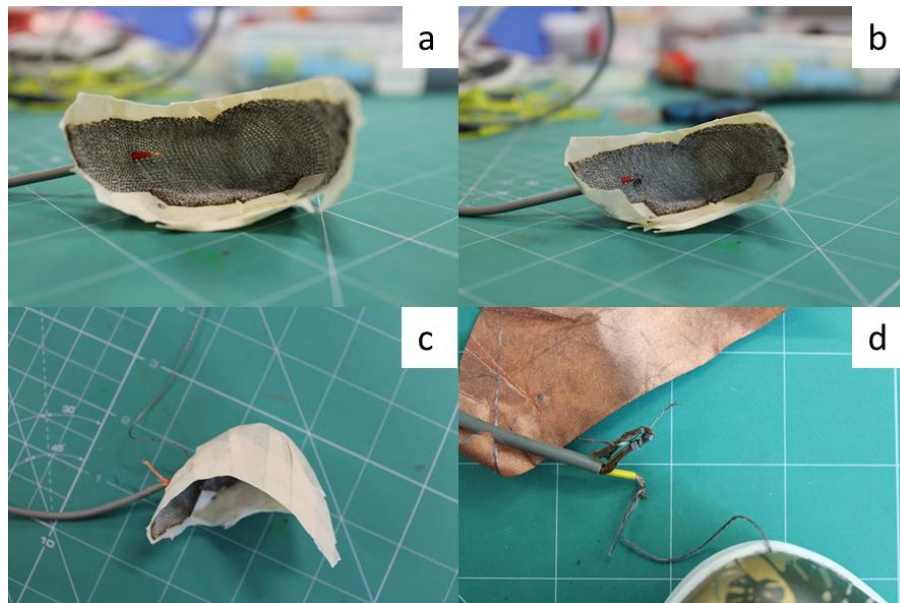
Figure 4.11: a) Inner Layer of shielded cable inserted between the knitted sensor. b) Stripped wire is sewn on to the knitted sensor using Pure Stainless Steel Thread c) Overview of the sensor with outer layer of shielded cable isolated. d) Pure Stainless steel thread is wrapped around the conductive braid of coaxial cable; same thread is sewn through the copper taffeta shielding.

4.1.3.4 Electrical/Electronic Components and Software

The electrical/electronic components will read the capacitance signals from the textile sensor and connections. There are 2 components used for the capacitance reading and for acquisition of data from the sensor to the PC

- MPR121

- Arduino 101
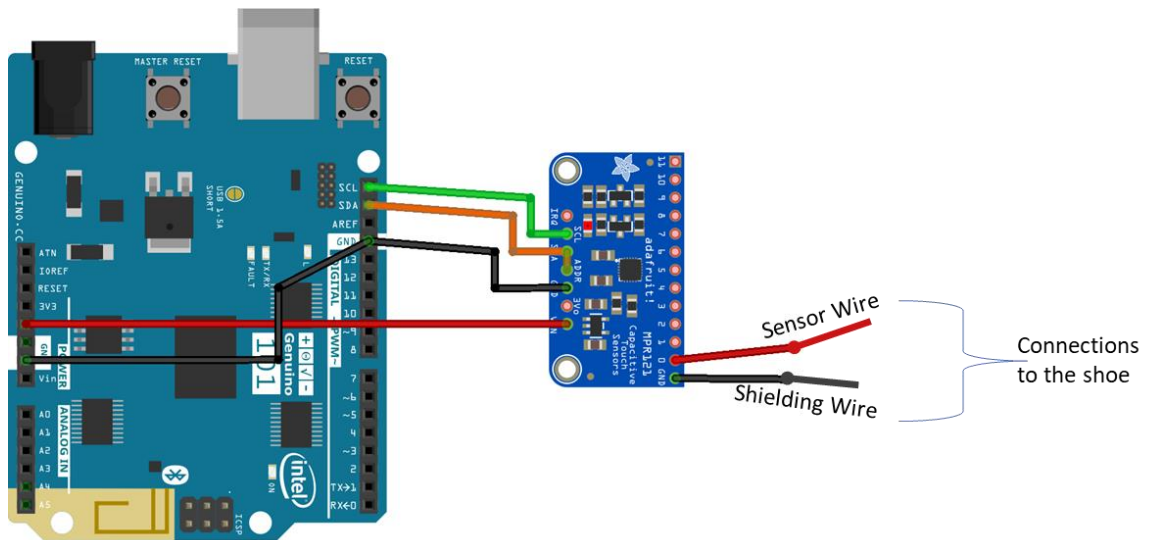
Figure 4.12: Connections between Arduino 101 and Adafruit MPR121
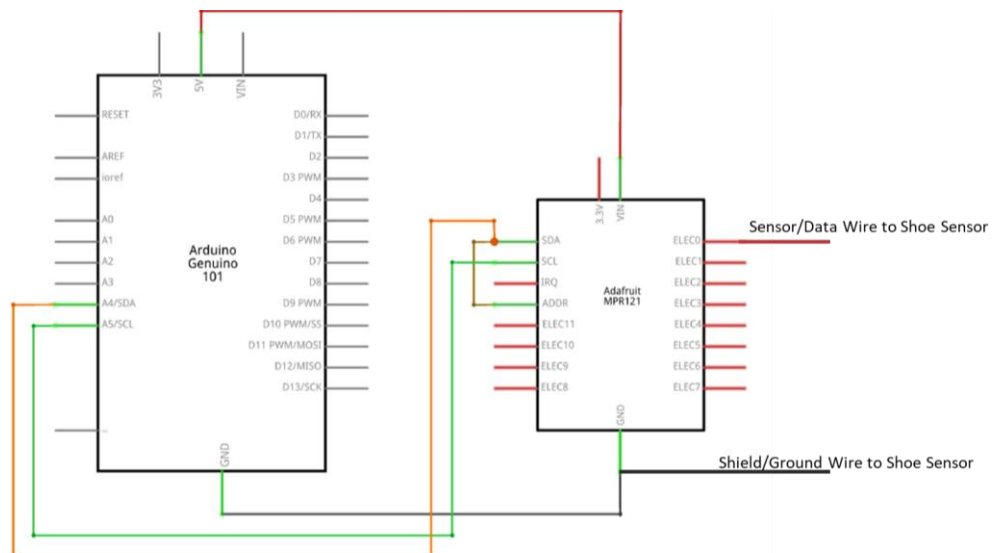
Figure 4.13: Electrical Schematic of Arduino 101 and MPR121

4.1.3.4.1 MPR121

The breakout board from Adafruit Industries includes an NXP semiconductor capacitive sensing chip called MPR121. This can have up to 12 electrode inputs. One input electrode is used in Chapter 4 : Foot Length Measurement, and eight input electrodes for the Chapter 5 : Foot Pressure Measurement. This board is chosen due to its small form factor and capacitive sensing range from 10 pF to 2000 pF with a resolution of up to 0.01 pF. This range is desirable due to the unknowns of the capacitance of the fabric sensors.
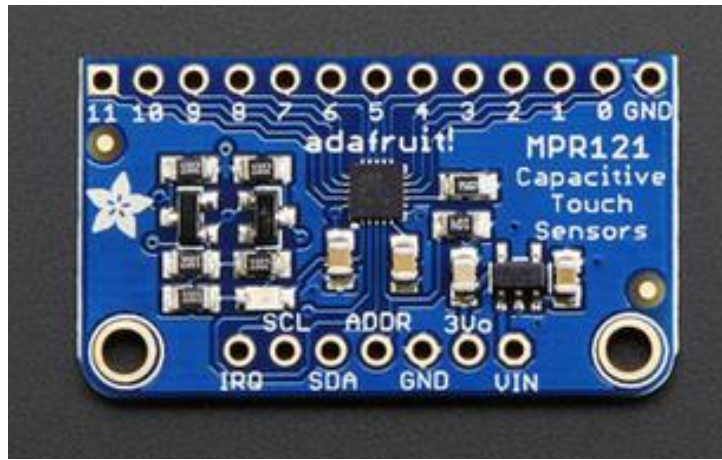
Figure 4.14: MPR121 Breakout Board (Adafruit, 2017)

This capacitive sensing module uses a CTMU to determine capacitance changes. This involves measurement of voltage, as the system assigns a known current on the sensor. The circuit then examines the shift in the voltage while constant current is being applied over a specified amount of time. Equation 4-3 shows how capacitance can be measured while voltage is changing.

$$I = C \frac{dV}{dt}$$

Equation 4-1

$$\Delta I = C \frac{\Delta V}{\Delta t}$$

Equation 4-2

$$C = \frac{I \times t}{V}$$

Current (I) is held constant for a fixed amount of time (t), therefore as these two are known and voltage (V) can be measured, Capacitance (C) can be calculated.

MPR121 can be set up as a touch and proximity sensor. In this case, it is set up as a proximity sensor. This microcontroller built in to Adafruit board is already wired so that it can step down higher voltages for up to 5V, as it only needs 3.3 V. MPR121 is also an I^2C Compliant device, it has a configurable I^2C address that can be used to change register values to programme the microcontroller as wanted.

4.1.3.4.2   Arduino 101

MPR121 is interfaced with an Arduino 101 Module, this allows communication and programming in Arduino IDE without having to change the source code. Communication is via I^{2}C, and the information from the sensing module is accessed through registers via serial data.

Figure 4.15: Arduino 101 Board (Arduino, n.d.)

4.1.3.4.3 Code Implementation[2]

For MPR121 to communicate and read the correct capacitance values an algorithm is followed as recommended by the MPR121 Data sheet. Open source code and libraries that are readily available online were used with alterations to fit this project's purpose.

---

[2] The same code is implemented for both Chapter 3 and 4.

A pseudocode is described below detailing the functions used in the programme.
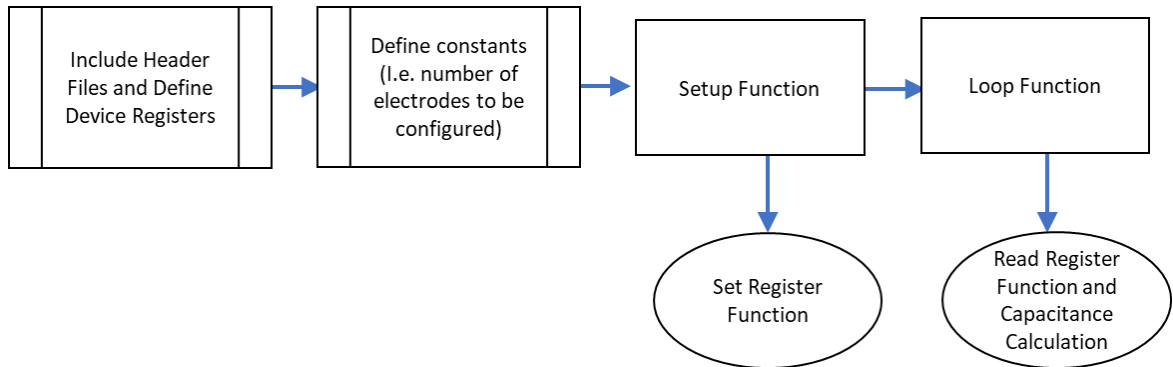
Figure 4.16: Pseudocode of the Arduino Algorithm

Include Header Files and Define Device Registers

As MPR121 is an external sensing chip, libraries and header files *(i.e. #include "Adafruit_MPR121.h")* is included so that variables inside this file can be easily accessed. After introducing the header files, the device addresses must be defined so that Arduino knows which information to access. Depending on where the ADDR pin on MPR121 is connected to, there is a different value for the address. In this case, ADDR is connected to SDA therefore the device address is 0x5C. There would be two device addresses if there are two MPR121 interfaced with the Arduino.

Define Constant, Reading and Configuration Registers

Once device is addressed and found, configuration registers are defined so that their values can be changed in the setup functions. There are corresponding values for these configuration registers and only some registers are selected as not all the electrodes are being used. For example, the electrodes need to be accessed to tell device that we only want one electrode to work. Accessing device address 0x5E according to MPR121 Datasheet (Freescale Semiconductor, 2013) gives access to setting up which electrode needs to be configured. (i.e. *#define ELEC_CFG 0x5E*). Some registers are not

64

configured. However, they are introduced here as they will be read later, in the loop function. These registers change based upon the changes made on the configuration register. The registers that need to be read are *ELEC_Current* - for reading the electrode's current, *ELEC_Time* – this is the register for electrode's charge time, and ADC Registers, *ADCLSB* and *ADCMSB* – these are for reading the electrode's voltage.

Setup Function

In the setup function, the baud rate is defined to know how fast the microcontroller samples and how often it gets information from the serial port. It is set to read at the fastest rate at 115200 baud. The introduced configuration registers are changed to its corresponding values to do what it needs. However, there is a certain order as to how this needs to be changed.

To set these registers to their new value, the device itself must be soft reset (*SOFTRESET*). This resets the registers into their default values. After this, the MPR121 is at stop mode (*ELEC_CFG* bit assignment is 0b10000000), so that remaining registers such as Auto Configuration Registers (*AUTOCONFIG0)* and Voltage Operation Limits (*UPLIMIT, LOLIMIT, TARGETLIMIT)* may be changed. Once registers are set, the MPR121 is changed to run mode so that these settings can be applied and used. To enable run mode, the electrode configuration register bit assignment changes to enable electrode detection and proximity sensing at electrode 0. The code detailing these changes is included in the Appendix 2.

The other variables that need to be determined are the Voltage Operation Limits, which are dependent on the Voltage Supplied and Auto Configuration Control.

Voltage Operation Limits are defined by the Voltage Supplied (V_s), in this case it is at 3.0V. Although the MPR121 is connected to 5V supply in Arduino 101, there is a built-in step-down voltage regulator in the Adafruit Breakout board. There are three registers that depend on V_s, Upper (*UPLIMIT*), Target (*TARGETLIMIT*) and Lower Limits (*LOLIMIT*). The values for these three registers are laid out below.

$$V_s = 3.0V$$

Upper Limit

$$UPLIMIT = \frac{V_s - 0.7}{V_s} \times 256$$

$$\therefore = \frac{3.0 - 0.7}{3.0} \times 256 = 196.27 \approx 196 \; or \; 0 \times C4 \; (hex)$$

Target Limit

$$TARGETLIMIT = \frac{V_s - 0.7}{V_s} \times 256 \times 0.9$$

$$\therefore = \frac{3.0 - 0.7}{3.0} \times 256 \times 0.9 = 176.64 \approx 177 \; or \; 0 \times B1 \; (hex)$$

Lower Limit

$$LOLIMIT = \frac{V_s - 0.7}{V_s} \times 256 \times 0.65$$

$$\therefore = \frac{3.0 - 0.7}{3.0} \times 256 \times 0.65 = 127.57 \approx 128 \; or \; 0 \times 80 \; (hex)$$

These Voltage Operation Limits are used inside the program to limit the region of where the voltage used is going to be.

The device runs optimally when it is set on Auto Configure (*AUTOCONFIG0)* as it can adjust capacitance readings whenever there is an environmental change. This register is set up based on the data sheet's recommendation. This register also determines how many samples the device, MPR121 needs per second, determining the sample rate, useful for timing the device.

Loop Function

In this function, certain registers are read to enable calculation of capacitance. As mentioned earlier, MPR121 operates using CTMU, which means that it needs current, voltage and time to calculate capacitance. These can be read from reading registers defined earlier (*ELEC_Current*, *ELEC_Time, ADCMSB and ADCLSB).*

The current register can be read as is and does not need any other conversions. The time register contains two values, each are correspondent of charge time for that electrode. The electrode used for sensor prototype 1 is Electrode 0, the time for this register is accessed on *ELEC_Time* register, however, this contains time values for electrodes 0 and 1.

According to the register map, Figure 4.17, to acquire the charge time for electrode 0, the bits are manipulated so that correct time is selected for the correct electrode.

ELE0, ELE1 Charge Time		CDT1		CDT0	0x6C	0x00
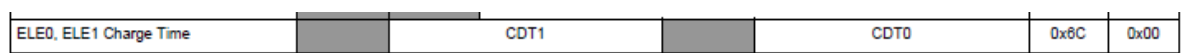
Figure 4.17: Electrode Register Map (Freescale Semiconductor, 2013)

This value is stored in another variable called *Timebyte_v*. This is also an integer value, therefore a calculation needs to occur to acquire the correct charge time converted in microseconds, as per datasheet,

$$chargetime = 0.5\,(2^{n-1})\,\mu s$$

$$where\ n = Timebyte\_v$$

The voltage is read from *ADCMSB* and *ADCLSB*. There are two registers that need to be read as each register can only hold 8 bits. 10 bits is needed to read the correct voltage reading. *ADCLSB* contains the full 8 bits and is joined together with *ADCMSB* which only contain 2 bits; when combined it equates to 10 bits, which is then stored in another variable inside the loop function called *ADCValue*. This variable call for the real voltage value sensed by the circuit.

All these are used to calculate the capacitance, as per the equation

$$C = \frac{IT}{V} = \frac{ELEC_{Current} \times chargetime}{V_s \times ADCValue/1024}$$

4.1.4 Sensor Material Evaluation and Code Verification Testing

As mentioned in Section 4.1.3, there are two different knit samples, each assembled in a shoe with the same shoe composition (Figure 4.2).

This is done to evaluate the following:

1. Whether the capacitance reading truly increases when the toe area gets closer to the sensor, which is laid out in a non-planar pattern.

2. If the programmed capacitive sensing circuit reads a similar output as the LCR Meter, which is a more reliable source of measuring readings.

3. Which of the two materials, Silver Knitted Threads or Stainless Steel Threads, are a better option in sensing proximity.
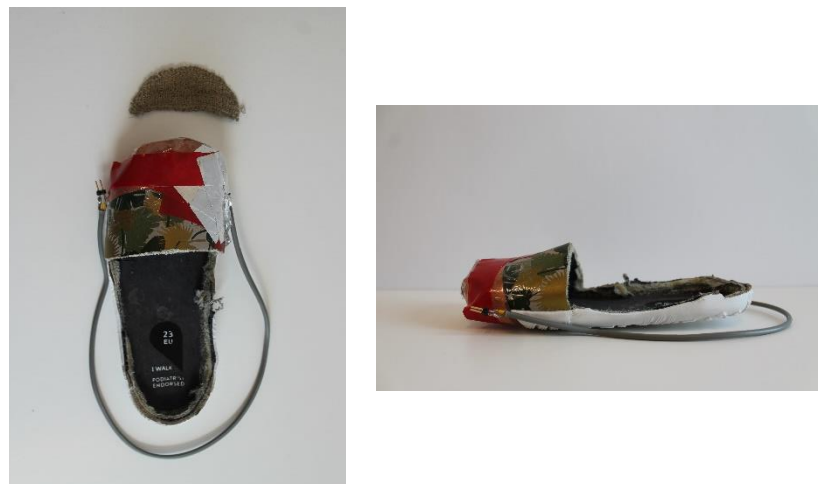
Figure 4.18: Example of completed shoe with textile sensor inside Bobux Shoe

To test whether capacitance truly increases when the toe gets closer to the sensor, 3D Printed shoe lasts were covered in aluminium conductive tape. This is to replicate the conductive characteristic of the human foot and, this will be referred to as the foot phantom for the following section of this thesis.

Although aluminium may not have the same conductivity and electrical behaviour as the human foot, these were sufficient to undertake the tests carried out for the sensor prototype 1. These lasts are of varied sizes, the range used is between size 20 – 23 with equivalent lengths between 13.5 cm (Size 20) – 15.5 cm (Size 23).

Figure 4.19: Foot Phantom, showing different sizes (Left to right showing sizes 20-23)

Figure 4.20: Test Setup

To compare whether the Arduino is programmed correctly, the textile sensors inside the shoes were connected to both Agilent E4980A LCR Meter and Arduino and the readings were observed using the Arduino Serial Data Window and recorded.

Finally, the results recorded from both materials were then evaluated. A criterion used to select a material is that, the capacitance should increase linearly as the foot approaches the textile sensor.

4.1.5   Sensor Prototype 1 Results and Discussion

Table 4: Capacitance Readings from both knitted textile sensors. Readings derived from LCR Meter and Arduino

| Shoe last inserted | Distance of toe last to the fabric sensor (cm) | Capacitance Readings (pF) | | | |
| | | Silver Samples | | Stainless Steel Samples | |
		Arduino	LCR Meter	Arduino	LCR Meter
No last	6	53.19	99.92	26.3	37
Size 23	2	54	101.26	29	39
Size 22	1.5	77	107.45	35.5	40
Size 21	1	75.5	105.4	42.5	42
Size 20	0	80.5	108	76	48
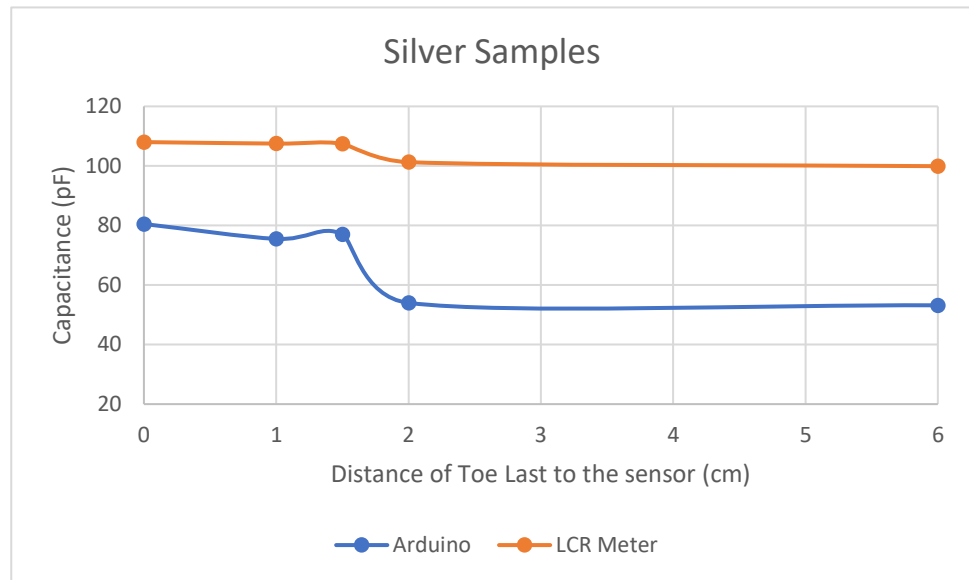
Figure 4.21: Silver Sample Capacitance Readings comparison between Arduino and LCR Meter
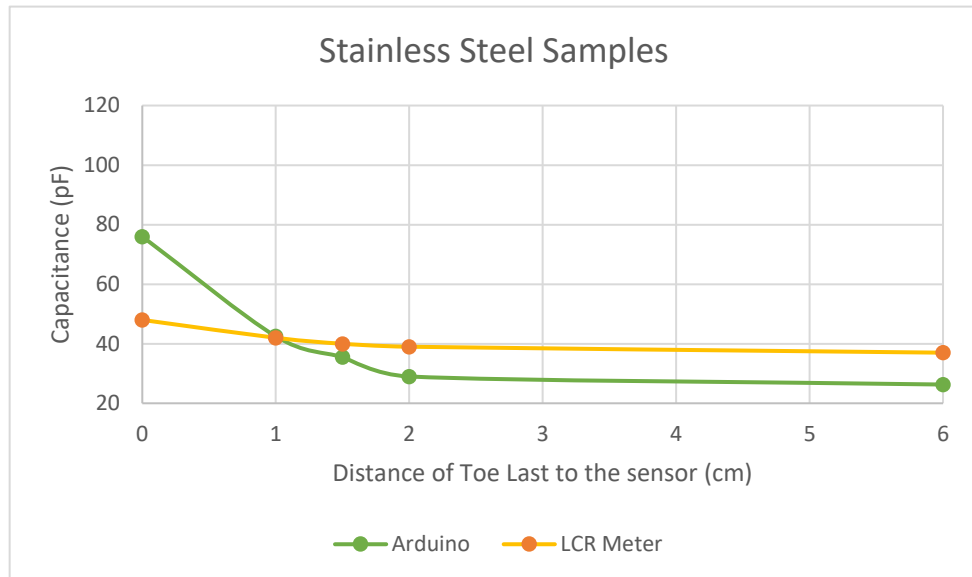
Figure 4.22 80/20 Polyester/Stainless Steel Sample Capacitance Readings comparison between Arduino and LCR Meter

4.1.5.1 *Measurement System Evaluation and Discussion*

Tests were performed to see whether the programmed MPR121 interfaced in Arduino 101 reads a similar output as the LCR Meter (Keysight Technologies, Agilent E4980A), which is a more reliable source of measuring capacitance. Figure 4.21 compares the capacitance readings of Silver Samples, and Figure 4.22 compares the capacitance readings of Stainless Steel Samples.

Both samples in Figure 4.21 behaved the same regardless of which measuring system was used, as the Arduino readings followed the same pattern as the LCR Meter. Although the scaling between the two readings are different because the readings do not have the same starting point and a large offset between the two readings. There is also an irregularity, where the reading of Arduino at 1.5 cm is higher compared to the readings at 1 cm.

Both samples in Figure 4.22 also behaved similarly regardless of the measuring system. As the phantom foot approached closer to the sensor, the capacitance increased. The trend for both Arduino and LCR Meter are similar, however between the 2 cm and 1 cm mark, they have two different slopes. Arduino detected a much larger change on the last centimetre compared to the LCR Meter. Resulting to a much steeper gradient and dramatic change as the foot came much closer to the sensor.

Although the readings from the Arduino are not exactly the same as the LCR Meter, both measurements followed the same trend/pattern. This is a good indication that the Arduino interfaced with MPR121 is good enough to measure the capacitance changes.

From the results in Table 4, Figure 4.21 and Figure 4.22, as the foot phantom comes closer to the fabric sensor, the capacitance increases. This is regardless of what material it is made of and the equipment it is being measured in. All the knitted sensors can sense up

until 2 cm distance away from it, as the graph starts to change its slope when the last reaches this part.

4.1.5.2 Material Evaluation
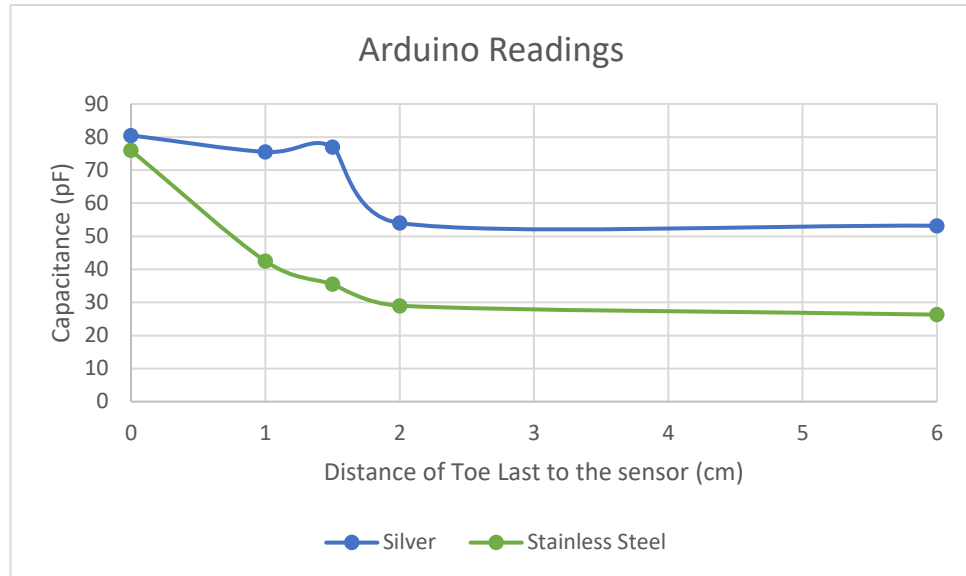
Figure 4.23: Capacitance readings using Arduino, comparing silver and 80/20 Polyester/stainless steel knitted samples

As observed from Figure 4.23, Polyester/Stainless Steel (SS) sample (green line) showed a steeper increase in capacitance compared to the Silver Sample (blue line). The SS Sample also showed a more distinct increase when the toe last gets closer to the fabric sensor whereas the Silver Sample exhibited an irregularity when it detected capacitance at the 1.5 cm mark. This may be because of the sensor not sitting flat in this area. As this sensor is shaped around a shoe last, there are areas in the sensor that may have more conductive material and so it bunched together, creating a thicker conductive plate. More conductive material in this area means that it could have picked up more capacitance compared to an area before or after this. The bunching of sensor material is also possible as the knit material of the silver sample felt softer and more limp compared to SS sample. The texture of the knit could have affected the readings when the lasts are inserted. The last could have shifted the sensor creating an irregularity in the reading.

From Table 4, comparing the Arduino results, the two samples garnered two different capacitance ranges. The SS Samples readings ranged from 26.3 to 76 pF which corresponds to a capacitance range of 50 pF over 6 cm, whereas the Silver samples varied between 53.19 to 80.5 pF. Hence a capacitance range of 27 pF over 6 cm. From these results, the sensitivity if the SS Sample is greater (8.3 pF/cm) over the silver samples (4.5 pF/cm). This indicates that the SS sample has better sensitivity which is more advantageous than the Silver sample. Higher sensitivity means that the sensor can have more resolution in readings. This is suitable, because when measuring foot length especially from ages between 11 months old to 36 months old, the foot length development is rapid. Therefore, a more sensitive sensor is able to pick up minor changes.

4.1.6   Sensor Prototype 1 Findings and Design Limitations

From Chapter 4.1.5, it was verified that the textile sensors placed in a non-planar pattern can still detect capacitance of volumetric shape, like the foot. This is verified by both LCR Meter and MPR121 interfaced with Arduino. The capacitance was tested on both because MPR121 needed validation to test if it would read the same way as the LCR Meter. Although the readings on both measurement system were not the same, it followed the same trend of increasing capacitance whenever the phantom foot got closer to the sensor

The evaluation also verified that the material more suitable for use is stainless steel threads. It showed that it was able to read a larger range of capacitance over a short amount of distance, despite its conductivity being less than silver's. The knit of the stainless steel held more structure, as it can be conformed around the last better than the silver knit. This is due to it being 80% Polyester, hence it was able to be shaped better.

This led to the result that the stainless steel will be used for the next design iteration. However, there are still issues that need to be addressed leading up to the next iteration. It was observed after repeated testing that sensor behaviour degraded to acting like a switch, where capacitance only was high or low, regardless of the foot location. This was thought to be due to:

- The physical connection of sewing copper wire and knitted textile sensors together using a stainless steel thread disconnecting. This is due to lack of flexibility of the shielded copper wire. The copper wire can easily slide out after repeated movement of the wire for plugging it in the Arduino. A more flexible alternative is needed and a more fibrous conductive core with insulation, so that

when wires are sewn onto a fabric, the fibres would interlock each other giving more strength at the connection.

- It was also observed that the physical structure of only having one local area of the sensor in the toe cap did not sit well with the rest of the shoe structure and felt unnatural. An obvious bump can be felt while it was still inside and did not seamlessly fit. To avoid this the sensor must be incorporated in the sock liner.

4.2 Sensor Prototype 2

This part of the chapter outlines how the issues from Sensor Prototype 1 are addressed. The main objectives were:

- Create a fully textile sensor and connection system so that it can conform to any shape and be more robust to flexing.

- Verify the experimental findings from Chapter 4.1, and validate whether the same results occur when real human feet are inside the instrumented shoe. A wireless system would be implemented to test this in a more natural manner.

- An enclosure must be created protect the electronics unit during testing with real human feet.

- Attempt to increase sensitivity of the fabric sensors, so that it can read larger range of values over a small distance.

4.2.1 Sensor Design

4.2.1.1 Sensor Pattern

From the results in Chapter 4.1.5, the maximum sensing range corresponds to a foot phantom 2 cm away from the sensor. This corresponded to the insole information provided in Figure 4.24a. This refers to the 2 cm mark which matches foot sizes 20 (13.5 cm) to size 23 (15.5 cm). From this information, a new striped pattern (Figure 4.24b) is devised to create a sensor that can sense a larger range, while also improving the structure of the knit integration with other threads to be implemented as a sock liner.
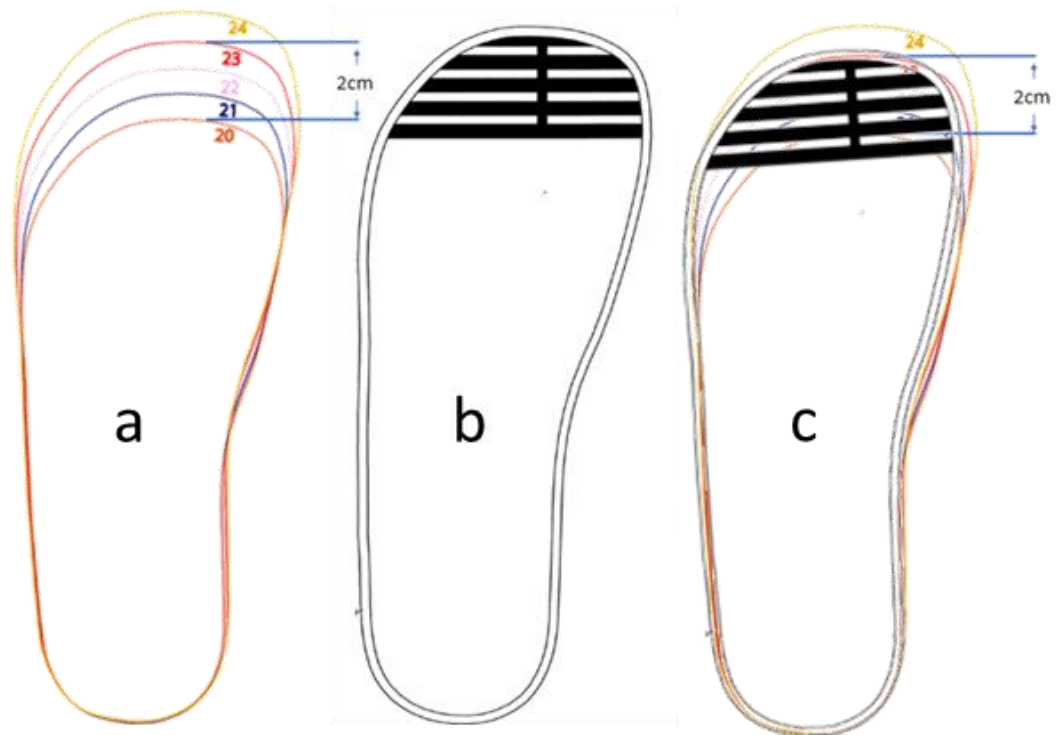
Figure 4.24: a) Insole information from Bobux showing the 2 cm mark. b) Sensor Pattern segmented but connected in the middle. c) Sensor Pattern overlapped with Insole Information

The striped pattern is drawn in Solidworks corresponding to a size 23 shoe insole and toe cap. The dimensions of the pattern are shown on Figure 4.25. The thickness of the conductive knits and gaps are determined by the minimum number of courses (rows) the knitting machine can do. SIG 123 SV 14-Gauge knitting machine is used and it can do a minimum of two courses.

Two courses are equivalent to 2 mm thickness, the conductive traces are knitted with 4 courses (w_c) and the non-conductive thread gaps (w_{nc}) are knitted with 2 courses.
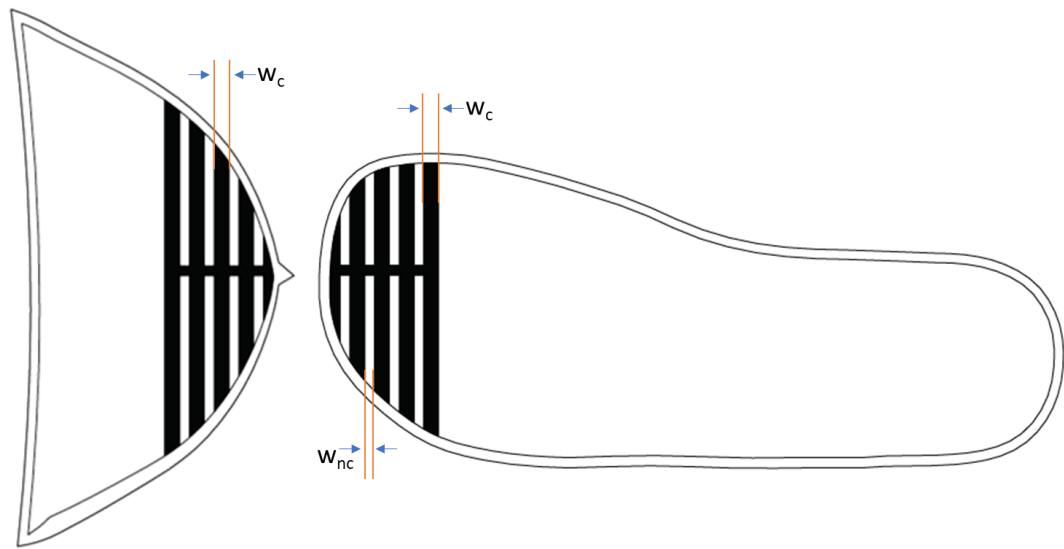
Figure 4.25: Striped pattern drawn on Size 23 toe cap (right) and insole (left); w_c = width of conductive knit, and w_{nc} = width of non-conductive knit.
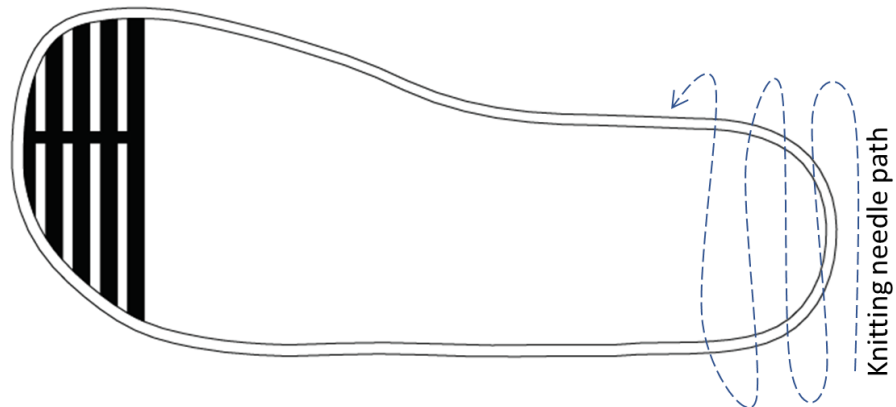
Figure 4.26: Knitting needle path

4.2.1.1.1 Sensor Pattern Validation Test

Before implementing the design to the knitting technician, the striped pattern was first implemented as a cut out of copper stripes. The template was printed to 1 to 1 scale, and copper tape cut out to the same scale. The stripe running across the conductive widths were replicated in the mock up (Figure 4.27) by connecting a pure stainless steel conductive thread and connecting this with a single header pin. Figure 4.27 contains an amber colour tape, called Polyimide tape, which provides insulation and electrical isolation from surrounding electronics and human touch.

Figure 4.27: Copper Tape stripes on the insole and the toe cap. Both sensors are joined by a conductive thread in the middle. This is knotted to a header pin, protected by a red electrical tape.

The mock up is to be plugged in to the Arduino with MPR121 unit, to see whether capacitance increases whenever a copper stripe is covered. This will be done by covering each stripe with each size of foot phantom (size 20-23) and observing whether there is an incremental change whenever a copper stripe is covered. The results are read and logged using the Arduino Serial Monitor built into the PC.

4.2.1.1.2 Sensor Pattern Test Findings

The mock up sensor is plugged in to the Arduino unit. The graph shown in figure 4.27 shows an incremental increase when each stripe is covered by the foot phantom size 20 - 23. Although, this proved that striped design works, this test is not an overall indication of the final design, as the final prototype is needed to be made of fabric and not paper and copper tape.
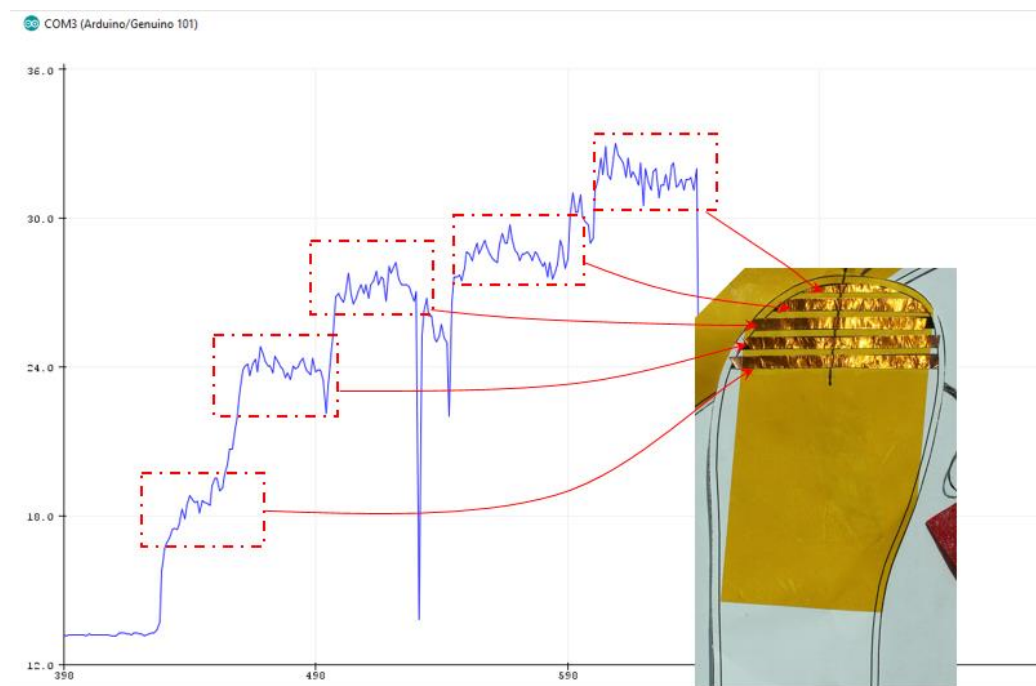
Figure 4.28: Incremental increase when lasts covered each copper stripe

4.2.1.2 Sensor Manufacturing – Sensor fitment iterations

Different iterations of sensors are assembled and visually evaluated. The layer layout of these design iterations is the same in Figure 4.4.

Figure 4.29: Version 1 - Laser cut fabric sensors fitted inside soft sole shoe. Black wire is the connection to the electronics unit

Figure 4.31: Version 1 inside out

Version 1 – Like the copper stripes but replaced with knitted 80 PES/20 SS Conductive thread. The conductive thread is knitted as a sheet, and is laser cut to shape to take the pattern of Figure 4.25. the knitted sheet is laser cut to prevent from fraying. The laser cut upper and sole patterns are glued to their corresponding places. Each corresponding stripe is hand sewn to create a connection (refer to Figure 4.30). The sensors are installed in a soft sole shoe for easy installation as it can be turned inside out. The black wire in Figure 4.29 is a coaxial cable. The innermost wire of this is connected to the fabric sensor inside the shoe and the braided cable is connected to the copper taffeta outside the shoe.

Figure 4.30: Hand sewn connections from the upper (Blue leather) to the sole (brown leather)

Visual inspection on the connections between each stripe (Figure 4.30), shows is not as thick as the rest of the striped sensor. This can get disconnected, if the hand sewn connections are not secured properly. The wires of coaxial cable are made of smooth copper, making it hard to secure connection to the textile sensor

as there is not enough "grip" for the copper to textile sensor.

Version 2 – The textile sensor is made and backed up with a polyester thread (white), to hold up the conductive stripes evenly (Figure 4.32). The stripes are also more complete as it does not have to be hand sewn together. The sensor is shaped over a last to conform with the foot shape as this is going to be inserted in a hard sole shoe. The connection from the fabric sensor to Arduino is made of a pure stainless steel with Teflon layer, which serves as an insulation (Figure 4.34). This replicates the innermost core of the coaxial wire pictured in Figure 4.10. The connection from the copper taffeta to Arduino Ground is a non-insulated Stainless Steel Conductive thread. This is wrapped around the insulated stainless steel wire, to replicate the braided conductive wire component in the coaxial wire. The overall wire connection is then clipped to an FCI Clincher connector (not pictured), creating an easier connection to the Arduino terminals.

Figure 4.32: Version 2 – knitted sheet of polyester with 80PES/20SS Conductive thread

Figure 4.33: The connection to Arduino is protected and held together by a red tape to prevent physical disconnection.
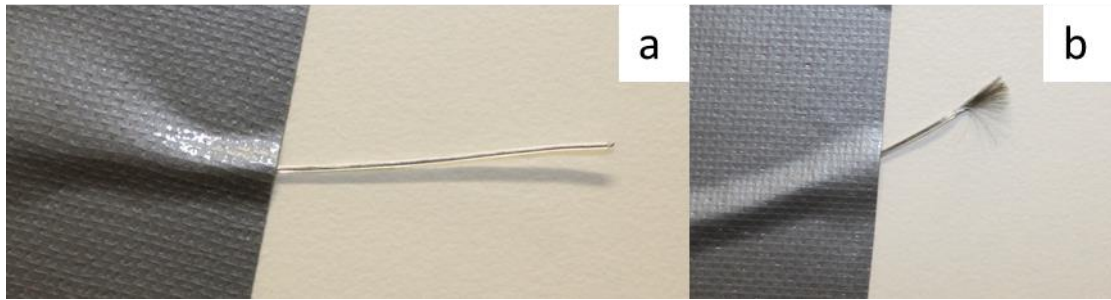
Figure 4.34: (a) Pure Stainless Steel wire covered with Teflon insulation. (b) Teflon insulation is stripped, exposing multifilament pure stainless steel conductive thread

Implementation of the new wire (pure stainless steel with Teflon), solved the textile connection issue, as it can be sewn securely on the fabric sensor. However, the fabric sensor itself did not have much structure and did not sit against the inner wall of the shoe. This could be because the upper is cut around the sole, and even if the installation was easier, it was found that the sensor did not stay inside the shoe properly.

Version 3 – knitted as a sock this eliminates the handwork of joining between the upper and the sole fabric sensor. The type of knitting used for samples in Figure 4.36 and Figure 4.37 are tubular knitting using Shima Seiki Whole Garment Technology. This technique allows for two different materials to be knitted together. It incorporates non-conductive polyester threads in between the conductive threads, allowing for a better mechanical structure preventing the conductive rows from touching each other. This also allows for

Figure 4.35: Knitted sock sensor with seamless connection at each stripe

Figure 4.36: knitted sensor as a sock

86

a seamless connection along the stripes, ensuring each row is connected as one round stripe.

The main connection from the fabric sensor is done the same way in version 2, where an insulated stainless steel thread is stripped and sewn on to the sensor (Figure 4.38). The knitted sensor sock is coated in PVA glue while it is inside a last. The glue is cured and dried inside an oven at100 ℃ until dry to touch. This is to keep the sensor in shape (Figure 4.37) and the insulated conductive thread connection in place, for easy installation inside the shoes.

Figure 4.38: knitted sensor with insulated stainless steel thread connected at the tip of the sensor.

Figure 4.37: Samples after curing glue in an oven.

4.2.2 Final Sensor Assemblies

The different versions were visually assessed, evaluated on ease of installation and achieved the objective. Version 3 was chosen for manufacturing of the final assemblies of the sock sensors because it achieved a full textile connection and seamless integration of the knitted sensor from upper to sole.

There were two knitted sock sensor samples created for test, characterised as Grounded Heel (GH) and Non-Grounded Heel (NGH) (Figure 4.39).

Both samples were knitted with a combination of non-conductive polyester thread and 80/20 PET/SS Conductive thread. GH contained a conductive knit patch on the heel and NGH does not. GH and NGH samples have the same knit layout on the toe area and were made the same way, as described in Chapter 4.2.1.2.

Figure 4.40: Two Samples Showing the same sensor pattern on the toe cap area
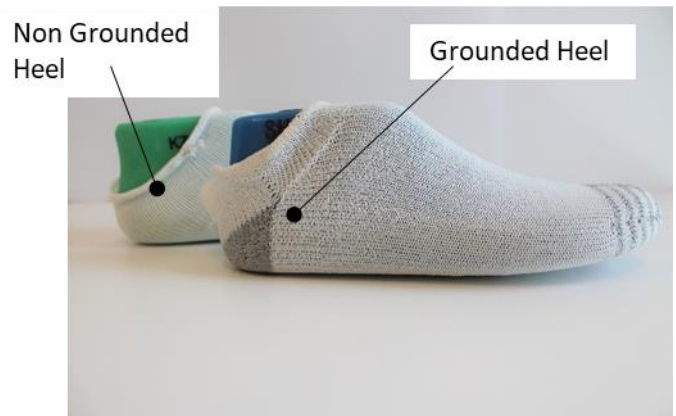
Figure 4.39: Two Samples showing Non Grounded Heel (NGH) Sample and Grounded Heel Samples (GH)

The sensors were installed inside Bobux shoes. NGH sensor would follow the layout in Figure 4.4. GH sensor contained an additional ground plane at the heel. This was connected to the shield layer on the outer upper of the shoe (Copper Taffeta) (Figure 4.41).
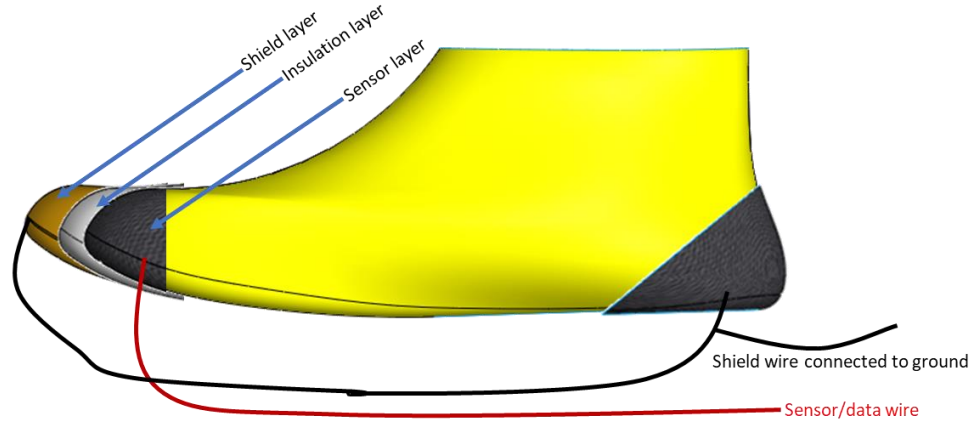
Figure 4.41: Layer and Connection Layout of GH Sensor

For both GH and NGH, insulated stainless steel thread (Figure 4.34) is used as the sensor wire, carrying data to the electronics unit. A non-insulated stainless steel conductive thread is wrapped around this thread, to replicate the shielding effect of a coaxial cable preventing noise from the environment.
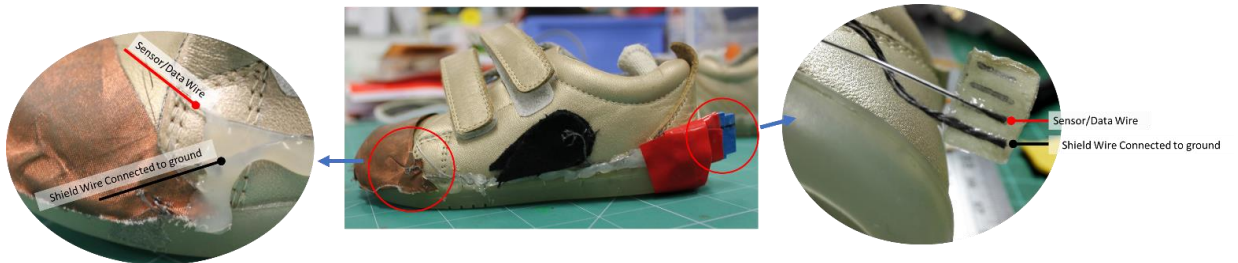
Figure 4.42: (Left) Connections from the Sensor and Shield Layer on the Toe Cap, (Middle) Overview of the Grounded Heel Shoe (Right) Connections of wires attached to a Z axis tape

Figure 4.42 shows the physical connections of the shoe with GH Sensor. The black cloth contains connections from the copper taffeta and the extra ground plane on the heel. The connections shown on Figure 4.42 (right), is connected and crimped to a blue Female FCI Clincher. This is used, as it gives the best contact for the traces while ensuring reliable contact between conductive threads and the electronics unit.

4.2.3 Pycom Expansion Board and WiPy 2.0

A wireless system is implemented so that it can be tested on children's feet. This is done to avoid any hazard that may come along during testing, such as broken connection between Arduino and the PC due to accidental disconnection while the child is walking.

The Arduino is replaced by two modules, Pycom Expansion Board and WiPy 2.0 (Figure 4.43). Pycom Expansion Board is used because of easy plug and play configuration while it allows for external microcontroller boards to be plugged in. In this situation, the MPR121 is still used and is plugged in to the exposed female pin headers in Figure 4.43 using a custom-made PCB.

The Pycom expansion board includes a mini USB Plug so that it can be easily programmed and deliver power using an external power source like readily available power banks. The expansion board contains a step-down voltage regulator so that when a higher voltage is plugged in, it would only take what is needed to prevent overvoltage (Pycom Ltd., 2017).

Figure 4.43: Pycom Expansion Board with WiPy 2.0 Module

WiPy 2.0 is a separate microcontroller that is attached by inserting the headers on the inner part of the Pycom Expansion Board. This microcontroller features Bluetooth Low Energy (BLE), Bluetooth Classic and Wi-Fi. This is advantageous as it can be integrated with older Android devices that do not support BLE. It can also communicate over Wi-Fi, therefore eliminating the need for a wired connection to log and acquire data. This is compatible with MPR121, as it can communicate with I^2C Bus protocol (Pycom Ltd., 2017).

An external custom made PCB shield is manufactured to decrease the amount of wires for connecting MPR121 to Pycom Expansion Board headers, Figure 4.44 and Figure 4.45. The routing layout of the custom-made PCB is discussed later.
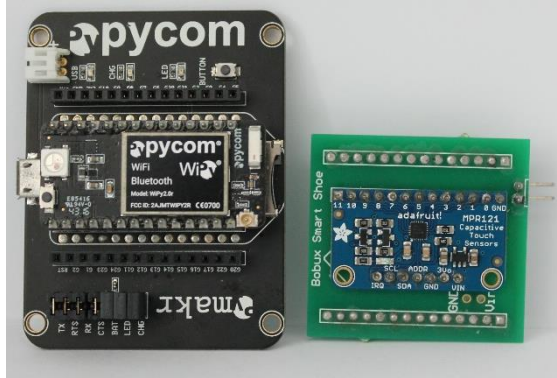
Figure 4.44: (left) Pycom Expansion Board with WiPy 2.0; (right) Custom-made PCB Shield with MPR121 soldered to it. With header pins to match with Pycom Board

Figure 4.45: PCB Shield assembled on top of the Pycom expansion Board

The Arduino 101 is replaced by the Pycom Expansion Board and WiPy 2.0 as it was more convenient to implement to the researcher's Android phone. Although both WiPy 2.0 and Arduino 101 supports Bluetooth Low Energy Module, the WiPy 2.0 also had Bluetooth Classic Version. This version had more software support in terms of open source code. It was also more compatible with older Android Phones as they only work with Bluetooth Classic version.

An Android app is made by a colleague using Android Studio. This allowed for seamless data collection creating a wireless data logging system. This meant that the electronics unit is capable of operating while it is strapped on a child, without worrying about physical disconnections.

The code of MPR121 implemented in Arduino (Section 4.1.3.4) is also implemented in WiPy 2.0, this provided the same reading conditions with a different electronics unit.

4.2.3.1   Hardware Enclosure

A hardware enclosure (Figure 4.47 and Figure 4.48) was created to prevent physical disconnections from the circuit and the shoe. The hardware enclosure also prevents possible electric shock that may come from low voltage electronics while it is being tested on children.

The design of the enclosure is based on an original Pycom enclosure provided on purchase. The original Pycom enclosure did not fit all the components in Figure 4.44.
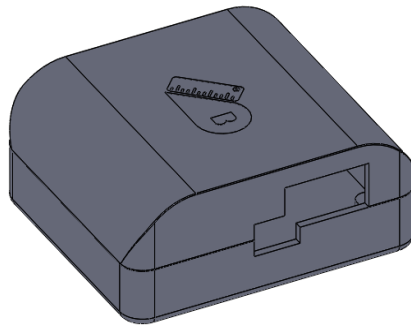
Figure 4.47: 3D Drawing of edited enclosure

Figure 4.46: 3D Printed Enclosure

Figure 4.48: 3D Printed Enclosure with elastic straps to fit to child's ankle.

4.2.4 Overall Connection and Assembly of Shoes and to Electronics Unit

In Chapter 4.1.3, the overall system layout considered the use of Arduino. In this section, Pycom with MPR121 is implemented. The overall physical connections with pin assignments are laid out in Figure 4.49
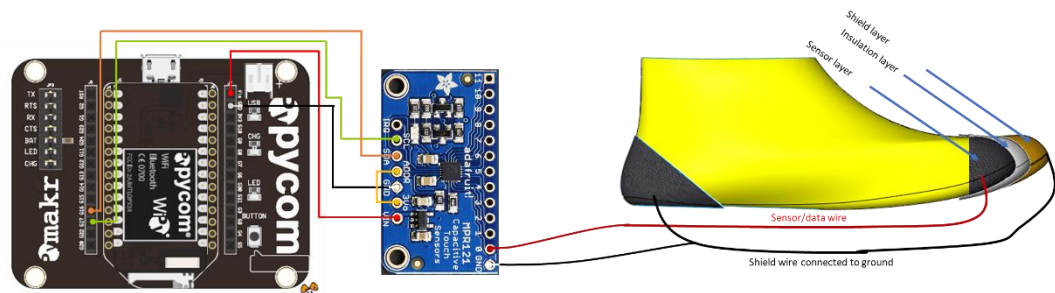
Figure 4.49: Physical Connection from the electronics unit to the shoe sensor unit.

The wires connecting the MPR121 and Pycom in Figure 4.49 are represented by a custom-made PCB Shield that sits on top of the Pycom Expansion Board as picture in Figure 4.45. Figure 4.50 shows how the connections/copper routes are placed in one plane of the PCB.
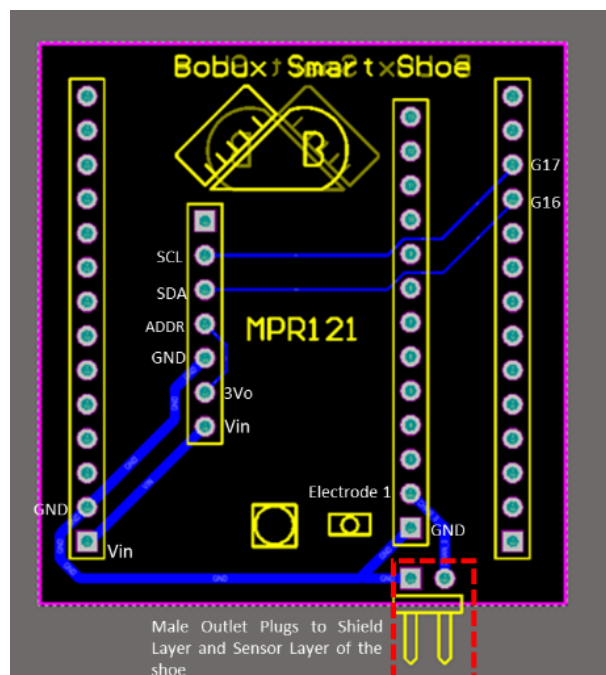
Figure 4.50: Electrical Schematic of connections of the custom made PCB Shield

93
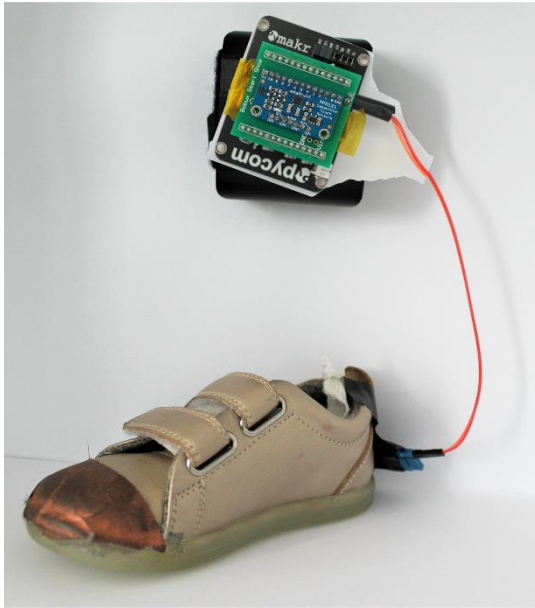
Figure 4.52: Non-Grounded Heel Sensor Connected to Pycom and MPR121

Figure 4.51: Grounded Heel Sensor Connected to Pycom and MPR121

4.2.5 Evaluation with Children

A study in children was undertaken to prove the effectiveness and reliability of the textile sensors. An ethics approval was granted by Auckland University of Technology Ethics Committee (AUTEC) under Ethics Application Number 17/381 Can in-shoe, textile sensors provide useful information to determine appropriate shoe sizes in young children.

4.2.5.1 Participant Recruitment and Setting

All children in this study were recruited from the general community using online platforms and email recruitment from the AUT Early Childhood Centre and from existing Bobux Customer Database. In person recruitment also occurred using posters put up in the Bobux Outlet Store.

Parents and/or guardians gave written consent and children assented to participate. During the test held in Bobux retail store, the parents and care givers needed to be present to give them familiarity in the environment. On the tests held in AUT Early Childhood Centre, the centre manager approached the researcher and introduced her to the children being involved.

The shoe prototypes were tested in 30 children, 14 data sets were taken from that. The other 16 results had to be excluded due to:

- The children's feet were long and/or too plump inside the shoe which changed the capacitance readings
- A coding error was found during shoe tests in December and February Shoe Testing causing the code to read the wrong electrode.

4.2.5.2 Inclusion and Exclusion Criteria

Inclusion criteria put in place for this study were: only developing children aged 11 – 36 months old will be included. Parents will be asked if their children have any known health conditions that could have an impact on walking. These include genetic conditions that change walking, neuromuscular conditions that are exhibited in tiptoe walking or orthopaedic conditions that results in foot structure change.

Necessary exclusion criteria were: only children that can stand and walk properly can participate, and children's foot length needed to be under the size of 150 mm, as the sensors are instrumented inside a Size 23 Bobux Shoe, which has a foot length of 150 mm.

Documents pertaining to this study are included in the Appendix 3.

4.2.5.3 *Testing Procedure during test with children*

The test procedure called for the participants/children to be in a static (standing position) with their heels all the way at the back of the shoe, with socks worn on both feet. During the test, the children were asked to count from 1 to 10 after physical measurements – i.e. Foot Length and Foot Circumference were measured.

During the test other parameters were also recorded such as

- Bobux Shoe Size (according to Bobux Shoe Ruler) – recorded by placing the child's heel at the heel curve of the Bobux shoe ruler, and the slider on the opposite end is slid until it touches the longest point of the foot (Figure 4.53)

Figure 4.53: Bobux Shoe Size Measurement

- Foot Length (Using tape measure) (Figure 4.54)

  A tape measure is placed at the back of the Bobux shoe ruler. This indicates the

  foot length in centimetres.

Figure 4.54: Foot Length measurement

- Foot Circumference (Using tape measure) (Figure 4.55)

  Tape measure is wrapped around the widest part of the foot while participant is

  standing up.
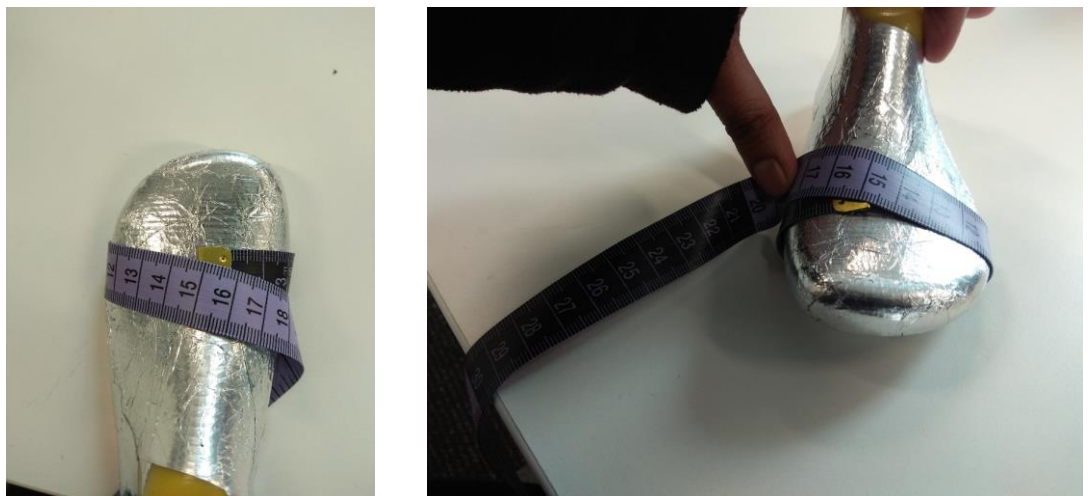
Figure 4.55: Tape measure wrapped around the widest part of the foot.

These are recorded to create comparison between capacitance readings, foot length,

indicative Bobux Shoe Size and possibly Foot Volume.

4.2.6 Sample Population and Data Analysis Approach

Sample Population

Out of the 30 children recruited between February and March 2018, 14 results were valid for data analysis. Valid results were identified by complete recording of the parameters. Two sets of readings were available for each child (GH and NGH sensor). For some children, this was difficult to achieve as the child would not always want to cooperate.

Of these 14, five were males and 9 were females. The average age of the sample group was 22 months, ages ranging between 14 – 27 months, and the average foot length is 13.5 cm, foot lengths ranging between 11.6 cm – 15 cm.

Data Analysis Approach

Of the two sock sensors, 14 data sets were recorded. Parameters recorded were the following:

- Capacitance – measured with the instrumented shoe with GH and NGH sensors connected with Pycom
- Time of test – recorded in the Android app
- Length of test time
- Foot Length
- Foot Circumference
- Bobux shoe size

The GH shoe was for the left foot, and NGH shoe is for the right. The foot lengths of both feet were recorded for each child. Some children have different foot lengths between their right and left foot. (i.e. right foot may be smaller than the left or vice versa).

Once recorded, data from the app was organised based on the baseline readings of the sensor (capacitance reading before feet is inserted and after feet was taken out), transition between when a child puts on the shoes and when they take it off, and time when they have the shoes on.

An example of raw data in Figure 4.56, shows the stages of the whole sensor behaviour when the foot goes inside the shoe. This is referred to as the touch profile
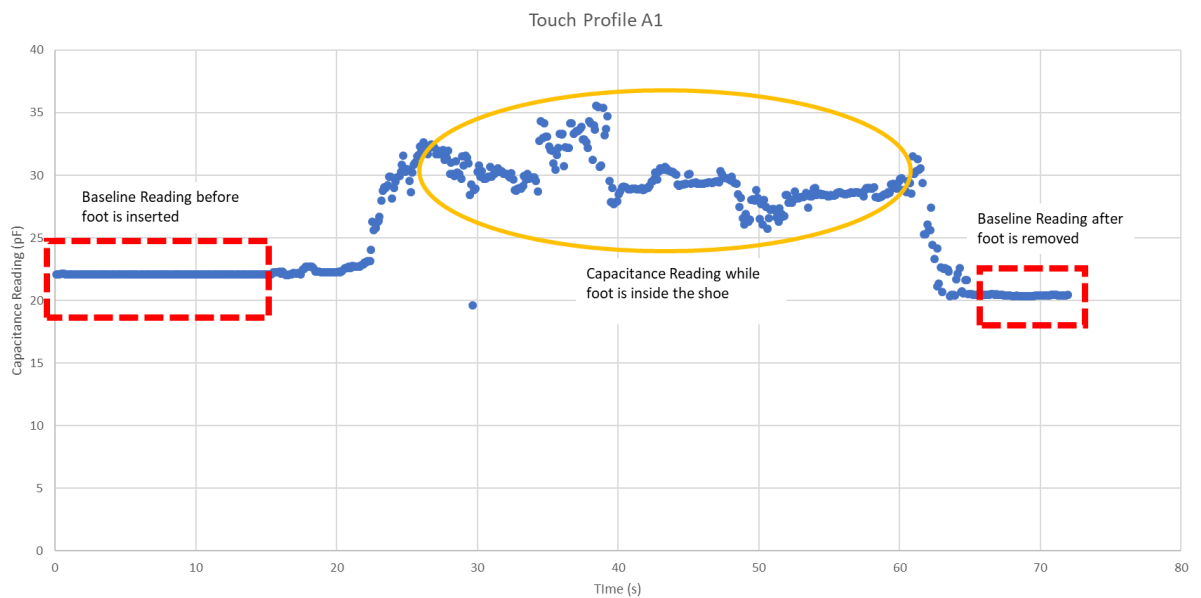
Figure 4.56: Example of raw data showing how sensor behaves over time.

There are 28 touch profiles, two for each child as there were two sensors tested. For each touch profile, the readings inside the yellow circle in Figure 4.56 were averaged.

The capacitance readings are compared to the foot length and foot volume. A MATLAB Script is written to observe the linear regression and statistical models of the results between GH and NGH sensors. For the statistical models, 95% Confidence Intervals are

derived and significance level of p value less than 0.05 is implied. If p value is greater than 0.05, results of the linear regression model are considered statistically insignificant.

4.2.7 Sensor Prototype 2 Result

4.2.7.1 Foot Length and Capacitance Relationship
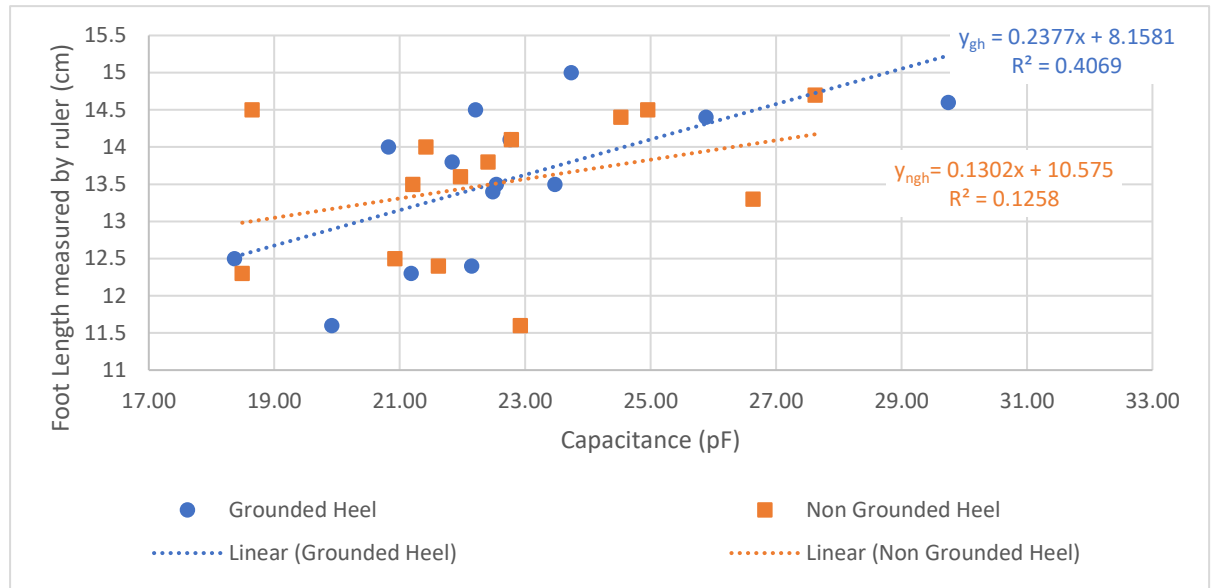
Figure 4.57: Graph of Foot Length and Capacitance

Table 5: Linear Regression – Statistic Analysis for Capacitance and Foot Length Relationship

	Linear regression model: $y = mx + c$ $y = equation\ for\ both\ GH\ and\ NGH\ shoes; m = gradient\ of\ the\ equation; c = y\ intercept\ of\ the\ model$		
	$m\ (lower\ CI, upper\ CI, SE)$	$c\ (lower\ CI, upper\ CI, SE)$	p
y_{ngh}	$0.130\ (-0.085, 0.346, 0.0991\ )$	$10.57\ (5.669, 15.48, 2.252)$	0.2135
y_{gh}	$0.238 (0.057, 0.418, 0.0829\ )$	$8.158\ (4.012, 12.2, 1.889)$	0.0141

Referring to Table 5, GH shoe sensor results possessed a statistically significant result (p < 0.05) and a steeper relationship compared to NGH (p = 0.2). The standard errors (SE) of GH is smaller, statistically indicating that it is unlikely for the true gradient to be negative.

4.2.7.2 Foot Volume and Body Capacitance Relationship

For these results, the circumference of the foot is taken from the widest part of the foot.

An assumption that was made is that the volume of the foot is approximated to have the section of an ellipse.

The volume of the foot is assumed as a cylindrical ellipse shape, semi minor axis is assumed to be ¼ of the semi major axis.
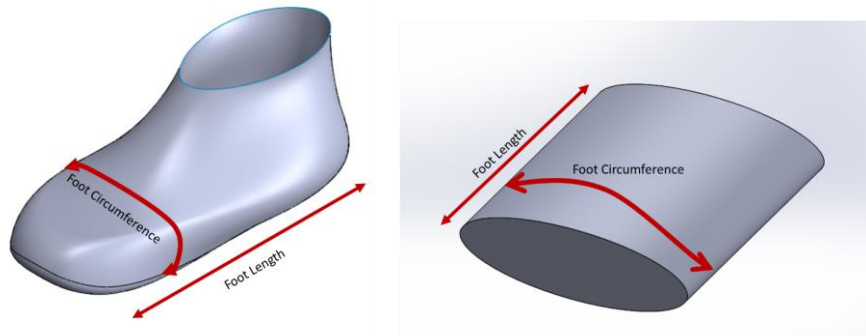
Figure 4.58: Assumption of foot as an ellipse shape.

The volume is calculated using the circumference equation of the ellipse:

$$C_{ellipse} = 2\pi \sqrt{\frac{a^2 + b^2}{2}}$$
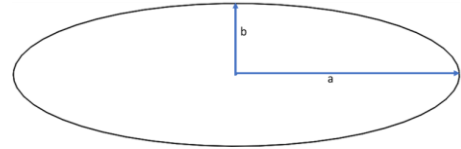
$a = radius\ from\ the\ semimajor\ axis;\ b = radius\ from\ the\ semiminor\ exis;\ C_{ellipse}$

$$= measured foot\ circumference$$

It is assumed that $b = \frac{1}{4}a$

$$\therefore C_{ellipse} = 2\pi \sqrt{\frac{7a^2}{32}}$$

Volume of elliptic cylinder is:

$$V_{ellipse} = \pi abh = \frac{\pi}{4}a^2h$$

103
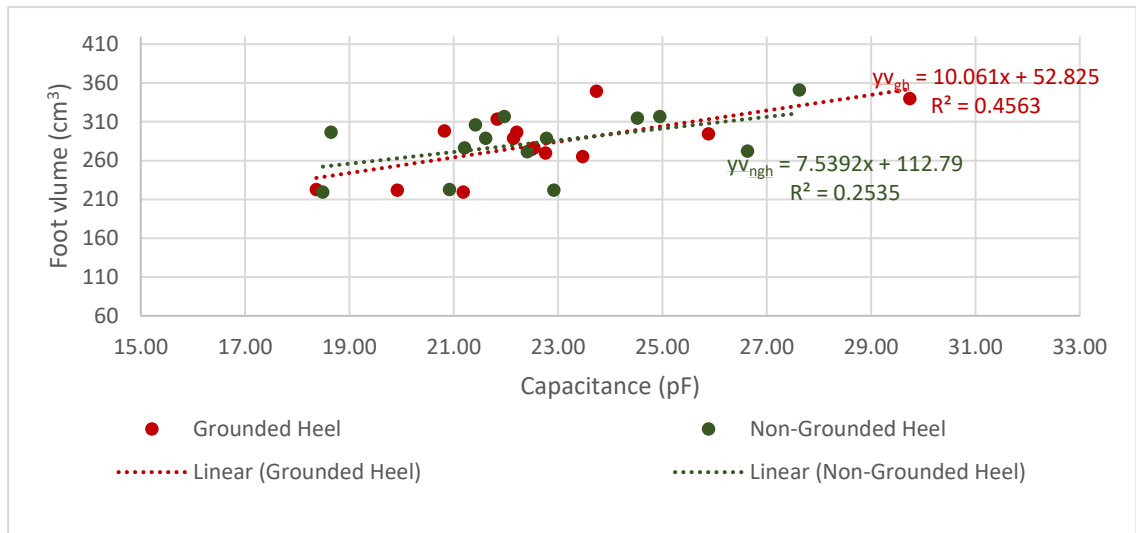
Figure 4.59: Graph of Foot Volume and Capacitance

Table 6:Linear Regression – Statistical Analysis for Foot Volume and Capacitance

Linear regression model $yv = foot\ volume\ regression\ equation = mx + c$		
$yv = equation\ for\ both\ GH\ and\ NGH\ shoes; m = gradient\ of\ the\ equation;$		
$c = y\ intercept\ of\ the\ model$		

	$m\ (lower\ CI, upper\ CI, SE)$	$c\ (lower\ CI, upper\ CI, SE)$	p
yv_{ngh}	7.54 (−0.60, 15.68, 3.73)	112.73(−72.11, 297.6, 84.83)	0.066
yv_{gh}	10.06 (3.15, 16.97, 3.16)	52.84 (−104.6, 210.3, 72.25)	0.008

Referring to Table 6, GH shoe sensor results possessed a statistically significant result (p < 0.05) and a steeper gradient relationship compared to NGH (p = 0.06). The standard errors (SE) of GH is smaller, statistically indicating that it is unlikely for the true gradient to be zero of negative.

4.2.8 Sensor Prototype 2 Discussion

The results shown in Figure 4.57 and Figure 4.59 showed the sensors are functioning when real human feet with socks on are inside the shoes. Both GH and NGH showed feasibility that the textile sensors can measure foot length. This was indicated by the positive gradients in Figure 4.57., which means as the longer foot is inserted inside the shoe, the capacitance readings increase.

In Figure 4.57, y_{gh} showed a steeper gradient and a larger r^2 value compared to y_{ngh}. This may be due to the extra conductive pad in GH sensor creating an effect which increases the sensitivity of the sensor. This extra conductive pad on the heel decreased the parasitic noise from the background. The result for y_{gh} in Table 5, also showed statistical significance as the p value is less than 0.05 (p = 0.01), whereas for y_{ngh} is greater than 0.05 (p = 0.2), hence GH shows a more credible result compared to NGH.

Additionally, both GH and NGH sensors showed feasibility for measuring foot volume. This can indicate how much of the human foot is expanding inside the shoe. This is indicated by the positive gradients in Figure 4.59, as larger volume indicated increase in capacitance. Although similar effect presented where yv_{gh} showed a steeper gradient and a larger r^2 value compared to yv_{ngh}. The p values in this linear regression model. In Table 6 depicted lower values compared to the foot length and capacitance in Table 5. Even though the values are lower, the GH shoe, yv_{gh} showed more statistically significant result due to its p-value being 0.008, whereas the NGH shoe, yv_{ngh} p value is 0.06. Again, this could have been the effect of the added extra conductive pad on the heel of the GH Shoe sensor.

The textile sensors appear feasible for sensing the foot length, especially the GH shoe sensor. However, the r^2 value of the GH shoe is less than 50% when capacitance is compared against foot length and foot value. This can mean that the linear regression model may not be a suitable model for characterising the textile sensors. Although the p values showed credibility and proved the concept, more information such as more variability in the foot lengths are needed to create a conclusive and more definite capacitance to foot length model.

4.3   Foot Length Measurement System Conclusion

To conclude, there were two aspects in this part of the research thesis. Sensor Prototype 1 tested the feasibility of textile sensors and Sensor Prototype 2 further improved the design of Sensor Prototype 1.

Both sensor prototypes went through an iterative design process to create final prototypes, and these were tested and validated throughout the design process for further verification and to help answer the research questions.

Sensor Prototype 1 showed that physical presence of a phantom foot increases the capacitance reading of the fabric sensor. This was proved by reading capacitance using gold standard measurement, Keysight E4980A LCR Meter. A smaller capacitance reading system was then implemented using Arduino and MPR121 to enable portable capacitance logging from the fabric sensor. The capacitance readings from both measurement systems provided comparable results. An issue found in this design iteration was that it was not sensitive enough to measure incremental changes. This means that the reading from a phantom foot 2 cm away from the sensor, was similar to 0.5 cm away from it.

A different sensor design was implemented in Sensor Prototype 2, to increase sensitivity of the fabric sensors. Two sensor configurations were tested, to see which design would work better. In vivo validation was performed to examine whether a child's foot would change the capacitance, the same way a phantom foot would in the GH and NGH shoe. During this testing, the child's foot length and the foot circumference were measured with a measuring tape. The foot length and the capacitance reading were plotted in a graph for the GH and NGH shoe prototypes. GH shoe indicated better performance compared to NGH shoe. This was indicated by the difference in slopes and difference in standard errors, using the information analysed from linear regression. The p-value also indicated that the placement of an extra conductive pad in the heel part (GH shoe) resulted in an increase in sensitivity of readings. This verifies the theory stated in Chapter 3 .

The positive increase of slope and small standard of error in the GH shoe indicated that, textile sensors can measure child's foot length. Nevertheless, there are also some limitations to this research:

1. Testing with more feet is needed to ensure that the trend is generally true.

2. It would be ideal if the same instrumented shoe is tested longitudinally on one child to observe the foot length growth trend. This study did not allow for this observation to happen due to time restrictions.

3. The sensors and connections are fully textile and is installed in one type of shoe. Ultimately, this sensor can also be implemented on other types of shoes with different materials. However, the effect of variable materials is unknown and was not explored in this study.

4. The prototype electronics worked for this. However if this were to be implemented on real shoes, smaller electronics would need to be implemented, which may affect the quality of the readings.

5. This research only considered estimating the foot length of the child. Other anthropometric parameters such as foot width, foot height, and foot volume would be ideal, as this would indicate to the parent or podiatrist whether their child have wide feet or have tall feet.

6. The fabric sensor is implemented inside a shoe with more rigid walls compared to a knitted shoe. The shoes used for testing may have constrained the foot instead of allowing it to relax and conform to its natural shape. Therefore, this could have affected the results.

Chapter 5 Foot Pressure Measurement

Insole foot pressure systems like Pedar and F-Scan are some of the gold standard devices that measure foot pressure. Podiatrists, clinicians and researchers alike benefit from devices like these. For example, clinicians benefit as they are able to check up on their patients to see if they are performing their foot treatments well. However, these devices are expensive, ostensibly due to their high sensitivity, high accuracy and complex software and electronics.

Children's foot pressure is highly dynamic. The foot pressure changes at a rapid rate as the foot grows. It is important for clinicians and designers to know how the child's foot pressure progresses, for them to create preventive foot care and to design shoes better.

This chapter examines the development of a built-in-shoe foot pressure sensor system for use inside children's shoes.

5.1 Objectives

The objective of the research described this chapter is to create a low-cost sensor assembly which mimics pressure sensing insoles like F-Scan Tekscan, e-med pressure sensing platform and Pedar. Design requirements were drawn up to achieve the objective. As for Chapter 4 , the design requirements are broken up to two categories, Mechanical and Electrical Components and Software:

Mechanical aspects include

- Sensor placement and topography
- Sensor Manufacturing
- Sensor Layer Layout

Electrical Components and Software include:

- Physical Connections from the sensor to the electronics unit – The development of the physical connection is discussed in the sensor manufacturing section as the sensors and connections are manufactured the same way.
- Data logging of capacitance readings using LabVIEW

This chapter mainly focuses on the mechanical aspects of the design. This is because the same electronics unit (Arduino 101 and MPR121) as was used for foot length is used and configured to read 8 sensors all at once. The implementation of this code was discussed in Section 4.1.3.4.

5.2 Methodology

To develop a built-in-shoe foot pressure measurement system, the following approach was taken:

1. Literature Review – existing in-shoe foot pressure measurement systems were explored including how clinicians and researchers use the data acquired from these systems.

2. Making and Manufacturing plantar pressure sensor – existing manufacturing techniques were researched and qualitatively assessed. The main focus for selecting a suitable technique was an inexpensive process whilst delivering a good quality sensor.

3. Testing, Validation and Calibration – Once the sensor was manufactured, the sensor was tested to check whether there were any connection faults. This was done by connecting the plantar pressure sensor to Arduino and MPR121 electronics unit, connected to LabVIEW for data logging and visualisation. This test is referred to as Validation Testing 1 (VT1).

   Calibration carried out after VT1 derived calibration curves from the plantar pressure sensor system. This was done by applying repeated loads on the sensor using controlled instrumentation. Hounsfield H10KS Tensile Testing machine was configured as a compression testing machine to apply loads to the sensor. This stage is referred to as Validation Testing 2 (VT2).

5.3   System Layout

The sensor system contains 4 components as shown in Figure 5.1:

1. Mechanical/Physical Sensor – This includes the sensor pads that mainly detects the pressure change.

2. Connections and Routing system – This includes the connection from the sensor pads to the electronic system

3. Electronics System – This includes the implementation of Arduino 101 and MPR121 that reads the capacitance of the sensor

4. Data Visualisation and Data Logger – This includes LabVIEW Setup for visualisation and logging of data for post processing.
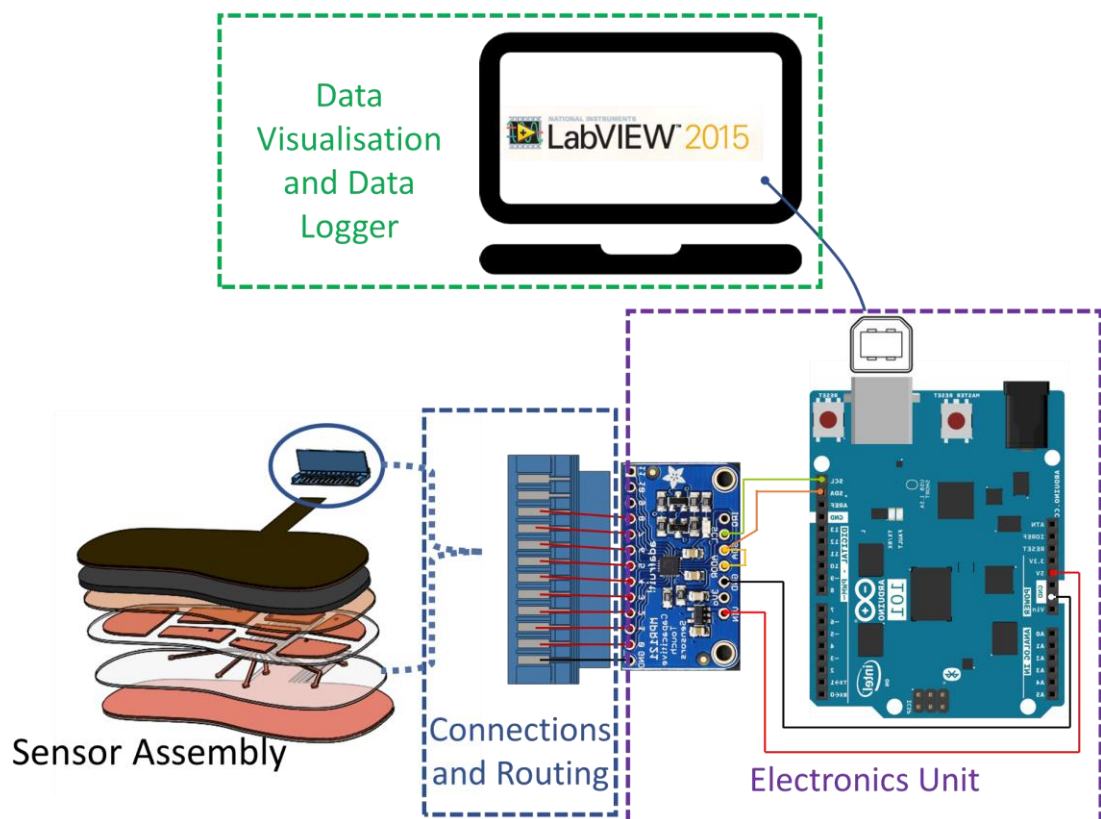
Figure 5.1: System Layout of Foot Pressure Measurement System

5.4   Sensor Design Layout

This section covers the mechanical design and development of the sensor assembly. This is comprised of the development of sensor topography/shapes and location, evaluation of materials and manufacturing techniques suitable for the creation of the sensors, and the assembly of the sensors.

5.4.1   Sensor Location

The plantar pressure sensor is aimed to measure the overall plantar pressure. The existing sensors introduced in Chapter 2.3.1 are placed where the insoles of the shoes are placed contacting the plantar surface. Ideally, the sensor needs to be fixed in a location where it is going to experience minimal movement during dynamic activity of the child.

The plantar pressure sensor can be placed in the strobel area which is located between the insole and the midsole of the shoes (Figure 5.2). The strobel holds the shape of the upper it is stitched together with the midsole or outsole (Motawi, 2015). If the sensor is placed here, the sensor would be fixed (i.e. not loose) preventing it from moving around. Having the sensor fixed in place decreases the amount of environmental noise hence a cleaner signal. This area is also ideal because the sensors can be layered with other protective materials, such as EVA and other lining materials. Figure 5.3 shows the cross section of Bobux shoe made with Strobel construction.
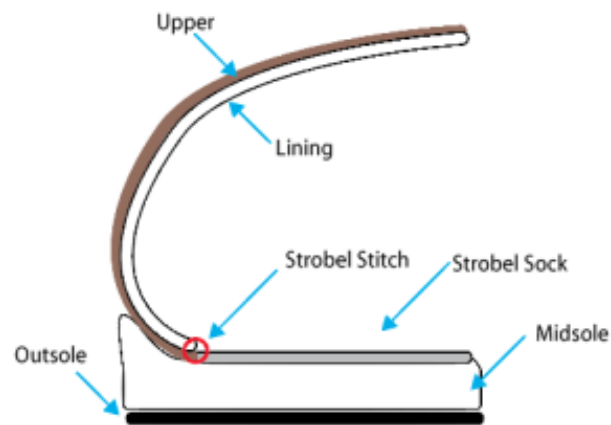
Figure 5.2: Strobel Construction Diagram (Motawi, 2015)

Figure 5.3: Bobux Shoe Cross Section with Strobel Construction

The plantar pressure sensor can be incorporated between the lasting board and the midsole

This can be done when shoes are constructed using a board lasting technique (Figure 5.4).

In this technique, the upper is pulled tight and bonded to a lasting board, this assembly is

also glued together with the midsole (Motawi, 2015). In Figure 5.5, a cross section of a

Bobux sandal is shown. The lasting board in this case is a thick EVA Foam. The ideal

place to put the sensor is below this lasting board as it can be protected by the EVA Foam.

The sensor can also be held in place when the thick EVA Foam is bonded to the midsole.
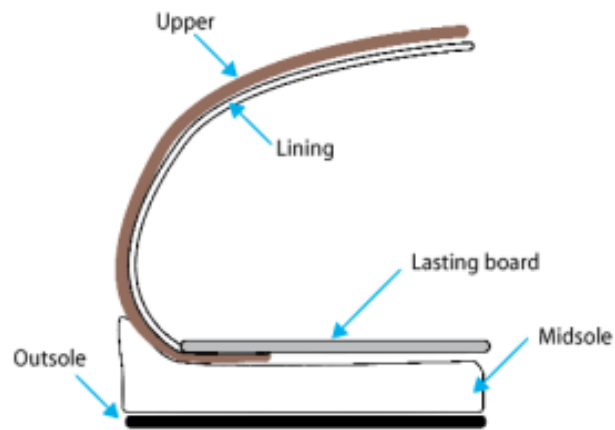
Board Lasting construction:

Figure 5.4: Board Lasting Technique (Motawi, 2015)

Figure 5.5: Cross Section of a Bobux shoe constructed with board lasting technique

The two examples shown in Figure 5.3 and Figure 5.5 are of two specific types of shoes. Figure 5.3 is a closed toe athletic shoe, whereas Figure 5.5 is a sandal. In this thesis, the sensor is not tested while it is inside a shoe. Instead, the characteristics of the layers on top of the sensor are observed and characterised.

5.4.2 Sensor Pattern/Topography

The sensor pattern is decided based on how clinicians and researchers use gold standard devices introduced in Chapter 2.3.1. These devices contain an array of sensors to capture all the pressure points of the plantar area and they have their own software. Masking is one of the functionalities in the accompanying software, where plantar areas can be divided up to observe areas of interest. The masks can be setup differently depending on clinician's and researcher's interests.
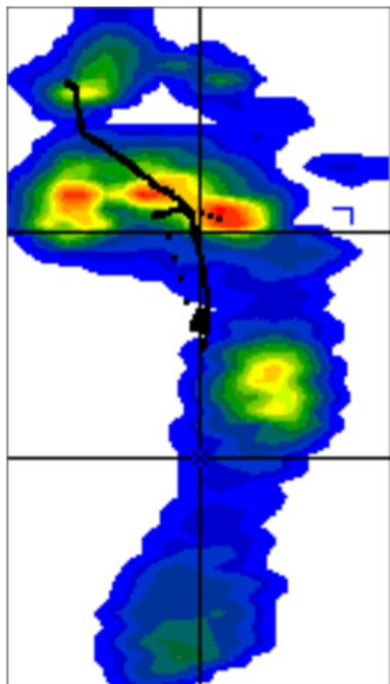
Figure 5.6: Typical foot pressure data divided into segments as per masking(Niiler et al., 2016)
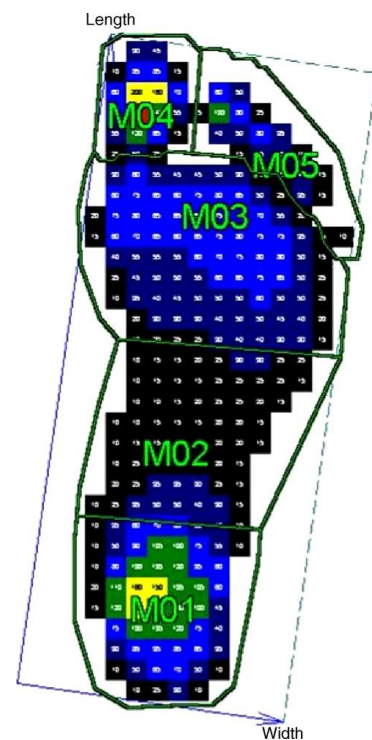
Figure 5.7: Foot Pressure Data derived from Emed Pressure platform(Bosch, Gerss, & Rosenbaum, 2007)

Technical data is available online for Pedar® insoles (Novel, 2017). This catalogue contains physical data for various feet size of children and adults. Children's feet size ranges from size 22 – 35 (EU Size) and Adult's feet size including wide and standard foot widths range from size 36-51 (EU Size).

As this thesis is focused on children's shoes, the smallest related size found in the Pedar®
catalogue is size 22. The foot length for this catalogue matches with the Bobux insole size
23. Using the sensor information extracted from Pedar® insole catalogue (Figure 5.9). A
custom mask is applied to Figure 5.9 to capture most of the pressure change on a
designated area while a child is walking. The mask was applied by counting the number
of rows from heel to toe (posterior to anterior), and this was divided in 4 regions among
medial, middle and lateral sides. The forefoot is divided into three to approximate and
detect movement on the metatarsals. The midfoot sections have longer lengths, covering
4 boxes along the length of the foot compared to the forefoot area which only covers 3
boxes (Figure 5.8). This is because of the absence of the longitudinal arch in toddlers
result in more contact of forefoot area with toddlers (Bosch et al., 2007).

Figure 5.9 is drawn using Solidworks to create the pattern for 8 different sensors for
different plantar areas in Figure 5.8.
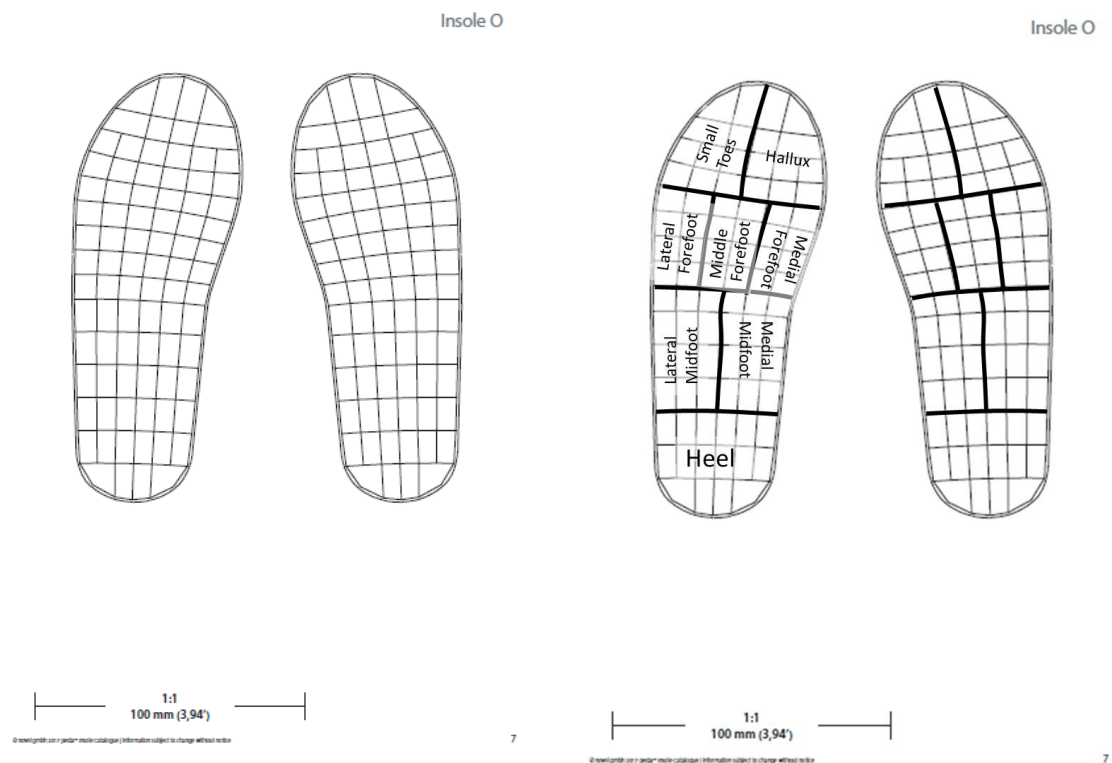
Figure 5.9: Pedar Sensor Information Size 22 (Novel, 2017)

Figure 5.8: Masked Areas using Pedar Sensor Information

A design is drawn using Solidworks to create a pattern for 8 different sensors for different plantar areas mentioned in Figure 5.8. Figure 5.10 shows the progression of design (Left to right)

Figure 5.10: (Left) Solidworks drawing of the Pedar Sensor Information. (middle) Solidworks drawing of , (Right) Design with gaps in between each sensor

The Figure 5.10 (middle), was changed to have larger gaps between each electrode (Figure 5.10 (right)). Having the electrodes close to each other can cause cross talk and therefore make it harder to get a clear signal. In MPR121 Application note, an ideal electrode design layout would be in blocks of 3.5-4.0 mm with gaps of 0.5 mm between the blocks (Jia, 2012).

The final design for the sensor pattern is shown Figure 5.11 as it captures most area with minimal amount of connections. Figure 5.11 shows different plantar areas with corresponding names and Table 7 shows the surface area of each sensor.
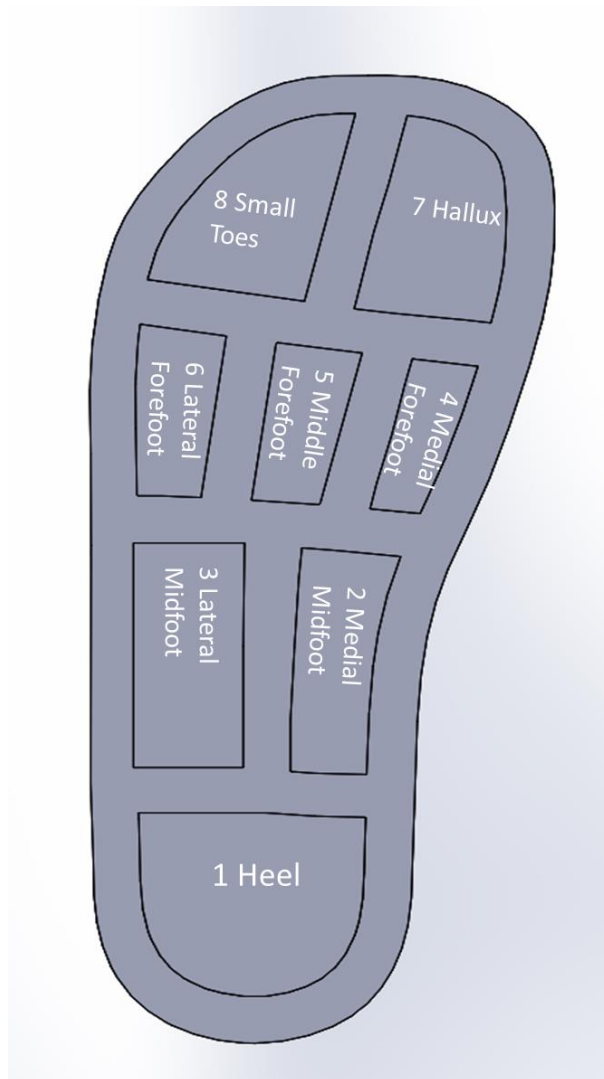
Figure 5.11: Final Sensor Topography

Table 7: Sensor Zones and Areas

Sensor Zone	Areas (mm^2)
1 Heel	787.88
2 Medial Midfoot	398.5
3 Lateral Midfoot	536.1
4 Medial Forefoot	199.28
5 Middle Forefoot	263.96
6 Lateral Forefoot	280.99
7 Hallux	513.68
8 Small Toes	506.81

5.4.3 Sensor Manufacturing and Routing

The sensor pads finalised from Chapter 5.4.2 need to be connected to the main electronics unit so that it can be used as a pressure sensor. Different manufacturing techniques were explored and qualitatively evaluated. Some techniques are readily available, and these techniques were applied in making the sensors. The physical sensors were visually assessed and their effectiveness was tested by connecting the assembled sensors to MPR121 and tested whether the capacitance would change with a fingertip touch (Testing Protocol in Section 4.2.1.1)

Manufacturing Techniques

A selection of manufacturing techniques were considered.

- **Screen-Printing** – A printing technique when ink or metal is forced on to a surface, through a screen of fine porous material to create a picture or a pattern (Oxford University Press, 2002). This technique is common when manufacturing flexible PCBs. This uses flexible silver conductive inks to create the traces. For the sensor pattern, the silver can be printed and can serve as the sensor itself. The routes of the sensor to the electronics can be printed together with the sensor pads. *Disadvantages*: Can be expensive if the equipment is not available.

- **Pattern Cutting and Sewing** – This can be used as there are conductive threads and fabrics available. The conductive fabric can be cut to any shape and sewn to any non-conductive cloth. The routes of the sensor can be the sewn on conductive threads.

Disadvantages: This can be labour intensive as the pattern needs to be cut accurately and the traces must be sewn carefully through small gaps so that it can fit small electronic connectors.

- **Pattern Cutting and Soldering** – This is similar to the previous technique but uses conductive adhesive (i.e. copper tape). As this can be cut to any shape and stuck on to any non-conductive substrate. Wires can be soldered on to the conductive adhesive and will serve as a route between the sensor pads to the electronics unit.
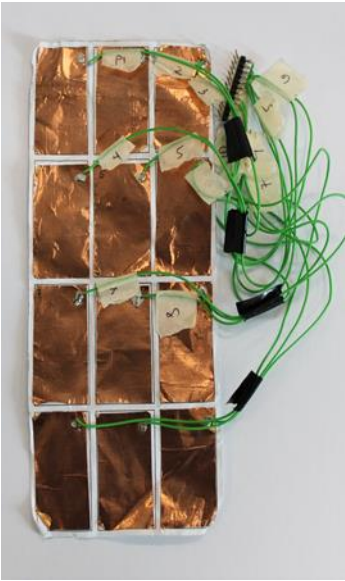
  Disadvantages: The conductive material can tear if there is no layering provided. The pattern needs to be cut accurately. Solder points can create stress raisers. If a force is applied on the joint, the solder point can tear off and disconnect itself from the sensor pad.
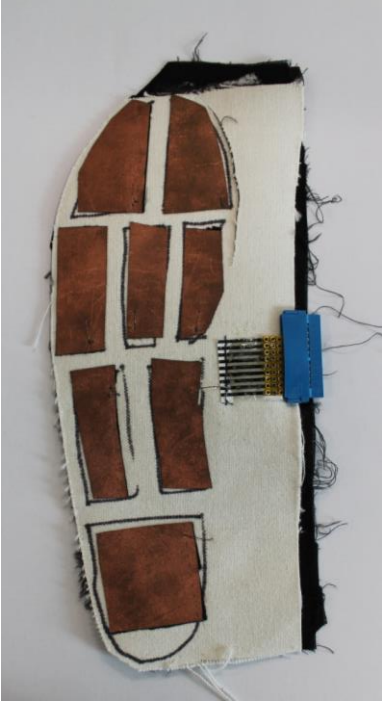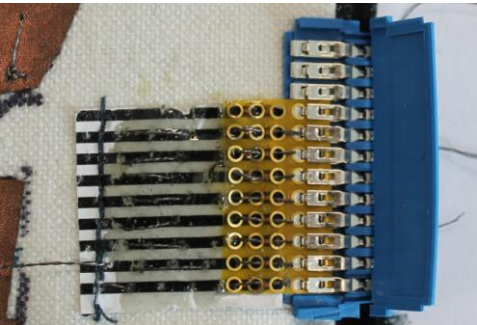
- **Laser Cutting** – This is a subtractive method where the conductive fabric or conductive tape can be laser cut instead of hand cutting the pattern. The routes can also be incorporated during the cutting process.
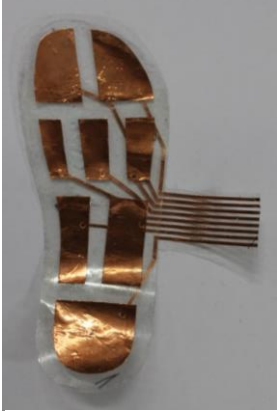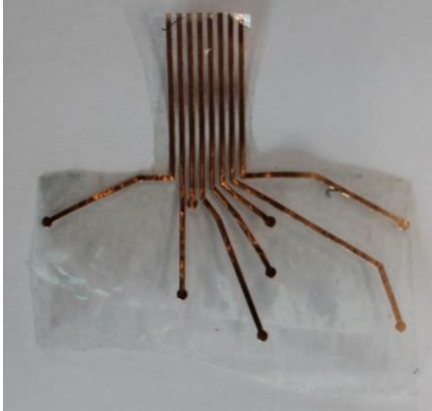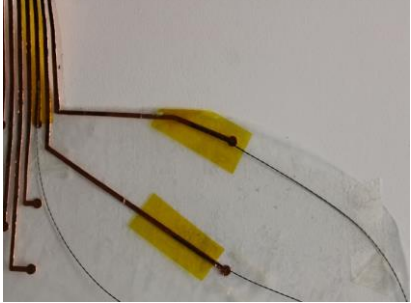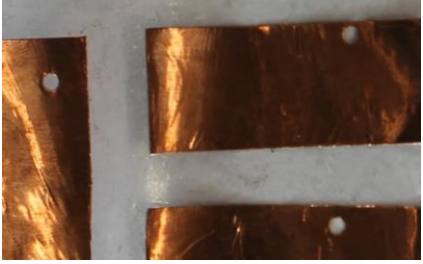
  *Disadvantages***:** Only special lasers can be used to cut conductive materials, as the reflection of metals can damage the laser. As this is a subtractive method, the material may not be utilized properly and not all of the material can be reused.

- **Vinyl Cutting** – This is also a subtractive method where there is a computerised blade that can cut the pattern. This is similar to laser cutting but instead of lasers the blades do the cutting.

  Disadvantages: As this is also a subtractive technique. The waste materials often cannot be utilised or reused.

Manufacturing Technique	Sensor Assembly	Sensor Connection
Pattern Cutting and Soldering	*Figure 5.12: Pressure Sensor made with copper tape and Wire connections*	*Figure 5.13: (top) well soldered connection; (bottom) lightly soldered connection*

Evaluation: The cut-out patterns of copper tape stuck well on paper. However, the edges of the copper tape frayed on the corners (Figure 5.13). The wire made a good connection when soldered well, however not all of them were consistent. Figure 5.13 (bottom), showed disconnection on the solder point. This could be due to the material flexing when transported and result in the connection snapping off.

Manufacturing Technique	Sensor Assembly	Sensor Connection
Pattern Cutting and Sewing	*Figure 5.14: Pressure sensor made with copper taffeta fabric and multi-layered connection*	*Figure 5.16: Conductive thread sewn at each fabric layer* *Figure 5.15: Conductive thread made to come out at the same area so it cna be inserted into a flexible breadboard and FCI Clincher*

Evaluation: The cut out patterns of the conductive fabric are sewn to a non-conductive fabric. Each sensor pad has its own route (conductive thread) and this is sewn through an individual layer of fabric to separate the routes (Figure 5.16). The non-conductive fabric also serves as an insulation to the routes as the conductive threads are not insulated. Figure 5.15, shows the line-up of the conductive threads and it is sewn through a flexible breadboard. The bare conductive thread leading up to this is covered with epoxy resin for insulation. This is then clipped on to an FCI Clincher connector.

Manufacturing Technique	Sensor Assembly	Sensor Connection
Vinyl Cutting	*Figure 5.18: Sensor and Route Layer* *Figure 5.17: Assembled Sensor installed on an outsole*	*Figure 5.21: Route Layer* *Figure 5.20: Route Layer with Conductive thread taped on* *Figure 5.19: Through holes in the sensor pad for the conductive thread to go through and join with route layer*

Evaluation: The cut out of the sensor areas shown in Figure 5.18 was done using a vinyl cutter, Roland CAMM-1 GS-24. The sheet fed on the vinyl cutter was a copper tape sheet with plastic backing. The vinyl cutter is setup to cut with the right amount of force so that it only cuts through the copper tape and not the plastic backing. The unnecessary areas of copper tape are weeded away only keeping the wanted sensor areas. The sensor route layer was also cut using the vinyl cutting machine. These are on a separate sheet to the

sensor pads. The sensor route layer and the sensor pads are connected by placing a conductive thread (Figure 5.20) on the sensor route and this is fed through the through hole (Figure 5.19) of the sensor pad sheet. The thread fed through the hole is secured with a conductive tape to ensure contact with the sensor pads.

Other materials like copper taffeta fabric were tested out and cut using the vinyl cutter (Figure 5.22). However, this technique is not ideal for cutting the copper fabric as it frays on the edges of the cut fabric. An example is shown in Figure 5.22 where copper taffeta was cut with dimensions of the connection end inserted to the FCI Clincher Connector.

Fraying of the copper taffeta. The loose strands connected to other tracks cause short circuit, making it one big sensor as opposed to 8 separate sensors.

Figure 5.22: Copper Taffeta cut using vinyl cutting machine

After visually assessing each manufacturing option, vinyl cutting copper tape on plastic backing was the preferred option. This provided a clean copper cut and most reliable connection as it does not fray on the edges. The connection inserted to the FCI Clincher tends to tear when an FCI Clincher is attached. To overcome this, a polyimide tape is used to cover the copper tape. This protects the sensor pads and the routing connections, to prevent the surface from tarnishing and gives more strength to the copper tape making it tear resistant.

5.4.4 Sensor Layer Layout

The sensor layout consists of the manufactured sensor pads and route layer using the vinyl cutting machine as pictured in Figure 5.23 and Figure 5.24.

Figure 5.23: Side View and Layers used for the sensor
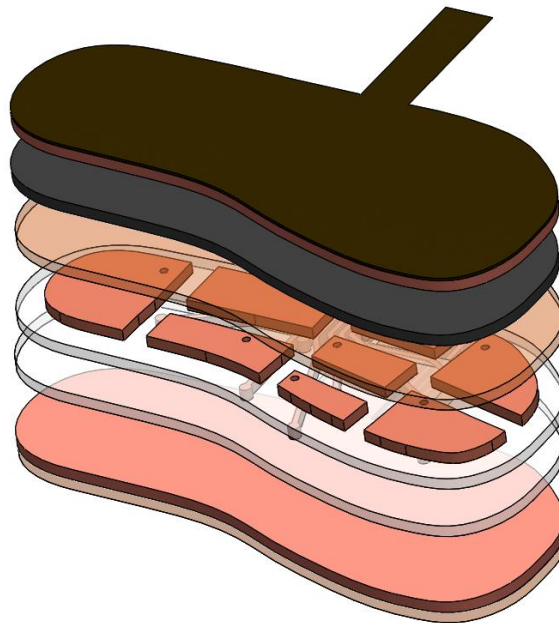
Figure 5.24: Isometric View of different sensor layers

These layers are based on the layer layout stated in Section 3.1.2. The functions of these layers are as follows:

- Cotton Cloth – Sock liner – This serves as the protection of the copper taffeta from the environment (e.g. sweaty skin). The copper taffeta tends to tarnish with moisture contact. This also functions as an insulator to the ground plane.

- Copper Taffeta – Ground Planes – these are present in both top and bottom layer of the sensor. These reduce the amount of interference from the environment (such

as RF Interference). One Ground Plane is located on the bottom of the sensor to block any interference coming from the bottom. The top ground plane serves as a part of the sensor: as the force applied changes, the top ground plane moves closer to the sensor pad (copper tape) changing the overall capacitance of the sensor.

- EVA Foam – Dielectric – This is the medium that allows the space between the top ground plane and sensor plane to change. This material is chosen because a conventional shoe would have this as their shoe insole providing cushion support on the feet. In a capacitive sensor, the EVA Foam acts as the mechanical element allowing distance between the two conductive plates to change when force is applied, and rebounds back to its original dimension when force applied is removed.

- Copper Tape – Sensor and Routes - This material is chosen as the sensor and the routes due to the ease of cutting in the vinyl cutting machine. There are two layers of copper tape and both are bonded to a plastic backing sheet. The top layer is for the sensor and the bottom layer is for the routes. This multilayer construction of the sensor is a common practice in flexible PCB Circuit printing to avoid any
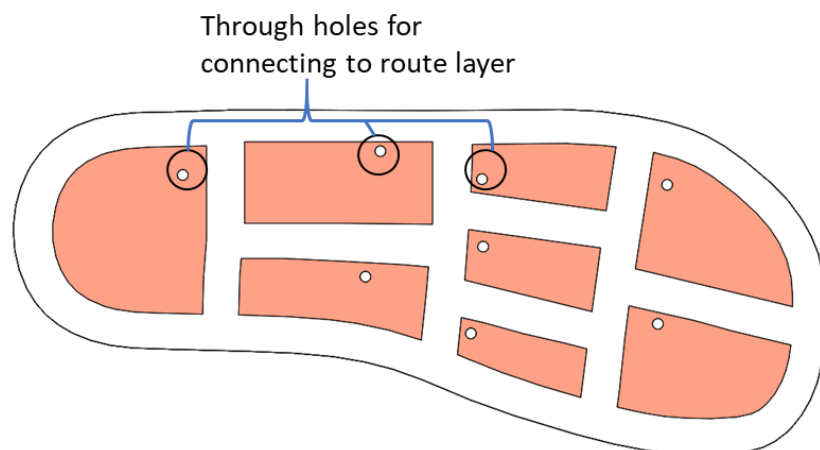
Figure 5.25: Through holes in the sense layer to connect to the route layer

crosstalk and interference between the routes and the sensor pads. (Jia, 2012). The top sensor layer contains a through hole so that it can be connected to the routes.

127

- Plastic backing – Insulator – This mechanically supports the copper tape sensor and routes during the vinyl cutting process and after the copper has been cut. This plastic backing is chosen due to its flexibility and being tear resistant during the cutting process. This also serves as an insulator and prevents the top sensor pad and bottom route layers come in contact.

- Polyimide Tape – Insulator – this mechanically supports both the copper taffeta and copper tape by keeping it in place and decreases the stress on the copper tape's surface. This is especially useful on the joint when the copper tape is punched through the FCI Clincher, helping to resist tear on the copper tape. This provides a protective layer from both the copper surfaces preventing it from tarnishing.

5.4.5 Sensor Assembly

The layers introduced in the previous section adhere to each other using pressure sensitive adhesives. Some materials selected already contain a layer of pressure sensitive adhesive, these being the polyimide tape, plastic backing and the copper tape.

The bottom copper taffeta is adhered to the plastic backing using polyimide tape. The top copper taffeta is adhered to the cotton cloth (sock liner) by an iron-on fabric glue interfacing. This is a heat sensitive material that melts and is usually placed between two non-adhesive materials (mainly fabric) to bond them together.

The top sensor layer and the bottom route layer are connected using a conductive thread this is secured on its corresponding track route by a piece of polyimide tape (Figure 5.20). This is then inserted in the through-hole and secured by a copper tape on the top sensor layer.

The completed sensor assembly is then connected using a 9 way connector to enable attachment to an electronics unit so that it can read the capacitance changes when force is applied.

Moreover, the intention for this sensor is to be built inside the shoe. This sensor assembly can be adhered to any outsole or midsole of the shoe assembly.

5.5 Sensor Validation and Calibration

For sensor validation a bigger sized sensor was made but the same design steps were taken to create this sensor. This is done so that validation can be made in comparison to a person with the same size foot as the sensor.
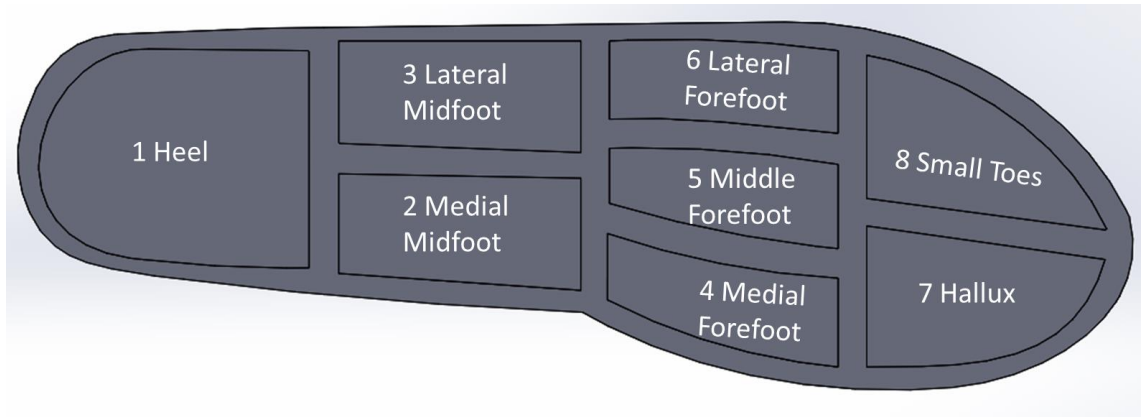
Figure 5.26: Size 36 Shoe with the same sensor segments as Figure 5.10

Table 8: Sensor Areas for Size 36 shoe

Sensor Zones	Areas (mm^2)	Sensor Zones	Areas (mm^2)
1 Heel	2163.12	5 Middle Forefoot	721.92
2 Medial Midfoot	1046.54	6 Lateral Forefoot	758.01
3 Lateral Midfoot	1057.13	7 Hallux	992.67
4 Medial Forefoot	754.45	8 Small Toes	1033.41

To validate the operation of this sensor, a 50 kg person stood on the sensor and recorded the change in pressures. This was recorded by connecting the sensor to an Arduino with MPR121, this is then connected to visualisation software programmed in LabVIEW. These results are compared to a static pressure recorded using an E-med pressure sensing platform, which is considered a gold standard device for measuring plantar pressure. This validation testing is referred to as VT1.

To validate and calibrate the sensor for repeatability, the sensor was tested under a compression testing machine, and tested for repeated loads. Other scenarios were also tested by changing the head speed of the compression testing machine to see whether this influences the operation of the sensor. During this, the sensor is connected to the Arduino with MPR121 acquiring capacitance and time data. At the same time, the force and displacement sensors from the Compression testing machine are being read in LabVIEW. This testing is referred to as VT2.

5.5.1 VT1: Validation after sensor assembly

For validation of the sensor assembly, a bigger sensor was made using the same manufacturing technique as described in the section on sensor assembly. To validate that sensor was working, a person of 50 kg mass stood on the sensor. The tester stood in a static position to generate a weight distribution. The same test was performed on the e-med pressure sensor platform, which recorded a higher resolution pressure distribution, and the results from the two different devices were compared.

5.5.2 VT2: Validation for Repeatability and calibration

To validate that sensor would deliver repeatable results, a testing jig was set up with the use of a machined foot phantom so that it can spread pressure evenly throughout the 8 sensors.
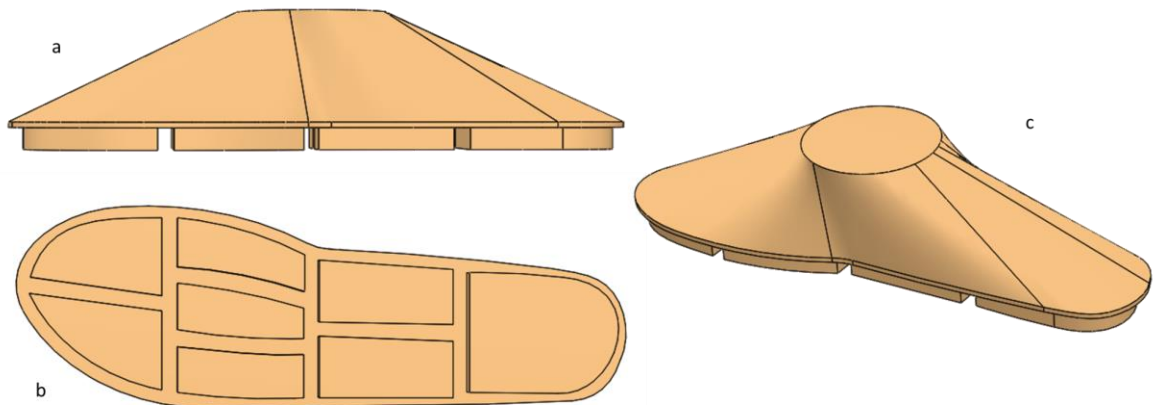
Figure 5.27: 3D Model of foot (a)Side view, (b) sensor areas, (c) isometric view showing tapered to distribute loads

Before machining, a deflection analysis was carried out in Solidworks to see whether three 18 mm panels of MDF would fail under 100 kg of load 100 kg is chosen because a Factor of Safety of 2 is assumed together with a 50 kg body mass.
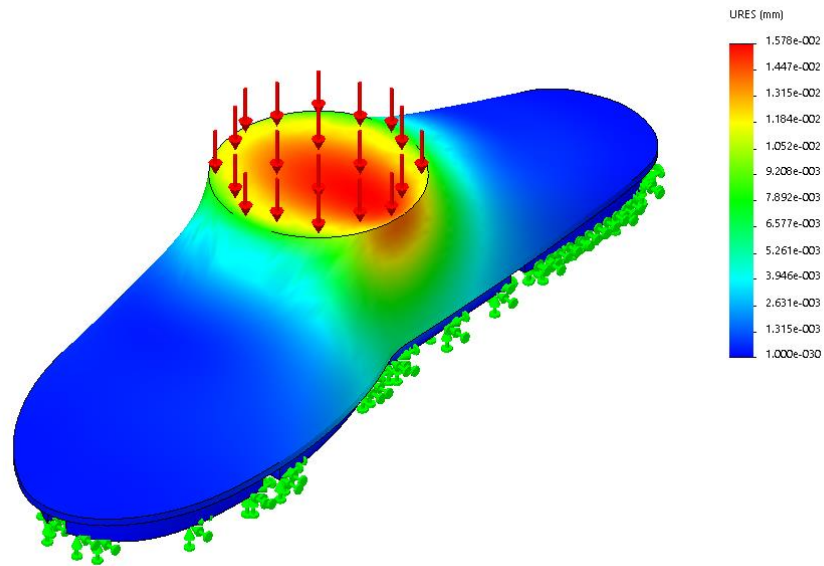
Figure 5.28: Solidworks Loading with 100 kg Load

A load simulation was done using Solidworks Simulation studies, to verify that 54 mm thick of MDF is enough to withstand 100 kg loads. Figure 5.28 shows that the most displacement is 0.0157 mm. This small deflection will ensure uniform loads across the sensors during testing.

To apply accurate loads, a compression testing Machine (Hounsfield H10KS) was configured to apply a 100 kg load. This machine is programmed and paired to using LabVIEW for Data Acquisition.
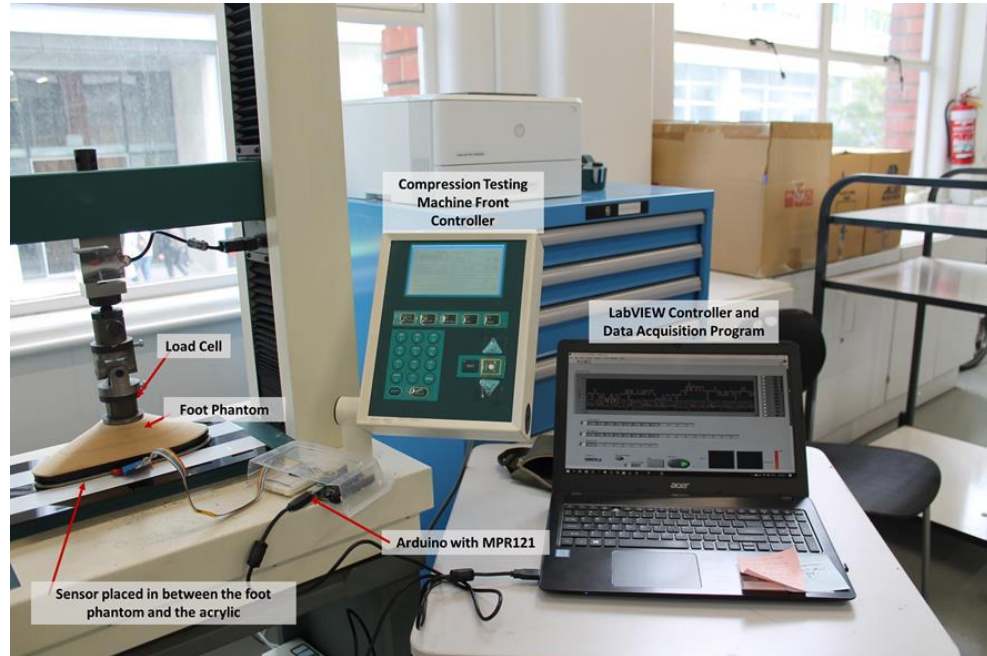
Figure 5.29: Testing Setup for VT2

5.5.2.1 *LabVIEW for Data Acquisition and With Arduino.*

A Virtual Instrument (VI) is put together to enable reading from the compression testing machine and Arduino paired with MPR121. The VI is needed so that both instruments are controlled and read synchronously. Block diagram below is showing the algorithm in the VI used. A copy of the code is included in appendix 4.

Setup	Data Manipulation	Data Extraction
Set options for the head speed and when to move for compression testing machine	Translation of ADC Data from compression testing machine to force (N) and displacement (mm)	Data extracted and translated from LabVIEW is converted as an Excel spreadsheet
Set options for the maximum force to be read	Extracting string data from both Arduino and Compression testing machine to numeric data	
Synchronise timing between Arduino and Compression Testing Machine.	Arranging data in a meaningful order	

Figure 5.30: Pseudocode of LabVIEW VI

5.5.2.2 *Test Methodology and Test Setup*

Two tests were carried out for validating repeatability of the sensors and for calibration

1. Loads were repeated 10 times, with the same loading and unloading rate

   For this test, the load is repeated 10 times with a single dielectric. The maximum load applied for the compression testing machine is set at 1000 N, as this is an approximate equivalent of a 100 kg mass. The loading and unloading rate is set at 10 mm/min. The sensor is resting on an acrylic sheet to stop it contacting the metal plate, at the base of the compression testing machine.

135

2. Loads are repeated 11 times, with different loading and unloading rates.

   The load is repeated 11 times, because it was found on the previous test that the first test would always be an offset to the remaining tests done. The loading and unloading rates varied from 15 – 50 mm/min with increments of 5 mm/min each test. A new dielectric is used, whenever the loading rate changed. The sensor again is resting on an acrylic sheet to stop direct contact with the metal plate base (Figure 5.31).
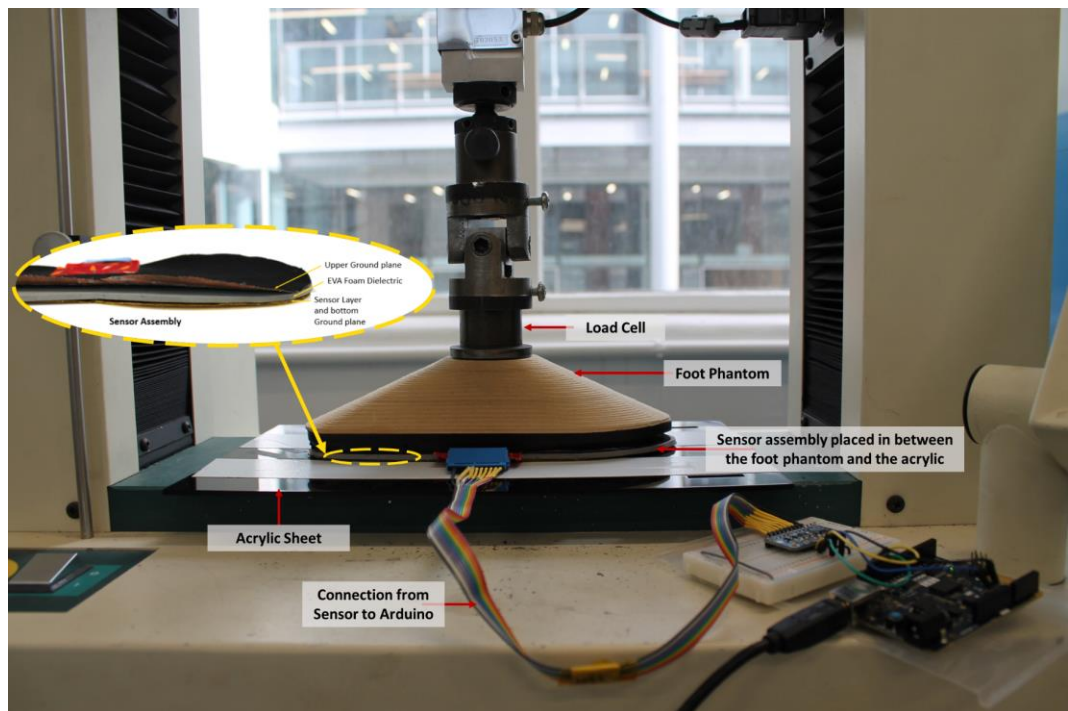
Figure 5.31: Test Setup for Test 1 and 2

5.6 Data Analysis

The data extracted from LabVIEW have 4 parameters.

- Absolute Capacitance

- Relative Capacitance

- Time

- Force

- Displacement of the load cell

- Visual interpretation of the foot print.

For the two validation tests, the data from these are analysed differently.

VT1: Validation after assembly

The visual representation of the foot print is will be compared with the pressure reading acquired from e-med pressure sensor.

VT2: Validation for repeatability and calibration

VT2.1: A MATLAB script is written to create time series plots of the capacitance to check whether it increases during application of load and decreases when unloaded. This is to test how reliable the connection is when put together manually. Additionally, Force and displacement plots are created per test to check how the material deforms under repeated load. Capacitance is then compared and plotted against displacement and force. This is to

VT2.2: There are 11 sets of data acquired for each loading and unloading rate. The 1st set for each rate is disregarded. This is because of it being reproducibly unfitting/outlier compared to the successive tests (tests 2-10). The loading and unloading rates are as follows: 15, 20, 25, 30, 35, 40, 45, 50 mm/min. A MATLAB script is written to

investigate three various aspects of the sensor.– a) force applied to the sensor and its corresponding displacement is plotted against each other to investigate the material properties during loading and unloading, b) relative capacitance read and displacement is compared together to investigate the electrical properties of the sensor according to displacement during load and unloading scenarios, c) relative capacitance and force applied to investigate electrical properties according to force applied during loading and unloading scenarios.

Each data set is separated to find the maximum readings for force and displacement which determines where to split the data. The first half of the data is loading data (i.e. when force is applied) and the second half of data is unloading data (i.e. when force is taken off). A curve fit algorithm is applied separately for each loading and unloading data.

The data acquired from MATLAB ran through a smoothing algorithm to remove 'spikes' in the data set. This is necessary so that data sets can be curve-fitted more accurately and resulted in r^2 values >0.95. The curve fits are selected using the built-in MATLAB curve fit application. The chosen equation is chosen based on which fit gives the highest r^2 value which indicated the goodness of fit. The same equation is used for all the other corresponding data sets, obtaining different coefficients for corresponding curve fit.

The coefficients of the curve fit are analysed by examining the spread of coefficients per load and unload rate. The median of each spread is extracted for further statistical analysis to see whether the load and unload rates affect the coefficients of the curve fit.

5.7 Results and Discussion

5.7.1 VT1: Validation after sensor assembly
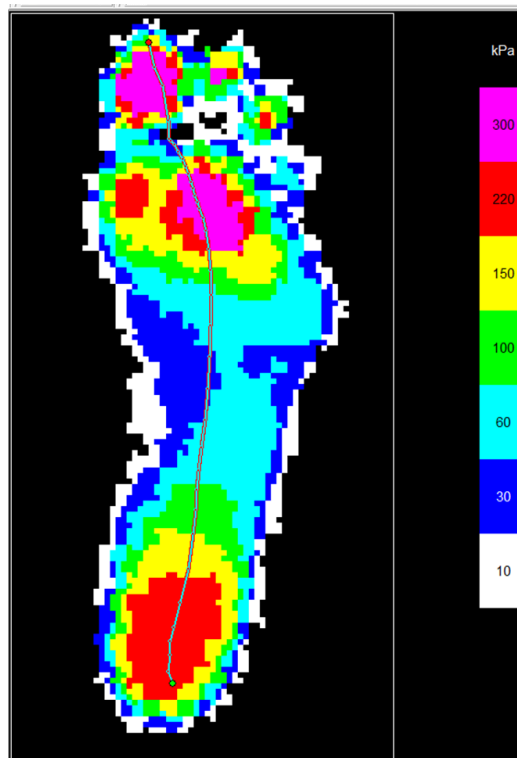
Figure 5.32: Result from E-med Pressure platform
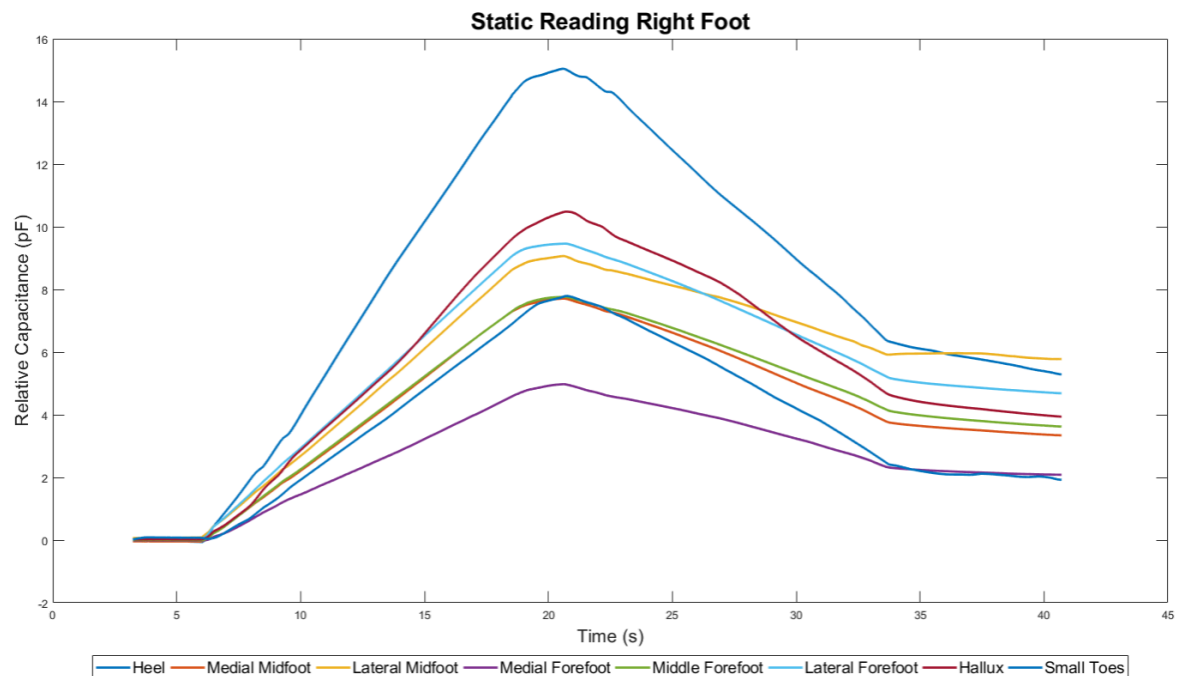
Figure 5.33: Line Graph of Sensor Prototype Readings from LabVIEW

A visual comparison is made between the results from e-med pressure platform Figure 5.32, which is a gold standard equipment for measuring pressure and LabVIEW results, Figure 5.33. The e-med result contains more resolution due to it having more pixels and so foot shape can be made out. The LabVIEW results are depicted as a line graph with 8 lines indicating each sensor pad.

The e-med and LabVIEW results are comparable to each other. The heel areas on both results show similar indication. The heel area on the e-med results shows a large red area, which means that there is a high concentration of force in that area. Similarly, the LabVIEW results shows that the heel area has the highest peak, indicating a high relative capacitance reading. This means that the highest concentration of force is also in the heel area.

Although the e-med result shows a large red area on the heel, this does not mean that it is the highest force read. The e-med result also shows magenta colour located on the hallux and the forefoot area. Similarly, LabVIEW results exhibited the second highest peaks after the heel readings for the plantar pressure sensor.

The LabVIEW results only show relative capacitance values, and not the amount of force for the corresponding capacitance reading. Testing was performed for second part of validation testing to further investigate electromechanical behaviours of material combinations. This would then help to characterise the sensors, resulting in an equation to calculate force from capacitance.

5.7.2 VT2: Results for repeatability and calibration

5.7.2.1 VT2.1 Results
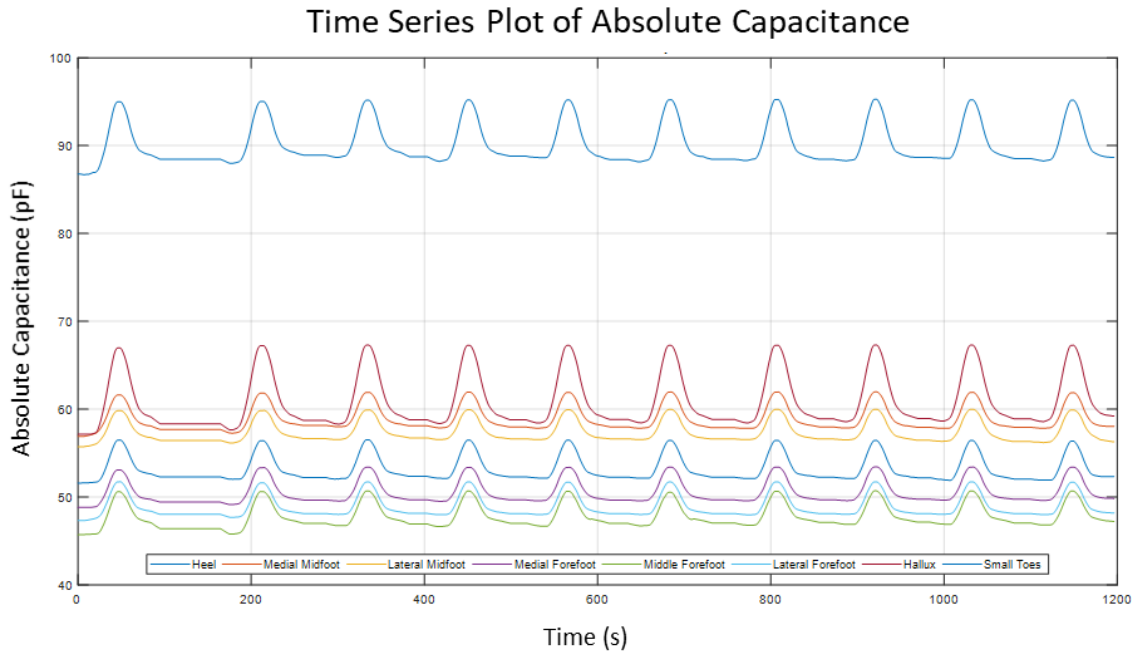
Figure 5.34: Time series graph of Absolute Capacitance of 8 sensor pads

The graph in Figure 5.34 shows the time series plots of the change in absolute capacitance during loading and unloading (loading cycle). The peaks indicate one loading cycle of the sensor. The left part of the peak indicated the loading of the sensor and the right part indicates unloading. In between these peaks, is an almost horizontal line. This indicates the time it took to reset and start the loading again.

Figure 5.34 displays 10 peaks indicating 10 loading cycles and 8 sets of plots, representing the 8 areas in the sensor. Each sensor showed different absolute capacitance values, indicated by the plots not overlapping each other. This is due to the sensors having different areas to each other. The highest reading in the graph indicates the heel sensor which had the largest area, whereas the other areas like the midfoot, forefoot and toes were twice as small as the heel area. Knowing that sensor areas are dissimilar to each other, results in the next set of testing were scaled based on area so that the sensors can be characterised easily.
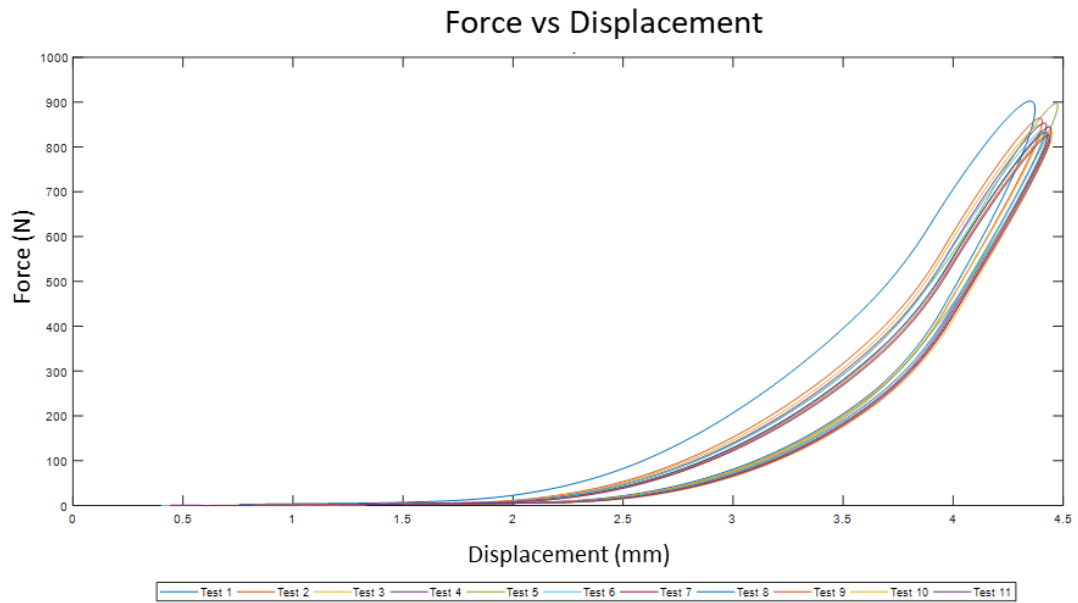
Figure 5.35: Force and Displacement plot of each test

The graph in Figure 5.35 shows the Force and Displacement plot of the sensor. This is plotted to observe the material characteristics of the EVA Foam. From this graph, it shows that Test 1 has a large gap between the other 10 consecutive tests (Tests 2-11). For the 2nd to 11th loading cycle, the offset between these lines is not as apparent as for Test 1. This could be due to the EVA closed cells deforming in the first load. When the 2nd load is applied, the foam is already deformed and does not go through the same deformation as the 1st test. Due to this result, Test 1 results will be disregarded when curve fitting is involved.
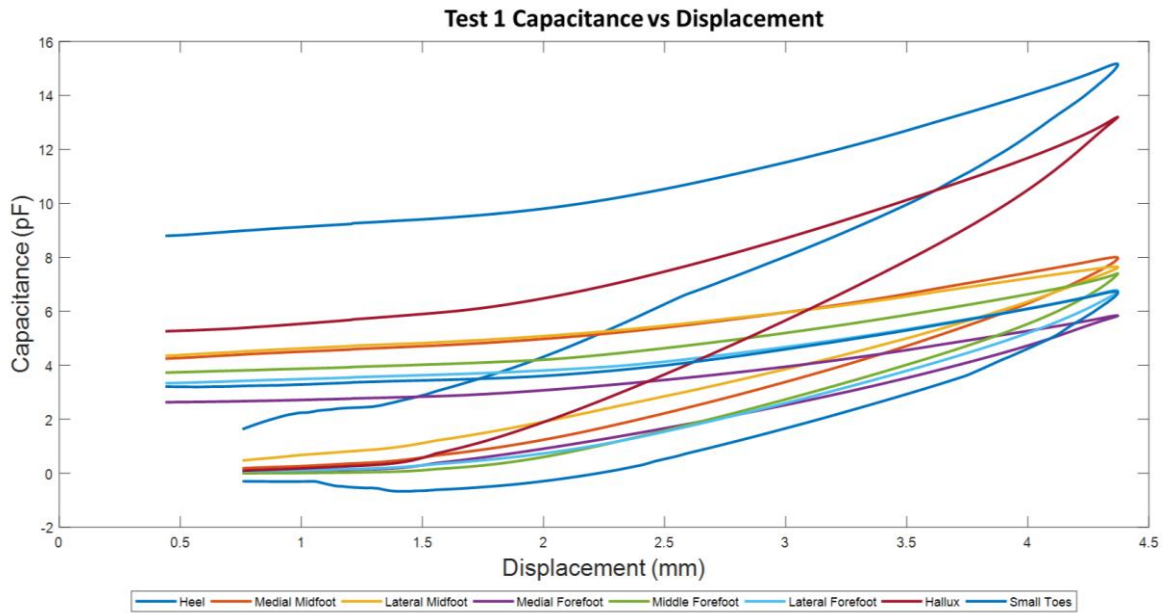
Figure 5.36: Test 1 Capacitance and Displacement plots for each sensor pad

The graph in Figure 5.36 shows the capacitance and displacement plots of test 1. There are 8 lines representing each sensor. The hallux and the heel plot are above all other readings. The heel readings may be higher than the other sensors because of it having the largest area amongst the other sensors. The hallux performed like the heel sensor, despite it being a smaller area and from the other end of the sensor assembly. This may be because of non-uniformity in the loading system on the foot shape.

143
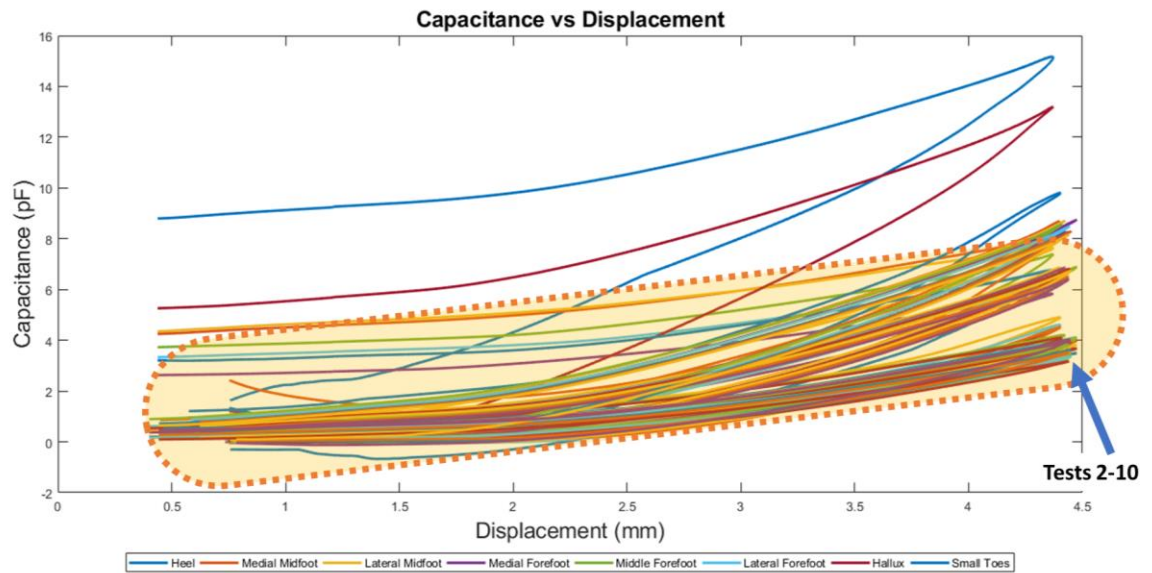
Figure 5.37: Capacitance and Displacement plots for 10 tests

When tests 2-10 were performed, the curves now have relative capacitance readings between 0 – 6 pF (Figure 5.37). The test 1 result is disregarded because the data trend obtained by the hallux and heel does not follow the results obtained by tests 2-10 as highlighted in Figure 5.37.

Comparable results were acquired and shown on the Capacitance and Force Plot (Figure 5.38), where the hallux and heel plot of test 1 is an outlier (Figure 5.39) .
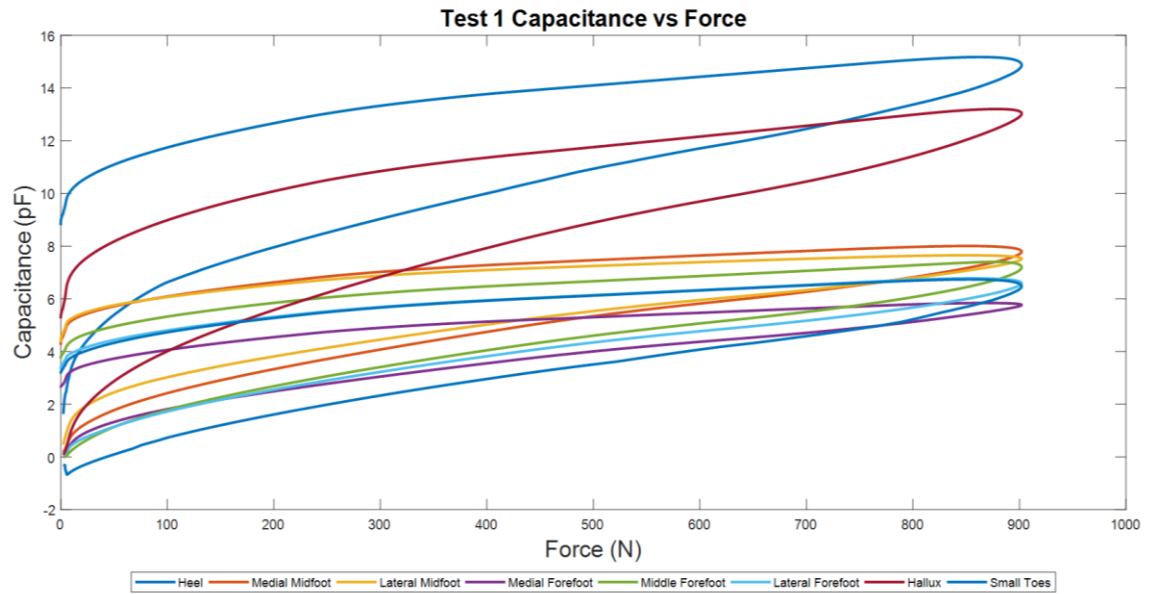
Figure 5.38: Test 1 Capacitance and Force Plot for each sensor
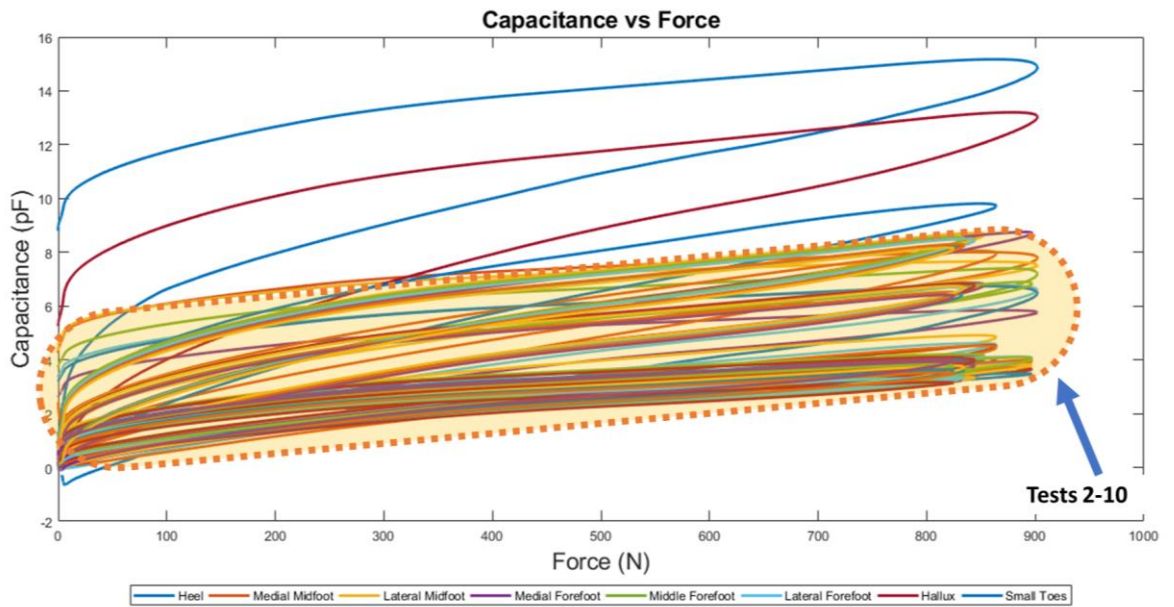
Figure 5.39: Capacitance and Force Plot for 10 Tests

145

5.7.2.2 VT 2.2 Results and Discussion

For this part of the results, three data sets were analysed. Each data set was analysed three ways, – a) Curves are fitted into each data set (Force and Displacement, Capacitance and Displacement, Capacitance and Force). Each data set has two curves, one for loading and unloading data; b) coefficients for the equations of the curve fit in each data set are collated, and their variability was observed amongst the same tests, and different load/unloading rates. These are represented as box plots; c) mean values of each data spread in the box plot were acquired and these are statistically analysed using linear regression techniques.

The equation used to acquire Force and Displacement Coefficients took the form of:

$$F = ad^b$$

where, a and b are coefficients, F is force and d is displacement
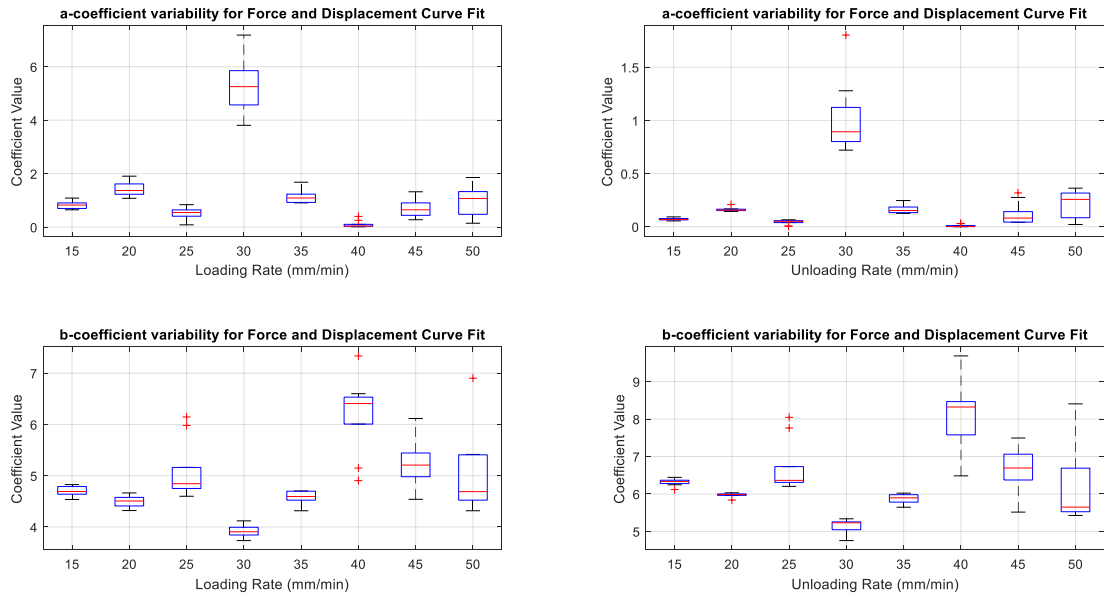
Figure 5.40: Box Plots showing coefficient variability for Equation 5-1

The variability of coefficient values per loading rate showed fluctuating ranges as shown in the spread in Figure 5.40. On the same figure, coefficient 'a' showed broad variability at both loading and unloading rates of 30 mm/min, compared to the rest of the loading rates. The 'b' coefficients showed a less consistent range throughout the different loading and unloading rates.
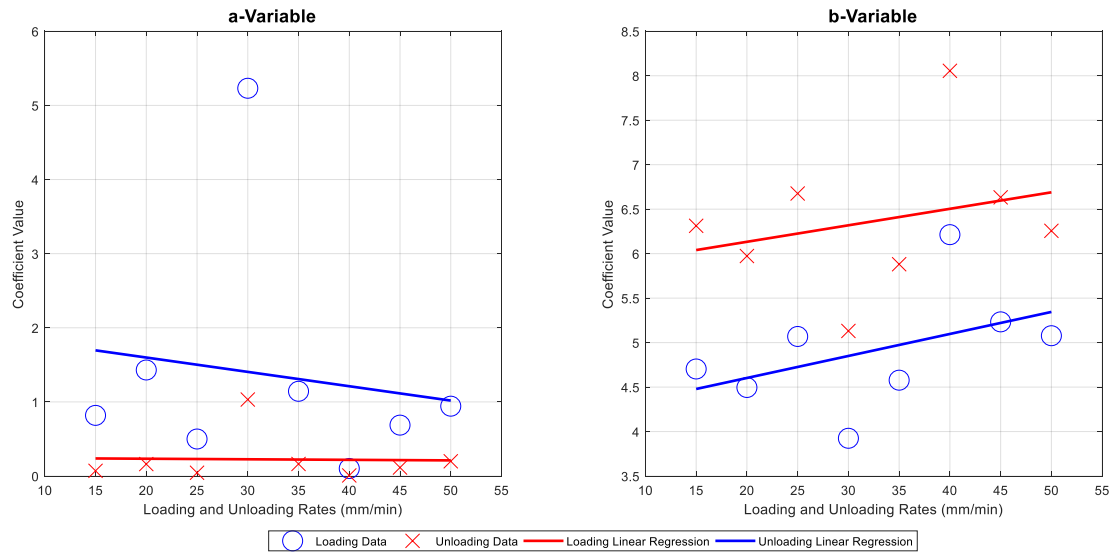
Figure 5.41: Plot of mean values for Figure 5.40 with Linear Regression Model Fitted

Table 9: Linear regression coefficient for mean coefficient values in Figure 5.41

	Linear Regression Model for evaluation of curve fit coefficients for $F = ad^b$ *m being the slope of the linear regression line, c being the intercept of the linear regression line.*		
	$m\ (SE)$	$c\ (SE)$	p
a_{load}	$-0.019\ (0.05)$	$1.99(1.84)$	0.73
a_{unload}	$-0.00074\ (0.01)$	$0.25(0.38)$	0.95
b_{load}	$0.024(0.011)$	$4.11(0.69)$	0.26
b_{unload}	$0.019(0.027)$	$5.76(0.93)$	0.52

The equation used to acquire Capacitance and Displacement Coefficients took the form

$$C = ad^2 + bd + c$$

where a, b and c are coefficients, C is capacitance and d is displacement.

Coefficient Variability for Capacitance and Displacement Curve Fit
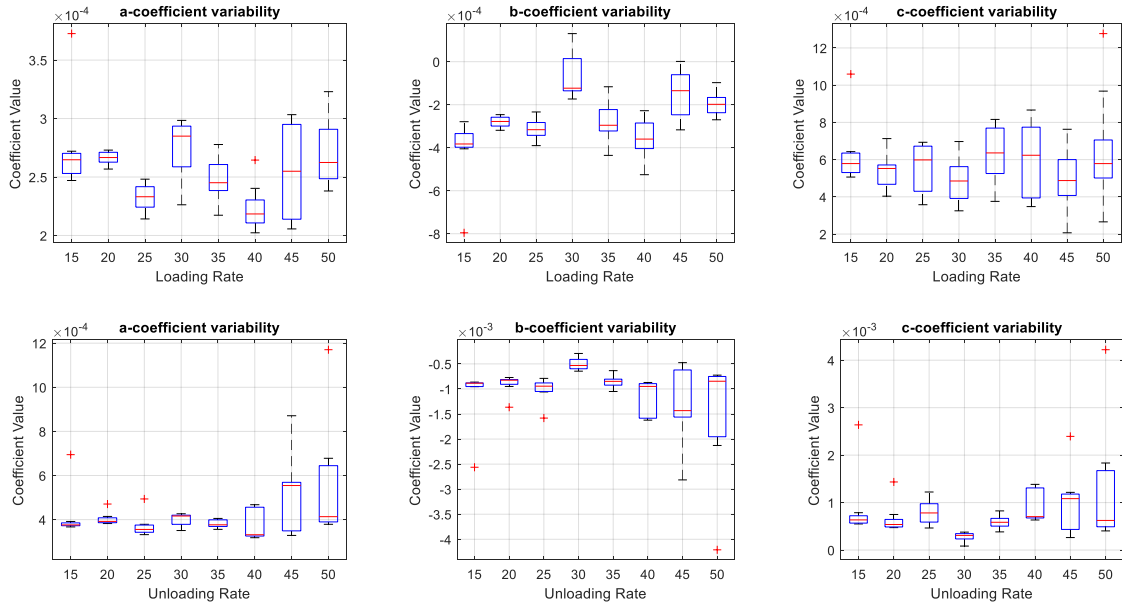
Figure 5.42: Box Plots of Coefficient Variability for Equation 5-2

The variability of all the coefficients at all loading rates in Figure 5.42 showed an inconsistent spread of coefficient values. However, the coefficient variability during unloading was more consistent. From 15 – 35 mm/min unloading rate, coefficients showed narrow variability, indicated by a narrow height of the box whereas on higher unloading rates between 40 – 50 mm/min, coefficients showed a larger spread of values.
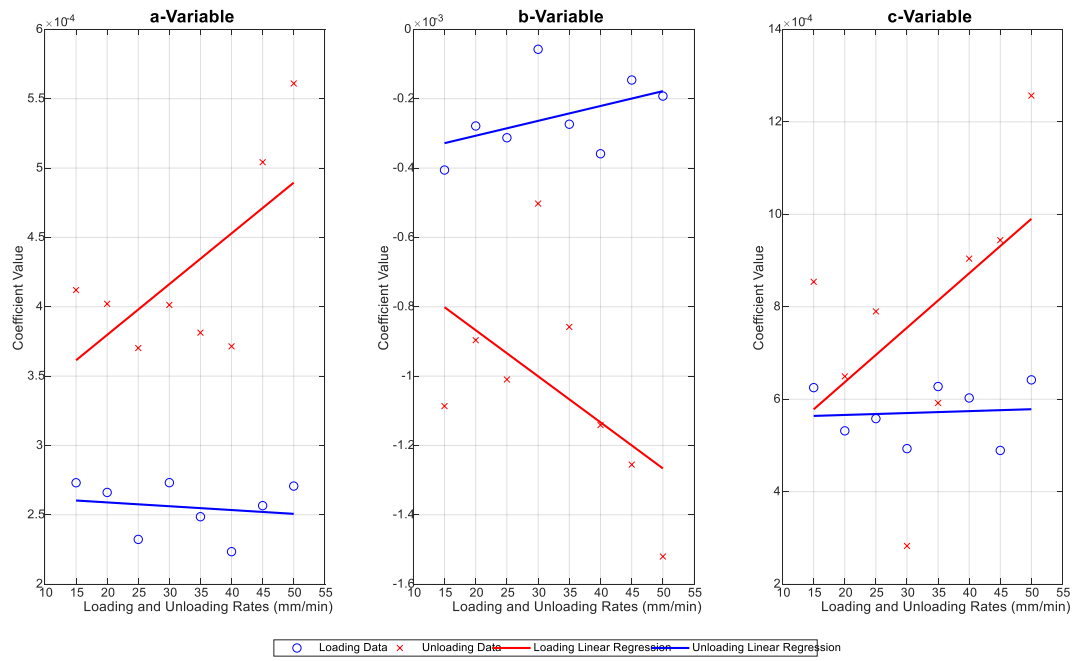
Figure 5.43: Plot of mean Values from Figure 5.42 with fitted linear regression model

Table 10:Linear Regression coefficients for mean of the coefficient values in Figure 5.43

	Linear Regression Model for evaluation of curve fit coefficients for $C = ad^2 + bd + c$ *m being the slope of the linear regression line, c being the intercept of the linear regression line.*		
	m (SE)	c (SE)	p
a_{load}	$-2.75 \times 10^{-7}(3.61 \times 10^{-7})$	$2.64 \times 10^{-4}(2.17 \times 10^{-5})$	0.68
a_{unload}	$3.66 \times 10^{-6}(1.77 \times 10^{-6})$	$3.07 \times 10^{-4}(6.10 \times 10^{-5})$	0.08
b_{load}	$4.29 \times 10^{-6}(3.41 \times 10^{-6})$	$-3.93 \times 10^{-4}(1.17 \times 10^{-4})$	0.25
b_{unload}	$-1.33 \times 10^{-5}(8.43 \times 10^{-6})$	$-6.02 \times 10^{-4}(2.9 \times 10^{-4})$	0.17
c_{load}	$4.15 \times 10^{-7}(2.05 \times 10^{-6})$	$5.58 \times 10^{-6}(7.06 \times 10^{-5})$	0.85
c_{unload}	$1.18 \times 10^{-5}(8.26 \times 10^{-6})$	$4.02 \times 10^{-4}(2.84 \times 10^{-4})$	0.20

The equation used to acquire Capacitance and Force Coefficients took the form

$$C = aF^b$$

where, a and b are coefficients, C is capacitance and F is force.

Coefficient Variability for Capacitance and Force Curve Fit
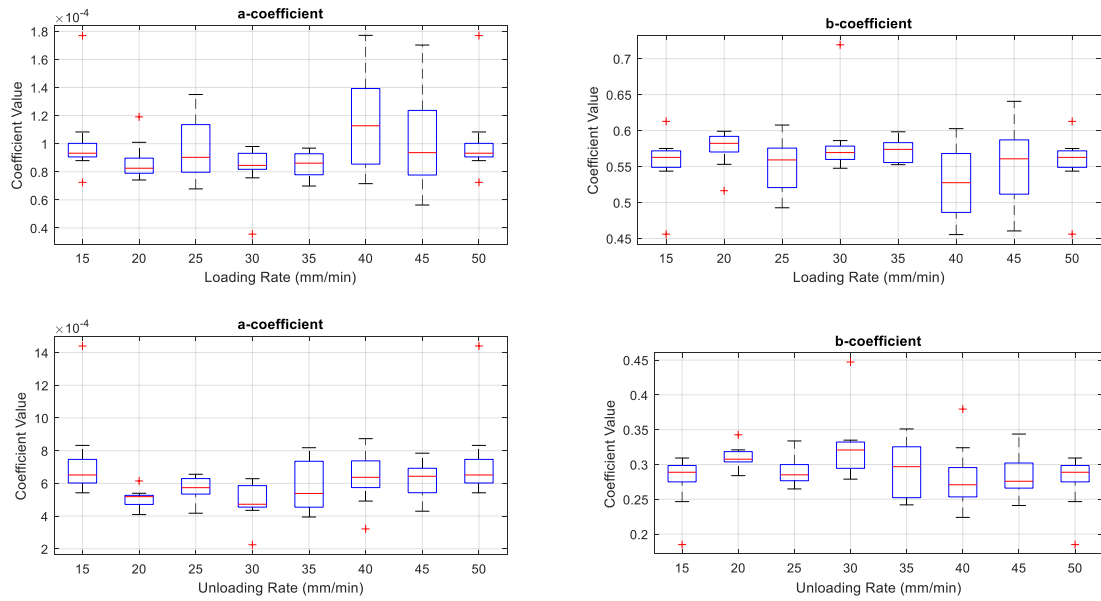
Figure 5.44: Box Plots for coefficient variability of Equation 5-3

The coefficient variability amongst both loading and unloading rates are inconsistent in Figure 5.44, this is indicated by the uneven heights of the boxes.
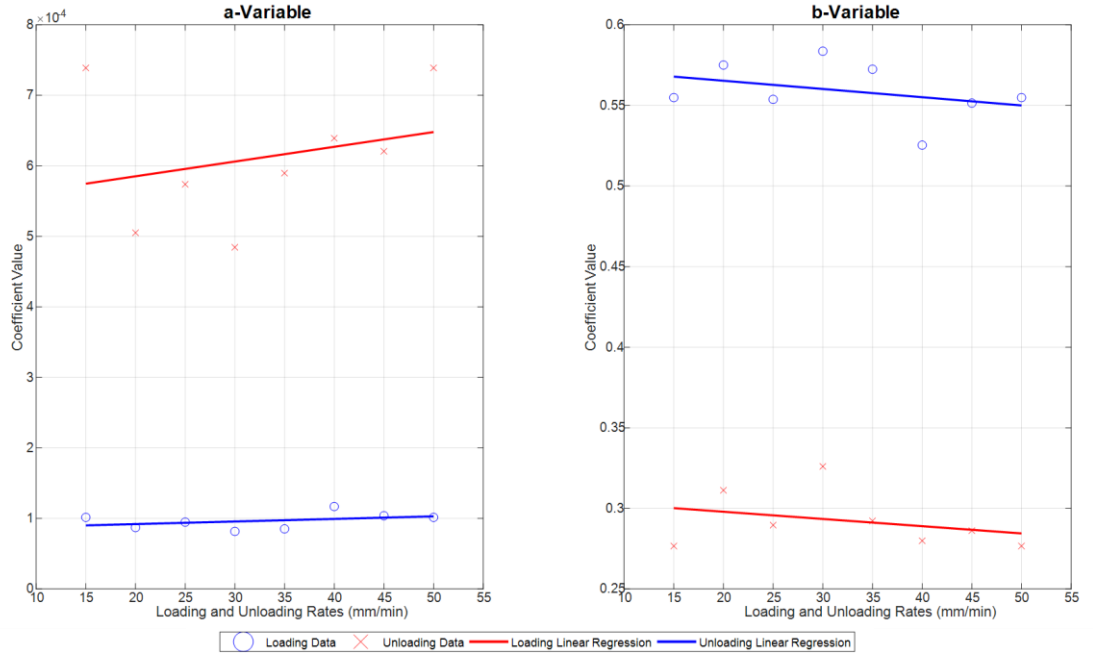
Figure 5.45: Plot of mean values for Figure 5.44 with linear regression model fitted

Table 11:Linear regression evaluation for coefficient values in Figure 5.45

	Linear Regression Model for evaluation of curve fit coefficients for $C = aF^b$ *m being the slope of the linear regression line, c being the intercept of the linear regression line.*		
	m (SE)	c (SE)	p
a_{load}	$3.66 \times 10^{-7} (3.61 \times 10^{-7})$	$8.47 \times 10^{-5} (1.24 \times 10^{-5})$	0.35
a_{unload}	$2.09 \times 10^{-6} (3.03 \times 10^{-6})$	$5.43 \times 10^{-4} (1.05 \times 10^{-4})$	0.51
b_{load}	$-5.10 \times^{-4} (5.67 \times 10^{-4})$	0.56 (0.02)	0.261
b_{unload}	$-4.48 \times 10^{-4} (5.60 \times 10^{-4})$	0.31 (0.02)	0.45

The results in Table 9, Table 10 and Table 11 shows the relevance of the strain rates in the role of curve fits for Equation 5-1, Equation 5-2, and Equation 5-3. Statistical analysis results were derived from MATLAB and in the tables mentioned, showed no p values less than 0.05, indicating that the loading and unloading rates do not affect the curve fits done on Force – Displacement, Capacitance – Displacement, and Capacitance – Force data sets with statistical significance.

Figure 5.41, Figure 5.43, and Figure 5.45 show the plots of mean coefficient values for both loading and unloading data. It is apparent that there is a difference in values of slopes between loading and unloading. This is indicated by the parameter 'm' (slope of the linear regression) shown in Table 9, Table 10 and Table 11. Additionally, there is an offset between the two linear regression lines indicated by different 'c' values (linear regression intercept) Table 9, Table 10 and Table 11.

As the loading and unloading rates do not affect the coefficients derived from the curve fits, mean values of the coefficients shown in box plots of Figure 5.40, Figure 5.42, and Figure 5.44were acquired to obtain suitable set of calibration curves. Figure 5.46 shows the curve fit graphs obtained using the mean coefficient values for each data set.
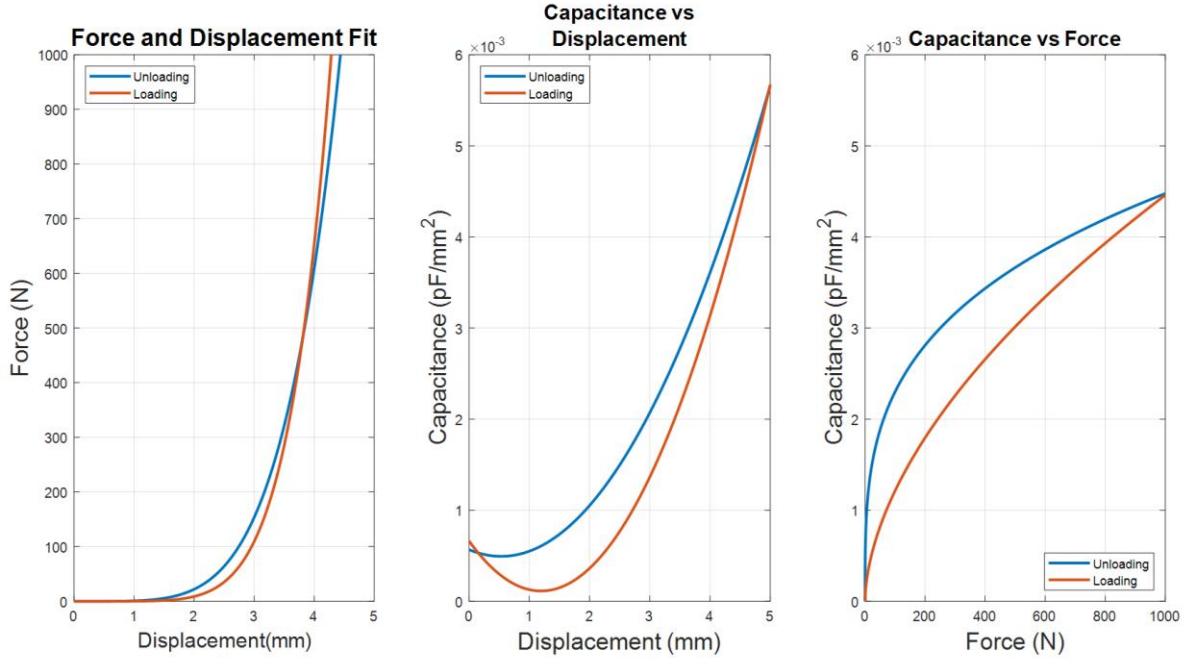
Figure 5.46: Calibration Curves for different data sets

Table 12: Equation of the curves in Figure 5.46

Curve Fit Type	Equation
	where $_l$ denotes equation during the loading phase, $_u$ denotes equation during unloading phase
Force and Displacement	$F_l = 0.795d_l^{4.78}$ $F_u = 0.119d_u^{6.21}$
Capacitance vs Displacement	$C_l = 1 \times 10^{-4}(3.84d_l^2 - 9.81d_l + 6.62)$ $C_u = 1 \times 10^{-4}(2.59d_u^2 - 2.76du + 5.67)$
Capacitance vs Force	$C_l = 9 \times 10^{-5}F_l^{0.57}$ $C_u = 6.08 \times 10^{-4}F_u^{0.29}$

Note: Equations are only applicable for loads between, $0 < F_l, F_u < 1000$ N and displacement between $0 < d_l, d_u < 5$ mm

5.7.2.3 Discussion of Results in Figure 5.46

Referring to Figure 5.46 there is a significant difference between the coefficients of loading and unloading parameters. It can be observed in the graph there is space between the loading and unloading curves in all the curve fits. This indicated a hysteretic behaviour due to the EVA Foam being an elastomeric material. The force and displacement showed little space between the load and unload curves. These curves crossed over each other at the point when displacement is at 4 mm and the force is at 400 N. This is an artefact of the curve fitting of different data sets. The same cross-over feature is starting to show in higher displacement on the capacitance vs displacement and force graphs.

Although the best fit was chosen for each loading and unloading curve, the mean values of the coefficients does not necessarily represent the best curve fit for the overall data set. A constraint can be given when carrying out the curve fitting, so that the loading curve would always be beneath the unloading curve within the operating range.

Both capacitance vs displacement and capacitance vs force showed large space between the loading and unloading curves, even though unloading lines were expected to overlap and be in the same place as the loading lines for Figure 5.46. This behaviour indicated that the readings from the sensor during loading are not the same during unloading phase. The hysteretic condition is more evident when capacitance is plotted against force and displacement.

The capacitance vs displacement curve fits took a quadratic form (Table 12). A characteristic in this curve is that both loading and unloading curves show a dip in the graph between displacement of 1 and 2 mm. They then show an almost constant slope with positive linear relationship from displacement of 2 to 5 mm (Figure 5.46).

This could reflect the behaviour of the EVA foam: when the EVA foam is in the early compression stage, the cell walls of the closed cells are bent but not completely collapsed. The uncompressed thickness of the EVA Foam is 3 mm, although this does not necessarily mean that allowable travel of the head displacement of the load cell is 3 mm. At 3 mm, the cell walls could have collapsed or completely fractured. Beyond 3 mm, cell walls have crushed together, leaving a non-foam EVA material.

The capacitance and force relationship showed a power function. Both loading and unloading curves in this graph have a distinct shape, where the loading curve is less curved compared to the unloading curve. At low and high force readings the curves converge a point. Visually, this graph contained more area between the two curves depicting higher hysteretic behaviour compared to force and displacement curves. This could also be due to the elastomeric behaviour of the EVA Foam but may include electrical phenomena as well.

The hysteretic phenomenon exhibited on Figure 5.46 is usually present when an elastomeric foam is under compression loads. Figure 5.47 shows a typical stress strain curve of an elastomer, where in the beginning of the curve, a linear stress strain relationship called linear elasticity is depicted. It is determined by bending of the cell walls of the closed cell. The plateau stage corresponds to gradual collapse of the cell wall, through elastic buckling or plastic yielding. The cell wall collapse is dependent on the material. Densification is the collapse of cell walls throughout the materials, causing the load to distribute against opposite cell walls (i.e. cell walls are now touching each other bearing the load) (Gibson, 2005).
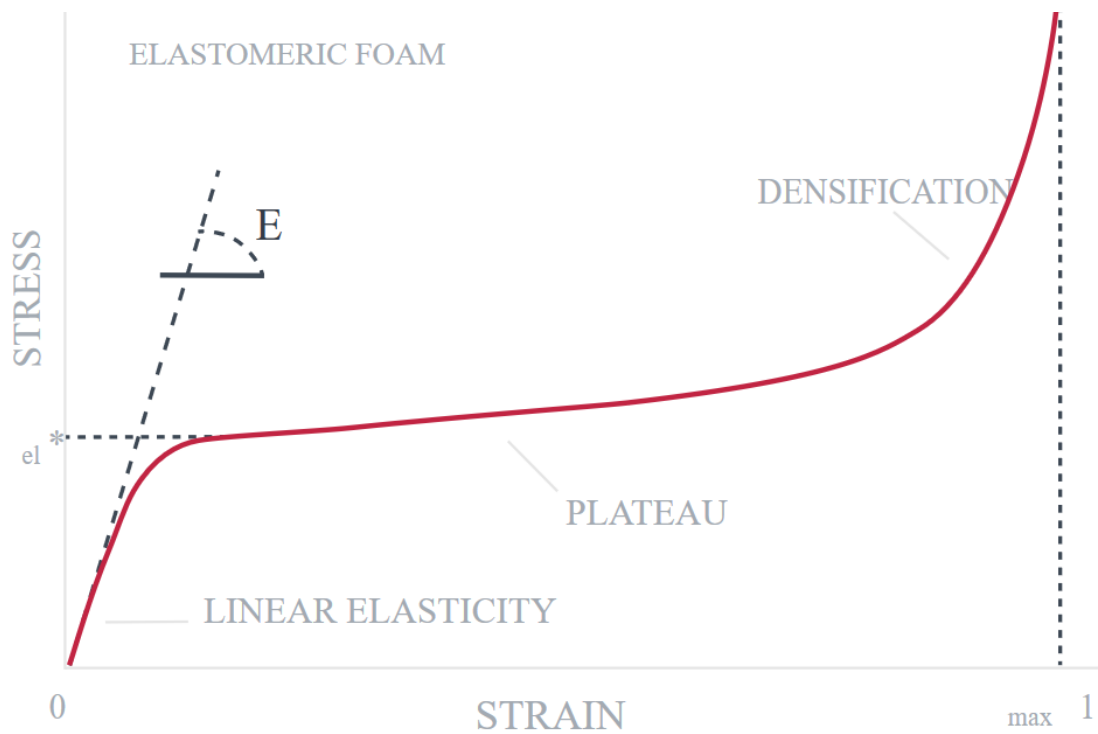
Figure 5.47: Stress vs Strain Curve of an elastomeric foam (Carbon (R), 2017)

For this investigation using EVA closed cell foam, a similar non-linear phenomenon can be seen in Figure 5.46. The curve fits and graphs in Figure 5.46 may not be representative of the whole data set, but are a representation of behaviour during loading and unloading stages.

In future work, the collapse of cell walls of the EVA could be modelled to better predict and anticipate the capacitance behaviour as it is dependent on force and displacement.

5.8   Foot Pressure Measurement System Conclusion

The objective related in this chapter was to develop a low-cost sensor assembly which mimics pressure sensing insoles and pressure sensing platforms.

Section 5.7 discussed the feasibility of a sensor assembly which mimics pressure sensing insoles. The final prototype for built-in-shoe pressure sensing was achieved through iterative design. Suitable manufacturing techniques were selected, having in mind how to design for manufacture. The vinyl cutting technique on copper tape and plastic backing was selected as this was the cheapest and most reliable option available. Screen printing would have been the best option as it would give more reliable connections without having to manually connect the route and the sense layer. However, the price of implementing this technique for prototypes is costly and time consuming.

The in-shoe pressure sensor has undergone two sets of validation testing. It fulfilled the requirement for the initial testing VT1, where it mimicked the pressure sensing characteristic of the e-med pressure platform. VT2 comprised of two types of testing, one for repeatability and calibration. VT2.1 repeatability testing showed satisfactory results as it showed 10 consistent peaks when the same load was applied 10 times.

VT 2.2 involved calibration tests to see whether different loading rates would affect the calibration curves. Different loading rates represented different landing rates for footfalls. Loading rates did not make a difference because the coefficient values of different parameters do not show a consistent range. Moreover, loading rates were found to not affect the sensor readings as they are not correlated with each other, as indicated by p values greater than 0.05 stated in Table 9, Table 10, and Table 11.

The curve fit and coefficient analysis proved the hysteretic behaviour of the EVA foam dielectric, hence causing the loading and unloading curves to not overlap each other. Three equations were derived from the data analysis, which can be initially used to translate capacitance to force readings. However, accuracy of these equations is limited to the ranges tested and there is some variability. Possible investigation and further development includes:

1. More accurate material modelling to better predict material properties. This can be modelling of the return (rebound) of EVA foam during cyclic loading. This can be combined by a study of electromagnetic fields of capacitive plates sandwiched between soft materials.
2. Implement a uniform area for all sensors. This is to make it easier for further test calibration, for the sensors to 'feel' the same amount of force when pressed.

Additionally, the testing done on the foot pressure measurement system is not representative of a real foot. The instrument used for compressing the sensors is made of wood, which is a hard material. Real feet, especially children's feet are not as rigid as wood. In fact, they are made with soft tissues with viscoelastic features.

Moreover, the foot pressure measurement system may still undergo through more development. The expenditure on making the physical sensor, without the electronics

costed at NZD 3.78 (detailed bill of materials is in the Appendix 5). However, no information on the cost of making the existing insole pressure sensors mentioned in Chapter 2.3 was available, apart from the cost of a used Pedar unit at USD 27000. Comparing the cost of the used Pedar unit and the plantar pressure sensor made during this research, the prototype made is of lower cost. However, other parameters needed to be taken in to consideration, such as, the software used for this plantar pressure sensor prototype which may not be as robust and presents less detailed information compared to the existing plantar pressure system.

Chapter 6 Conclusions and Future Recommendations

The aim of this research was to study the technical feasibility of textile sensors in measuring foot anthropometrics, specifically foot length and plantar pressure. Chapter 4 covered the creation and validation of an in-shoe foot length measurement system and Chapter 5 discussed the creation and validation of a built-in-shoe plantar pressure measurement system.

The motivation behind the aims of creating two different sensors was to help lessen the uncertainties that parents have around their children's foot health between ages of 11 months to 36 months, as children experience a rapid foot growth during this time. Additionally, Bobux is also interested in deciphering podiatrists' issues around children's foot development, as well as using foot anthropometric data to design shoes better. As Bobux is a shoe manufacturer, they are specifically looking at implementing new and innovative technologies in their shoes to help address the issues mentioned.

Chapters 4 and 5 discussed the creation of two prototypes that can help to address the issues specified in Chapter 1.1.

An iterative design process was taken to create final prototypes. The prototypes were tested and validated in many ways for further verification to answer and justify the research aims.

Chapter 4 explored the development of knitted shoe sensors to measure foot length. Sensor prototype 1 proved that knitted conductive threads can be used as sensors. Sensor prototype 2 was created to improve the design challenges and problems found in sensor prototype 1. Sensor Prototype 2 technically proved that knitted textile sensors can be implemented inside shoes to measure foot length. This is evident in Figure 4.57, showing

a positive increase in capacitance as the foot inserted inside the shoe gets bigger. Table 5 also shows the statistical validity of the results acquired in Figure 4.57. Although this research technically proved that knitted sensors can be used to measure foot length of children, more feet and information are needed to ensure that trend stays true.

Chapter 5 explored the development of built-in-shoe plantar pressure measurement. The final prototype for this was achieved through an iterative design process. Suitable manufacturing techniques were selected, to fit the prototyping environment. This meant that the technology explored was only limited to what is available to the university. The final prototype of plantar pressure measurement underwent validation testing and the results technically proved that it can mimic existing pressure sensing systems, as related in the discussion of Chapter 5.7. However, this system did not go through the same evaluation as Chapter 4, as it was not tested with children. The simulated results from the instrumented testing machine may not be the same as when human feet are involved in testing the sensors.

6.1 Future Recommendations

The evaluations of prototypes in Chapter 4 and Chapter 5 gave a better understanding on how these sensor systems work. This research also uncovered specific areas that warrant future research. These recommendations for future directions of investigation include:

1. In Chapter 4, the foot length is the anthropometric parameter investigated. Estimating other parameters such as foot width, foot volume and foot height, would be ideal, as this would indicate an overall shape. This information is more useful than foot length alone, as it gives an indication on how 'full' the shoe is while it is inside the shoe. Length, width and height would also be ideal as this

would give podiatrists a better indication of the feet size and posture by not having to virtually investigate the foot shape.

2. In Chapter 4, the fabric sensor is implemented inside a shoe with more rigid walls compared to a knitted shoe. The shoes used for testing may have constrained the foot instead of allowing it to relax and conform to its natural shape. Therefore, this could have affected the results. Applicability to other shoe constructions should be investigated.

3. In Chapter 5, more accurate material modelling to better predict material and sensor properties would be helpful. This includes modelling of the return of EVA foam during cyclic loading and unloading. This can be combined by the study of electromagnetic fields of capacitive plates sandwiched between soft materials.

4. In Chapter 5, uniform sensor shapes should be implemented, this would make it easier to calibrate the sensors, as they should all experience the same amount of change during the loading cycle.

The development of different sensors mentioned in Chapters 4 and 5 showed feasibility of the smart textile technologies. This thesis covered the creation and development of proof of concepts, established boundaries and parameters on what needs to be considered if it was to be designed for manufacture. The information in Chapters 4 and 5 lay a foundational knowledge that can be used to further investigate whether these technologies are appropriate for clinical requirements or suitable for commercial consumer markets.

In summary, the findings of this research achieved the objectives and the research aims. It creates a new body of knowledge that may help address issues that parents, clinicians and designers face. The technical results may not solve immediate problems that parents face, but this research increased foot health and footwear literacy, through the validation

test carried out with children detailed in Chapter 4.2.5. Similarly, with podiatrists and clinicians, this research does not give them an immediately usable tool. However, it presents new knowledge regarding new and innovative technologies that are available that can possibly solve more of their issues with further development. The development of both sensors described in Chapter 4 and Chapter 5 helped Bobux in exploring other materials and new manufacturing techniques that can help solve the issues of podiatrists and parents alike.

Appendix 1 – Leather Material Data

General information

Designation

Leather

Typical uses

Belts and seals, shoes, bags, cases, clothing, fancy goods.

Composition overview

Compositional summary

Collagen (protein)/12% H_2O

Form	Other	
Material family	Natural	
Base material	Biological	
Renewable content	100	%

Composition detail (polymers and natural materials)

Natural material	100	%

Price

Price	* 23.5	-	29.3	NZD/kg
Price per unit volume	* 1.9e4	-	3.08e4	NZD/m^3

Physical properties

Density	810	-	1.05e3	kg/m^3

Mechanical properties

Young's modulus	0.1	-	0.5	GPa
Specific stiffness	0.108	-	0.544	MN.m/kg
Yield strength (elastic limit)	2	-	5	MPa
Tensile strength	20	-	50	MPa
Specific strength	2.15	-	5.48	kN.m/kg
Elongation	18	-	75	% strain
Compressive strength	1	-	2	MPa
Flexural modulus	0.1	-	0.5	GPa
Flexural strength (modulus of rupture)	3	-	6	MPa
Shear modulus	0.03	-	0.1	GPa
Bulk modulus	* 1	-	2	GPa
Poisson's ratio	0.05	-	0.48	
Shape factor	3.8			
Hardness - Vickers	* 2	-	3	HV
Elastic stored energy (springs)	8.29	-	60.3	kJ/m^3
Fatigue strength at 10^7 cycles	4.5	-	9	MPa

Impact & fracture properties

Fracture toughness	* 3	-	5	MPa.m^0.5
Toughness (G)	28.3	-	159	kJ/m^2

Thermal properties

Glass temperature	* 110	-	130	°C
Maximum service temperature	* 110	-	130	°C
Minimum service temperature	* -83	-	-73	°C
Thermal conductivity	0.156	-	0.16	W/m.°C
Specific heat capacity	1.53e3	-	1.73e3	J/kg.°C
Thermal expansion coefficient	* 40	-	50	µstrain/°C
Thermal shock resistance	* 133	-	750	°C
Thermal distortion resistance	* 0.00316	-	0.00395	MW/m

Electrical properties

Electrical resistivity	* 1e8	-	1e10	µohm.cm
Electrical conductivity	1.72e-8	-	1.72e-6	%IACS
Dielectric constant (relative permittivity)	* 2	-	10	
Dissipation factor (dielectric loss tangent)	* 0.01	-	0.05	
Dielectric strength (dielectric breakdown)	* 6	-	8	MV/m

Magnetic properties

Magnetic type	Non-magnetic

Optical, aesthetic and acoustic properties

Transparency	Opaque			
Acoustic velocity	304	-	799	m/s
Mechanical loss coefficient (tan delta)	* 0.1	-	0.5	

Critical materials risk

Contains >5wt% critical elements?	No

Durability

Water (fresh)	Acceptable
Water (salt)	Acceptable
Weak acids	Limited use
Strong acids	Unacceptable
Weak alkalis	Limited use
Strong alkalis	Unacceptable
Organic solvents	Unacceptable
Oxidation at 500C	Unacceptable
UV radiation (sunlight)	Fair
Flammability	Slow-burning

Primary production energy, CO2 and water

Embodied energy, primary production	102	-	113	MJ/kg

Values marked * are estimates.
No warranty is given for the accuracy of this data

CO2 footprint, primary production	4.08	-	4.5	kg/kg
Water usage	* 1.09e4	-	1.2e4	l/kg

Recycling and end of life

Recycle	✘			
Recycle fraction in current supply	6.65	-	7.35	%
Downcycle	✔			
Combust for energy recovery	✔			
Heat of combustion (net)	* 19.4	-	20.4	MJ/kg
Combustion CO2	* 1.39	-	1.46	kg/kg
Landfill	✔			
Biodegrade	✔			

Notes
Warning

Leather is a very variable material. Its properties depend on source, age, moisture, tanning agents etc.

Other notes

Leather is a protein. It has a remarkable profile of properties, making it attractive for numerous applications even today.

Links

ProcessUniverse
Reference
Shape

Appendix 2 – Arduino Code

```
#include <Wire.h>
#include "Adafruit_MPR121.h"

//include cpp files

// Default address is 0x5A, if tied to 3.3V its 0x5B
// If tied to SDA its 0x5C and if SCL then 0x5D
//Device Addresses
#define MPR 0x5C          //Device 1 Default Address - MPRAddress in Arduino - C Connected to
SDA
//#define MPR 0x5B // Connected to Vin
//Configuration Registers
#define CHARGE_CURRENT 0x5C    //CDC Config
#define CHARGE_TIME 0x5D        //CDT Config
#define ELEC_CFG 0x5E        //Electrode Config
#define ELEC_Current 0x5F     //Electrode 0 - Current Set
#define ELEC_Time 0x6C        //Electrode 0 - Time Set

//Auto Configuration Registers
#define AUTOCONFIG0 0x7B
#define UPLIMIT 0x7D
#define LOLIMIT 0x7E
#define TARGETLIMIT 0X7F
#define SOFTRESET 0x80

//Constants
uint8_t N = 8; //Number of sensors
uint8_t Num_of_devices = 1;
uint8_t devices[] = {MPR};



void setup()
{

  // Debug console
  Serial.begin(19200);
  Wire.begin();

  set_register(MPR,SOFTRESET,0x63);
  set_register(MPR,ELEC_CFG,0b01000000);
  set_register(MPR,AUTOCONFIG0,0x15);//ARE disable
  //set_register(AUTOCONFIG0,0x16); //refer to MPR121 datasheet p17 ACE Disable
  //set_register(AUTOCONFIG0,0x17);//ACE enable
  set_register(MPR,UPLIMIT,0xC4);//Upper Limit C4 (196) because refer to p7 AN3889 Datasheet
  set_register(MPR,LOLIMIT,0x80);//Lowerlimit 80 (128) refer to p8 AN3889 Datasheet
  set_register(MPR,TARGETLIMIT,0xB1); //Target Limit B1 (177) refer to An3889
  //set_register(CHARGE_CURRENT,0x70); //
  //set_register(CHARGE_TIME,0x4C); //
  //set_register(ELEC_CFG,0x31);//Electrode config 0001 0001 enable electroce 0 for proximity sense
```

```
  set_register(MPR,ELEC_CFG,0b01111001);//Electroce config 0001 0001 enable electroce 0 for
proximity sense
}

uint32_t past=0;

void loop()
{
  uint32_t present=0;
   double capacitances[8];
   for (int j=0;j<Num_of_devices;j++)
   {
     for(int i=0;i<N;i++){
       capacitances[i] = read_capacitance(devices[j],i);
       Serial.print(capacitances[i]);
       Serial.print('\t');
       }
   }
   present=millis();
   Serial.print(present);
   past=present;
   Serial.print('\n');
   //delay(100);
}

double read_capacitance(uint8_t addr, uint8_t channel)
{
  uint8_t chargeReg;
  uint8_t timeReg;
  uint8_t timeShift;
  uint8_t lsbReg;
  uint8_t msbReg;

  chargeReg=0x5F+channel;
  timeReg=0x6C+(channel/2);
  timeShift=(channel%2==0)?0:4;
  lsbReg=0x04+2*channel;
  msbReg=0x04+2*channel+1;



  byte chargeCurrent = read_register(addr,chargeReg);
  byte Timebyte = read_register(addr,timeReg);
  unsigned int Timebyte_v = (Timebyte>>timeShift)&7; //to get the right most 3 bits, mask the target
byte with 111 (3bits) by logic AND (&)
  double chargeTime =0.5*pow(2,(Timebyte_v-1)); //
  byte ADCLSB = read_register(addr,lsbReg); //reading electrode 0
  byte ADCMSB = read_register(addr,msbReg);//reading MSB of electrode 0
  double ADCvalue = ((ADCMSB<<8)|ADCLSB);
  //calculation based on C=I*T*1024/(VDD*ADC)
  double cap1 = 3.3*ADCvalue/1024;
```

```cpp
  double cap2 = (1.*chargeTime*chargeCurrent)/cap1;
  return cap2;
}

//write function
void set_register(uint8_t addr, uint8_t r, uint8_t v)
{
 Wire.beginTransmission(addr);
 Wire.write(r);
 Wire.write(v);
 Wire.endTransmission();
}

//read register
byte read_register(uint8_t addr, uint8_t reg)
{
 Wire.beginTransmission(addr);
 Wire.write(reg);
 Wire.endTransmission(false);
 Wire.requestFrom(addr,1);
 byte reg_check = Wire.read();
 return reg_check;
}

//read ADC
 unsigned int ADC_check(uint8_t addr, uint8_t r1)
 {
  Wire.beginTransmission(addr);
  Wire.write(r1);
  Wire.endTransmission(false);
  Wire.requestFrom(addr,2);
  byte LSB=Wire.read();
  byte MSB=Wire.read();
  unsigned int ADCv=((MSB<<8)|LSB);
  return ADCv;
 }
```

Appendix 3 – Ethics Approval

AUTEC Secretariat

Auckland University of Technology
D-88, WU406 Level 4 WU Building City Campus
T: +64 9 921 9999 ext. 8316
E: ethics@aut.ac.nz
www.aut.ac.nz/researchethics

1 December 2017

Andrew Lowe
Faculty of Design and Creative Technologies

Dear Andrew

Re Ethics Application: **17/381 Can in-shoe, textile sensors provide useful information to determine appropriate shoe sizes in young children**

Thank you for providing evidence as requested, which satisfies the points raised by the Auckland University of Technology Ethics Committee (AUTEC).

Your ethics application has been approved for three years until 1 December 2020.

Standard Conditions of Approval

1. A progress report is due annually on the anniversary of the approval date, using form EA2, which is available online through http://www.aut.ac.nz/researchethics.
2. A final report is due at the expiration of the approval period, or, upon completion of project, using form EA3, which is available online through http://www.aut.ac.nz/researchethics.
3. Any amendments to the project must be approved by AUTEC prior to being implemented. Amendments can be requested using the EA2 form: http://www.aut.ac.nz/researchethics.
4. Any serious or unexpected adverse events must be reported to AUTEC Secretariat as a matter of priority.
5. Any unforeseen events that might affect continued ethical acceptability of the project should also be reported to the AUTEC Secretariat as a matter of priority.

Non-Standard Conditions of Approval

On the poster:

1. Clarify if the 'known conditions' are an inclusion or exclusion criteria;

2. Include the total cost of time i.e. up to 45 minutes

Non-standard conditions must be completed before commencing your study. Non-standard conditions do not need to be submitted to or reviewed by AUTEC before commencing your study.

Please quote the application number and title on all future correspondence related to this project.

AUTEC grants ethical approval only. If you require management approval for access for your research from another institution or organisation then you are responsible for obtaining it. You are reminded that it is your responsibility to ensure that the spelling and grammar of documents being provided to participants or external organisations is of a high standard.

For any enquiries, please contact ethics@aut.ac.nz

Yours sincerely,

Kate O'Connor
Executive Manager
Auckland University of Technology Ethics Committee

Cc: zahdeguzman@gmail.com

Appendix 4 – LabVIEW Code for Data Acquisition

SET-UP

Compression Machine

Tab Control

Hounsfield
Testing Machine

19200

Zero and Set Velocity VI.vi

Time Delay
Delay Time (s)

Start Moving.v

Arduino

19200

DATA ACQUISITION

Force Read
(N)

Instr
Bytes at Port

0.001

Head Displacement(mm)

10000

Capacitances

Number of Inputs

Arduino Millis

Set Zero

Zero Levels

True

Zeroed Values

Waveform Chart

False

Zeroed Values

stop

error out 2

error out

DATA RECORDING

Excel

Record Reading

Appendix 5 – Bill of Materials – Sensor Assembly
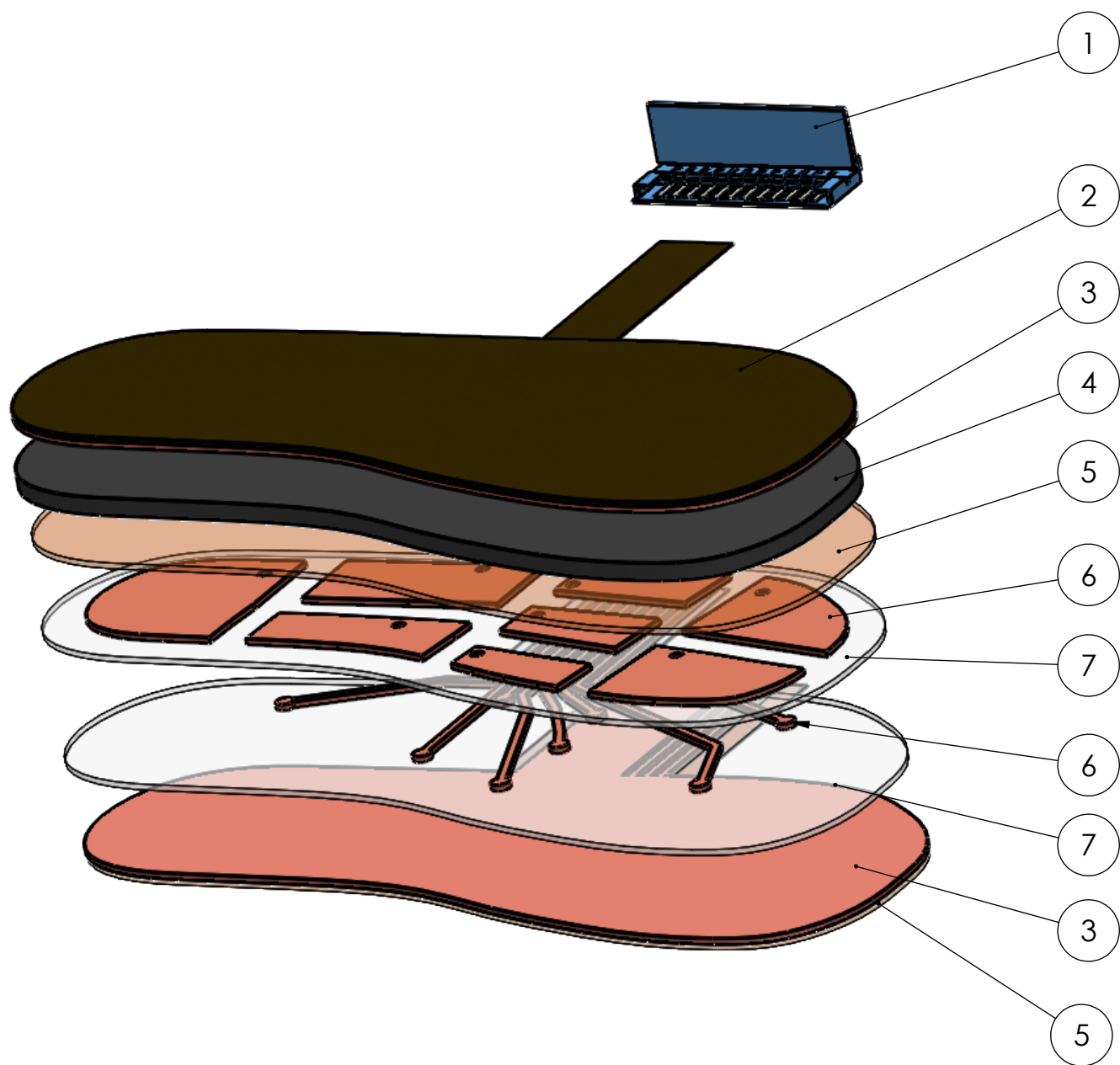
ITEM NO.	PART NUMBER	QTY.	Price (NZD)	Amount Used	Price of amount used (NZD)
1	FCI 12 Way Connector	1	2.50/piece	1	2.50
2	Cotton Sock Liner	1	NZD 1.30/sq.m	0.01 sq.m	0.013
3	Copper Taffeta	2	NZD 60/sq.m	0.02 sq.m	1.20
4	EVA Dielectric Foam	1	NZD6/sq.m	0.01 sq.m	0.06
5	Polyimide Tape	2	NZD 0.66/m	0.02 sq.m	0.01
6	Copper Tape	1	NZD 0.2/sq.m	0.0044 sq.m	0.00088
7	Plastic Backing	2	NZD 50/sq.m	0.02 sq.m	1
Total price of sensor (NZD)					3.78

References

Adafruit. (2017). *Adafruit MPR121 12-Key Capacitive Touch Sensor Breakout Tutorial*. Retrieved from https://learn.adafruit.com/adafruit-mpr121-12-key-capacitive-touch-sensor-breakout-tutorial/overview

Aliau-Bonet, C., & Pallas-Areny, R. (2013). A Novel Method to Estimate Body Capacitance to Ground at Mid Frequencies. *IEEE Transactions on Instrumentation and Measurement, 62*(9), 2519-2529. https://doi.org/10.1109/TIM.2013.2258240

Anderson, M., Blais, M., & Green, W. (1956). Growth of the normal foot during childhood and adolesced: length of foor and interelations of foot stature, and lower extremity as seen in serial records of children between 1-8 years of age. *American Journal of Physical Anthropology, 14*.

Ankhili, A., Tao, X., Cochrane, C., Coulon, D., & Koncar, V. (2018). Washable and Reliable Textile Electrodes Embedded into Underwear Fabric for Electrocardiogarphy (ECG) Monitoring. *Materials, 11*(256). https://doi.org/doi:10.3390/ma11020256

Arduino. (n.d.). *Getting Started with the Arduino/Genuino 101*. Retrieved November 14, 2017, from https://www.arduino.cc/en/Guide/Arduino101

Asics. (2017, 11 August 2017). The Anatomy of a Running Shoe. Retrieved from https://www.asics.com/nz/en-nz/blog/article/the-anatomy-of-a-running-shoe

Baadh, V. (2014). Why Barefoot is Best. *Education.com*. Retrieved from https://www.education.com/magazine/article/Barefoot_Best/

Barisch-Fritz, B., Schmeltzpfenning, T., Plank, C., & Grau, S. (2016). Foot deformation during walking: differences between static and dynamic 3D foot morphology in developing feet *Ergonomics, 57*, 921-933. https://doi.org/10.1080/00140139.2014.899629

Baxter, L. K. (2000). Capacitive Sensors. Retrieved from http://www.capsense.com/capsense-wp.pdf

Bilal. (2017). *Charge Time Measurement Unit of PIC Microcontrollers*. Retrieved from http://microcontrollerslab.com/charge-time-measurement-unit-ctmu-of-pic-microcontrollers/

Biomch-L. (2016). Novel Electronics Pedar System for Sale. https://biomch-l.isbweb.org/threads/29238-Novel-Electronics-Pedar-System-for-Sale

Bosch, K., Gerss, J., & Rosenbaum, D. (2007). Preliminary normative values for foot loading parameters of the developing child. *Gait and Posture, 26*, 238-247.

Brannock USA. *Ultra Fit Jr Brannock Device*. Retrieved from https://brannock.com/collections/products/products/ultra-fit-jr-brannock-device

Buckland, M. A., Slevin, C. M., Hafer, J. F., Choate, C., & Kraszewski, A. P. (2014). The Effect of Torsional Shoe Flexibility on Gait and Stability in Children Learning to Walk. *Paediatric Physical Therapy*. https://doi.org/DOI: 10.1097/PEP.0000000000000084

Busscher, I., Kingma, I., Wapstra, F. H., Blustra, S. K., Verkerke, G. J., & Veldhuizen, A. G. (2011). The Value of Shoe Size for Prediction of the Timing of the Pubertal Growth Spurt. *Scoliosis*. https://doi.org/http://doi.org/10.1186/1748-7161-6-1

Carbon (R). (2017). *Rethinking foam—Carbon's lattice innovation*. Retrieved from https://www.carbon3d.com/stories/rethinking-foam-carbons-lattice-innovation/

Chandra Das, S., & Chowdhury, N. (2014). Smart Textiles-New Possibilities in Textile Engineering. *IOSR Journal of Polymer and Textile Engineering, 1*(1), 1-6.

Chappell, P. H. (2016). *Mechatronic Hands : Prosthetic and Robotic Design* [Book]. London: The Institution of Engineering and Technology. Retrieved from http://ezproxy.aut.ac.nz/login?url=http://search.ebscohost.com/login.aspx?direct=true&db=nlebk&AN=1251287&site=eds-live

Cherenack, K., & van Pieterson, L. (2012). Smart textiles: Challenges and opportunities. *Journal of Applied Physics, 112*. https://doi.org/http://dx.doi.org/10.1063/1.4742728

Clarks. *Toddler Gauge*. Retrieved from https://www.clarks.co.uk/c/Toddler-Gauge/p/203524220000

Connolly, T. (2012). *The World's Oldest Shoe*. Retrieved August 17, 2018, from https://pages.uoregon.edu/connolly/FRsandals.htm

Davidson, B. (2011, September 15). *Techniques for Robust Touch Sensing Design*. Retrieved January 22, 2018, from https://www.digikey.co.nz/en/articles/techzone/2011/sep/techniques-for-robust-touch-sensing-design

Digi-Key North American Editor. (2016). Don't Touch! Designing Capacitive Proximity Sensing into IoT, Industrial & Automotive Applications. Retrieved from https://www.digikey.co.nz/en/articles/techzone/2016/aug/dont-touch-designing-capacitive-proximity-sensing-into-iot

Du, W. Y. (2015). *Resistive, Capacitive, Inductive and Magnetic Sensor Technologies*. Boca Raton: CRC Press.

Ehrmann, A., Heimlich, F., Brucken, A., Weber, M., & Haug, R. (2014). Suitability of knitted fabrics as elongation sensors subject to structure, stitch dimension and elongation direction. *Textile Research Journal, 84*(18), 2006-2012. https://doi.org/DOI: 10.1177/0040517514548812

Electronics, L. a. Capacitive Voltage Divider. *Learning About Electronics*. Retrieved from http://www.learningaboutelectronics.com/Articles/Capacitive-voltage-divider.php

ESD, A. (2010). Fundamentals of Electrostatic Discharge. In E. Association (Ed.), *Part Five -- Device Sensitivity and Testing*. Rome, New York.

Ethical Elephant. (2017). *How to Know if Shoes are Vegan*. Retrieved from https://ethicalelephant.com/how-to-find-vegan-shoes/

Evans, A., Morrison, S., & Williams, C. (Eds.). (2015). *The Paediatric Foot*. Retrieved from http://www.jfootankleres.com/series/paediatric_foot

Freescale Semiconductor. (2013). MPR121 Proximity Capacitive Touch Sensor Controller.

Gaddis, R. (2014). What Is The Future of Fabric? These Smart Textiles Will Blow Your Mind. *Forbes*. Retrieved from https://www.forbes.com/sites/forbesstylefile/2014/05/07/what-is-the-future-of-fabric-these-smart-textiles-will-blow-your-mind/#25ad3e26599b

Galloway, J. C., & Thelen, E. (2007). Feet first: Object exploration in young infants. *Infant Behaviour & Development, 27*, 107-112. https://doi.org/doi:10.1016/j.infbeh.2003.06.001

Gibson, L. (2005). Biomechanics of cellular solids. *Journal of Biomechanics, 38*(2005), 377-399. https://doi.org/doi:10.1016/j.jbiomech.2004.09.027

Goncalves, **C.**, da Silva, A. F., Gomes, J., & Simoes, R. (2018). Wearable E-Textile Technologies: A Review on Sensors, Actuators and Control Elements. *Inventions, 3*(14).

Gould, N., Moreland, M., Alvarez, R., Trevino, S., & Fenwick, J. (1989). Development of the child's arch. *Foot & Ankle, 9*(5).

Gould, N., Moreland, M., Trevino, S., Alvarez, R., Fenwick, J., & N, B. (1990). Foot Growth in Children Age One to Five Years. *Foot Ankle*, 211-213.

Granta Design. (2018). Leather.

Gusev, V. G., Demin, A. Y., Galina, L. M., & Mikhal'chenko, E. S. (2009). Study of Electrical Properties of Human Skin. *Biomedical Engineering, 43*(3), 124-127. Gusev2009. https://doi.org/10.1007/s10527-009-9107-7

Hallemans, A., Clercq, D. D., Dongen, S. V., & Aerts, P. (2006). Changes in foot-function parameters during the first 5 months after the onset of independent walking: a longitudinal follow-up study. *Gait and Posture*(23), 142-148. https://doi.org/doi:10.1016/j.gaitpost.2005.01.003

Harms, H., Amft, O., & Troster, G. (2012). Does loose fitting matter? Predicting sensor performance in smart garments*BodyNets'12 Proceedings.* Symposium conducted at the meeting of the 7th International Conference on Body Area Networks, Oslo, Norway.

Harris, C. (2015). Quality not quantity is Bobux founder Chris Bennerr's money mantra. Retrieved from https://www.stuff.co.nz/business/70810337/quality-not-quantity-is-bobux-founder-chris-bennetts-money-mantra

Herbaut, A., Chavet, P., Roux, M., Gueguen, N., Barbier, F., & Simoneau-Buessinger, E. (2017). The influence of shoe aging on children running biomechanics. *Gait & Posture*. https://doi.org/doi: 10.1016/j.gaitpost.2017.05.011

Hillstrom, H., Buckland, M. S., CM, Hafer, J., Root, L. B., SI, Kraszewski, A., Whitney, K., . . . Scherer, P. (2013). Effect of shoe flexibility on plantar loading in children learning to walk. *Journal of American Podiatric Medical Association, 103*(4), 297-305.

Indexmundi. *World Demographics Profile 2018*. Retrieved from https://www.indexmundi.com/world/demographics_profile.html

Inglis, J., Kennedy, P., Wells, C., & Chua, R. (2002). *The Role of Cutaneous Receptors in the Foot* (Vol. 508). Boston: Springer. https://doi.org/https://doi.org/10.1007/978-1-4615-0713-0_14

Jia, K. (2012). *Designing a Touch Panel using the Xtrinsic MPR121 Capacitive Touch Sensor Controller*.

Keim, R. (2016). Introduction to Capacitive Touch Sensing. Retrieved from https://www.allaboutcircuits.com/technical-articles/introduction-to-capacitive-touch-sensing/

Kessler, L., & Fisher, W. K. (1997). A study of the electrostatic behavior of carpets containing conductive yarns. *Journal of Electrostatics, 39*(4), 253-275.

Kirby, K. A. (2017). Longitudinal arch load-sharing system of the foot. *Revista Española de Podología, 28*(1). https://doi.org/http://dx.doi.org/10.1016/j.repod.2017.03.003

LessEMF. *Pure Copper Polyester Taffeta Fabric*. Retrieved from https://www.lessemf.com/fabric4.html

Maier, E. (1999). Über den Gestaltwandel der kindlichen Beine und Füße. *Orthopädieschuhtechnik*, 24-30.

McPoil, T. G. J. (1988). Footwear. *Oxford Academic, 68*(12). https://doi.org/https://doi.org/10.1093/ptj/68.12.1857

Morrison, S. C., Price, C., McClymont, J., & Nester, C. (2018). Big issues for small feet: developmental, biomechanical and clinical narratives on children's

footwear. *Journal of Foot and Ankle Research*. https://doi.org/https://doi.org/10.1186/s13047-018-0281-2

Motawi, W. (2015). *How Shoes are Made: A behind the scenes look at a real factory*: CreateSpace Independent Publishing Platform.

Motawi, W. (2017). *Shoe Material Design Guide*

Niethard, F. U. (1997). *Kinderorthopädie*. Stuttgart: Thieme Verlag.

Niiler, T., Church, C., Lennon, N., Henley, J., George, A., Taylor, D., . . . Miller, F. (2016). Reliability and minimal detectable change in foot pressure measurements in typically developing children. *The Foot, 29*, 29-35. https://doi.org/http://dx.doi.org/10.1016/j.foot.2016.10.001

Novel. *The emed systems*. Retrieved from http://www.novel.de/novelcontent/emed

Novel. (2017). Pedar Insole Catalogue. In N. GMBH (Ed.), (pp. 36).

Ohmura, N., Ogino, S., & Okano, Y. (2014). Optimized Shielding Pattern of RF Faraday Cage. *Institute of Electronics, Information and Communication Engineers*.

Orpyx. (2018). *SurroSense Rx* Retrieved from http://surrosense.orpyx.com/

Oxford Dictionary. (2018). Sensor. In *Online Oxford Dictionary*. Retrieved from https://en.oxforddictionaries.com/definition/sensor

Oxford University Press. (2002). Screen-print. In *Oxford American College Dictionary*

Pedar. *The pedar system - The quality in-shoe dynamic pressure measuring system*. Retrieved from http://novel.de/novelcontent/pedar

Penkala, S. (2012). Health Literacy: Implications for Shoe Choices Promoting Foot Health in Children. *The International Journal of Health, Wellness & Society, 1*(4), 87-97.

Price, C., Morrison, S. C., Hashmi, F., Phethean, J., & Nester, C. (2018). Biomechanics of the infant foot during transition to independent walking: A narrative review. *Gait and Posture, 59*, 140-146. https://doi.org/http://dx.doi.org/10.1016/j.gaitpost.2017.09.005

Pycom Ltd. (2017). Expansion Board 2.0. In P. Ltd. (Ed.).

R.E. Serrano, M. G., O. Casas, R. Pallas-Areny. (2003). *Power Line Interference in Ambulatory Biopotential Measurements*. presented at the meeting of the 25th Annial International Conf. Eng. Medical Biology Society, Cancun Mexico.

Razak, A. H. A. (2012). Foot Plantar Pressure Measurement System: A Review. *Sensors*, 9884-9912.

Renesas. (2017). RX Family CTSU Capacitive Touch Electrode Design Reference. In Renesas (Ed.).

RS Electronics. *RS Pro PVC Insulated, Shielded Single Core Microphone Cable 0.5 mm² CSA, PVC Sheath, 3.4mm OD 100m* Retrieved from https://uk.rs-online.com/web/p/single-core-microphone-cable/7492560/

Schneegass, S., & Amft, O. (Eds.). (2017). *Smart Textiles: Fundamentals, Design, and Interaction*: Springer International Publishing.

Sessoms, G. (2017). Foot Growth in Children. *Livestrong*. Retrieved from http://www.livestrong.com/article/514495-foot-growth-in-children/

Simon, S., Quesada, P., Pisciotta, J., & Leurgans, S. (1994). Dynamic Foot Pressues in the Early Months of Walking. *Orthopedic Research Society*, 661.

Skopljak, A., Muftic, M., Sukalo, A., Masic, I., & Zunic, L. (2014). Pedobraography in Diagnosis and Clinical Application. *Journal of Academy of Medical Sciences of Bosnia and Herzegovnia, 22*(6), 374-378. https://doi.org/10.5455/aim.2014.22.374-378

Staheli, L. (1991). Shoes for Children: A Reviews. *Pediatrics, 88*(2), 371-375.

Statex Productions & Vertriebs GMBH. (2010). *Technical Data Sheet; Conductive Sewing Thread* Retrieved from https://www.sparkfun.com/datasheets/E-Textiles/Sewing%20thread%20catalog.pdf

Stimpert, D. (2017). *What is the Sole of a Shoe*. Retrieved from https://www.liveabout.com/what-is-the-sole-of-a-shoe-2987688

Stimpert, D. (2018a). *Shoe Glossary: Lining*. Retrieved from https://www.liveabout.com/shoe-glossary-lining-2987683

Stimpert, D. (2018b). *The Upper of a Shoe and Its Parts*. Retrieved from https://www.liveabout.com/the-upper-of-the-shoe-and-its-parts-2987685

TekScan. *F-Scan System*. Retrieved from https://www.tekscan.com/products-solutions/systems/f-scan-system

Textile School. (2018). *Textiles - an introduction*. Retrieved from https://www.textileschool.com/119/textile-an-introduction/

Uddin, A. J. (2010). *Novel technical textile yarns*

Van Langenhove, L., & Hertleer, C. (2004). Smart Clothing: a new life. *International Journal of Clothing Science and Technology, 16*(1/2), 63-72. https://doi.org/https://doi.org/10.1108/09556220410520360

Walther, M., Herold, D., Sinderhauf, A., & Morrison, R. (2008). Children sport shoes - A systematic review of current literature. *Foot and Ankle Surgery, 14*(4), 180-189.

Wegener, C., Hunt, A. E., Vanwanseele, B., Burns, J., & Smith, R. M. (2011). Effect of Children's Shoes on Gait: A Systematic Review and Meta-Analysis. *Journal of Foot Ankle Research*.

Wells, J. P., Hyler-Both, D. L., Danley, T. D., & Wallace, G. H. (2002). Biomechanics of growth and development in the healthy human infant: A pilot study. *Journal of the American Osteopathic Association, 102*(6), 313-319.

Wenger, D. R. (1983). Foot Growth Rate in Children Age One to Six Years. *Foot & Ankle*.

Whelan, T. (1994). *Polymer Technology Dictionery*. Retrieved from https://books.google.co.id/books?id=7Qq_vknrP4kC&printsec=frontcover#v=onepage&q&f=false

Williams, A. (2014). The Sneaker Comes of Age. *New York TImes*. Retrieved from https://www.nytimes.com/2014/06/12/fashion/the-sneaker-comes-of-age.html

Young, H. D., & Freedman, R. A. (2008). *Sears and Zemansky's University Physics with Modern Physics*. San Francisco: Pearson Education Inc.

Zhang, X., & Tao, X. (2001a, July). Smart Textiles: Active Smart. *Textile Asia,* 49-52.

Zhang, X., & Tao, X. (2001b, June). Smart Textiles: Passive Smart. *Textile Asia,* 45-49.

Zhang, X., & Tao, X. (2001c, August). Smart Textiles: Very Smart. *Textile Asia,* 35-37.